

CHAPTER 5

SAR Methods for Mapping and Monitoring Forest Biomass

Sassan Saatchi, Senior Research Scientist, Carbon Cycle and Ecosystems Section, Jet Propulsion Laboratory, California Institute of Technology

ABSTRACT

Forests play a major role in the global carbon cycle, sequestering more than 25% of the carbon emitted to the atmosphere from fossil fuel consumption and land-use changes. The accumulation of carbon in forests has therefore become an effective strategy for mitigating climate change and an important mechanism for countries to meet their emission requirements under many international protocols and agreements. Remote sensing techniques are considered the most promising approach for providing up-to-date information on the status of forest cover and carbon stocks at different scales. Among remote sensing techniques, Synthetic Aperture Radar (SAR) sensors at long wavelengths have the advantage of strong sensitivity to the forest Above Ground Biomass (AGB) and the ability to quantify and monitor carbon stocks at the scale in which human activities occur. This chapter provides a summary of the methodologies and techniques for estimating forest AGB and monitoring changes from existing and future SAR satellite systems. The material in this chapter is designed to help both practitioners and remote sensing students and experts use SAR imagery for mapping and monitoring forest biomass. The examples and the bibliography capture the state of the art in SAR remote sensing of vegetation structure and biomass, and provide resources for enthusiasts to follow future developments in the technology and the methodology.

5.1 Background

5.1.1 GLOBAL DISTRIBUTION OF FOREST BIOMASS

Vegetation in terrestrial ecosystems takes up a significant fraction (~30%, or 3 PgC year⁻¹) of carbon released to the atmosphere from fossil fuel and deforestation (LeQuere et al. 2018, Schimel et al. 2015) and creates the land residual sink with a destiny dependent on future climate conditions and human activities (Ciais et al. 2013, Bonan 2008). Almost all of this sink is in forests, covering about 3.8 billion ha (FAO 2015) of the land surface (~30%) and storing large reservoirs of carbon, approximately double the amount in the atmosphere (Canadell & Raupach 2008, Sabine et al. 2004). Together, the carbon stored and sequestered in these ecosystems are major contributors to mitigating climate change and the economic benefits of emission Reductions from Deforestation and Degradation (REDD) (IPCC 2007, Gibbs et al. 2014). There are, however, large uncertainties surrounding the magnitude of the carbon stored in forests, particularly at landscape scales (1–100 ha) where mitigation benefits and ecosystem services are evaluated (Gibbs et al. 2007). A recent attempt to

put together the information from different types of measurements on a global scale captures the overall distribution of forest Above Ground Biomass (AGB) and carbon stored in global ecosystems (Fig. 5.1).

The structure of forests (i.e., the three-dimensional arrangement of individual trees) is a direct indicator of how much carbon is stored in the ecosystem. Carbon stored in an ecosystem has a profound effect on how the ecosystem functions (i.e., how it cycles

carbon, water, and nutrients). Additionally, there is an increased need to understand local to global storage and dynamics of carbon in ecosystems, as carbon storage is a prerequisite to understanding the coupling of the biosphere to other components of Earth systems. For example, the amount of carbon in a system determines how much is eventually emitted to the atmosphere (as CO₂, CO, and CH₄ through burning and decay) when ecosystems are disturbed due to

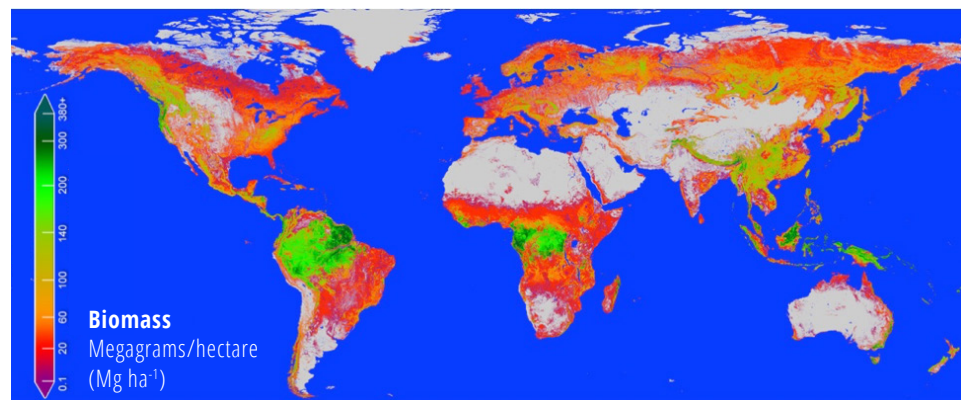


Figure 5.1 Distribution of forest AGB density in global ecosystems showing the high biomass in tropical rainforest regions and relatively lower biomass in extratropics extending to temperate and boreal regions with vast areas of forest cover. Map is produced at 1-km spatial resolution using a combination of ground, lidar, and radar measurements by Saatchi's team at the Jet Propulsion Laboratory, California Institute of Technology.

deforestation and degradation or from climate-driven stress and fire. The amount of carbon stored in the system can be estimated from AGB, which is estimated from measurements of structure (e.g., the size and density of trees) and the mass of trees. As such, AGB is considered a crucial variable for a range of applications, including forest fire assessment, management of the timber industry, monitoring land-use change, and other ecosystem services such as biodiversity and production of food and fiber, as well as greenhouse gas accounting.

Although many of these applications may be accounted for by using operational satellite observations of forest cover change, the understanding of changes in terrestrial AGB remains rudimentary (Saatchi et al. 2011). For example, it is known that changes in land use, largely from tropical deforestation and fire, are estimated to have reduced biomass globally, while the global carbon balance suggests that terrestrial carbon storage has increased; albeit the exact magnitude, location, and causes of this residual terrestrial sink are still not well quantified (Schimel et al. 2015a, Sellers et al. 2018). There is strong evidence that the residual sinks are spread in different forest ecosystems with locations that may change due to climate change and anomalies. Yet the magnitude and fate of these terrestrial sinks are crucial to future climate projections, and any uncertainties in the spatial locations or the temporal behavior of them directly influences the current status of global carbon cycle and climate (Houghton et al. 2018, Schimel et al. 2015a).

5.1.2 GROUND INVENTORY OF FOREST BIOMASS

Knowledge of the distribution and amount of AGB is based almost entirely on ground inventory measurements over an extremely small (and possibly biased) set of samples, with many regions left unmeasured (Fig. 5.2). Conventional forest inventory data known as the National Forest Inventory (NFI) are based on systematic sampling of forests and are mainly designed for monodominant, evenly aged forests in managed temperate and boreal regions. Although the basic statistical techniques can be used for tropical forests, there are differences in terms of

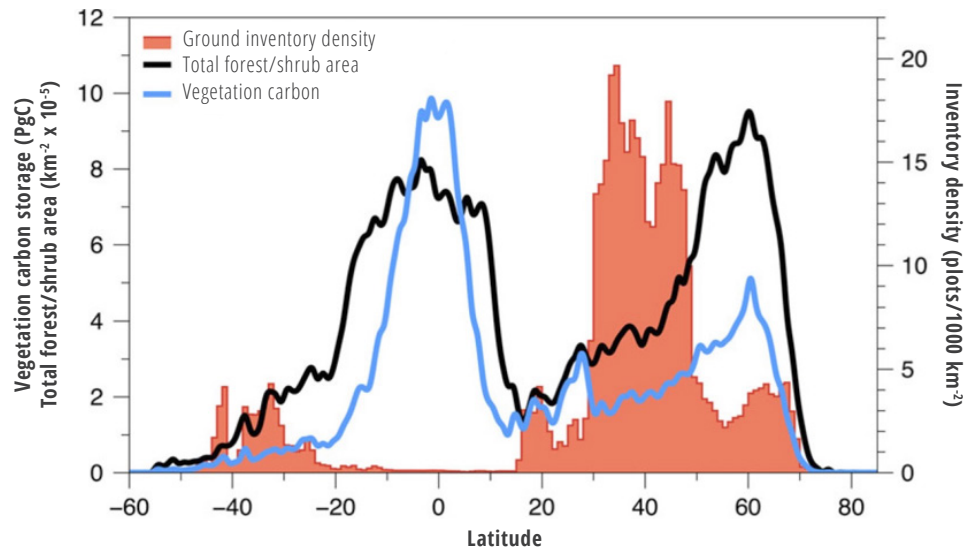


Figure 5.2 The distribution of woody (forest and shrubland) area and biomass derived from a variety of sources from field and remote sensing data. The red histogram shows forest inventory plot density in 1,000 km² grid cells (Schimel et al. 2015b), suggesting an uneven distribution of inventory plots in the Northern Hemisphere and a lack of data in tropical regions.

plot size, number of plots, and plot locations that have not been worked out for tropical forests.

- Conventional NFI can provide accurate estimates of forest carbon density at the national and potentially subnational levels depending on the density of the plots. However, they cannot provide spatial maps unless combined with remote sensing data.
- In tropical and unmanaged forests, implementation of NFI is extremely difficult, because of limited access to the site and the cost of establishing and monitoring plots over time. Using the protocols of the U.S. or northern Scandinavian NFI to the tropics requires a large number of plots.
- Conventional NFI data include 5–10 years of repeated measurements, and the timing of the measurements is not coordinated among the countries, making it difficult to conduct a global assessment for any period. For Greenhouse Gas (GHG) emissions, the use of a national inventory along with remote sensing estimation of forest cover change can provide national-level emissions estimates, but those estimates may involve uncertainty due to the lack of forest estimates in areas where deforestation occurs.

At large scales, robust AGB estimates are acquired

from ground-based forest censuses that are based on labor-intensive fieldwork (plot inventories) conducted by trained operators. As such, these plot inventories cannot be repeated frequently or at a low cost everywhere. Thus, plot inventories are limited to managed forests in a number of developed countries in the Northern Hemisphere where systematic sampling of forest inventories are performed on a regular basis (5- to 10-year cycles). Information on most carbon-rich global forests is missing, particularly in developing and tropical countries, even though this is where most living biomass is located (63% of carbon in intact tropical forests versus 15% in boreal forests and 13% in temperate forests, according to a recent and comprehensive estimate (FAO 2015)). Furthermore, land-use activities, along with increasing disturbances from climate and human stresses, are rapidly changing plot inventory requirements to include more frequent observations of forest ecosystems.

5.1.3 REMOTE SENSING OF FOREST BIOMASS

There is a strong synergism between ground and remote sensing measurements for quantifying AGB (Fig. 5.3). Ground data (generally consisting of all tree diameters above a threshold, a sampling of tree heights, and species identification that permits

inference of wood densities) are more comprehensive locally than remote sensing data that generally measure aggregate canopy height (in the case of lidar sensors) or some indicators of forest height and volume (in the case of radar sensors). In contrast, airborne or satellite remote sensing-based data are far more extensive, with millions of measurements over regional or continental scales compared to plots and providing a more spatially comprehensive measure of forest biomass variations. However, both ground inventory and remote sensing observations focus on measuring some physical properties (e.g., height or diameter, volume, etc.) that are not forest biomass (Clark & Kellner 2012). Both efforts rely on statistical techniques to estimate biomass, using single-tree allometry in the case of field plots and plot-aggregate allometry in the case of satellite data. Furthermore, both approaches are subject to several measurement and algorithmic errors.

A variety of remote sensing sensors provide measurements of biophysical and structural characteristics of forests based on the interaction of light or microwave energy with forest canopy and woody components. These sensors are typically categorized into passive sensors, such as spectrometers or radiometers that measure reflected or emitted radiation from the Earth's surfaces, and active sensors, which internally generate and emit energy and then measure different attributes of the returned energy bouncing back from the surface. Passive remote sensors measure different ranges of wavelengths of reflected solar radiation (optical and microwave), providing two-dimensional information that can be indirectly linked to biophysical properties of vegetation (Rosette et al. 2012, Shugart et al. 2010). Examples of passive systems include Landsat (measuring the visible spectrum), QuickBird (visible to near-infrared), AVIRIS, and MODIS, with the latter two measuring from visible to infrared (Hyde et al. 2006). On the other hand, active sensors are designed to work at limited wavelengths, such as lidar in visible or near-infrared wavelengths (Drake et al. 2002) or radar in microwave long wavelengths (Shugart et al. 2010). For more details on remote sensing techniques for forestry applications, see Zhang & Ni-meister (2013), Wulder & Franklin (2012), Zolkos

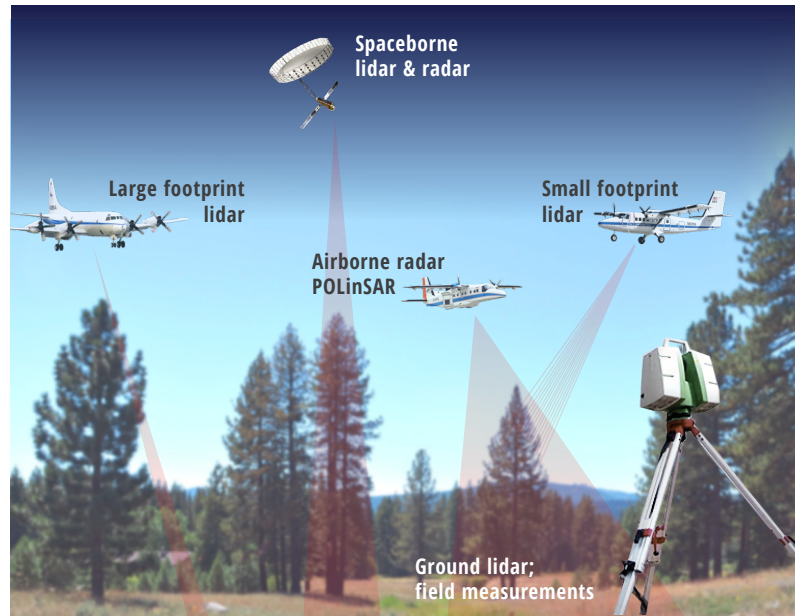


Figure 5.3
Ground and remote sensing measurement techniques to quantify forest structure and AGB.

et al. (2013), Saatchi et al. (2011b), and LeToan et al. (2011). Here, for the sake of brevity, the remote sensing techniques for forest structure and biomass are divided into two categories:

- (1) The first category refers to remote sensing observations that provide the most direct measurements of forest structure, such as canopy height from lidar sensors on either airborne or spaceborne platforms. Lidar sensor measurements must be treated similarly to ground measurements such as tree height measurements using a laser ranger or clinometers in the field. In both cases, the measurements are relatively direct. Height is measured from laser altimetry from air or space, and from distance and angle measurements in the ground. There is strong evidence that tree height can be measured as accurately if not better than ground measurements using small-footprint (<1 m) lidar systems (Asner et al. 2010). Here, the measurement errors can be treated the same as measurement errors in the field (Dubayah et al. 2000, Lefsky et al. 2002, Lefsky 2010).
- (2) The second category refers to active remote sensing observations that provide indirect measurements of forest structure, such as active radar sensors for forest volume or biomass and height. In this case, radar backscatter

measurements provide strong sensitivity to forest structure and biomass. This sensitivity may be asymptotically reduced when biomass increases to a range of more than 100 to 150 Mg/ha at L-band wavelengths (~25 cm) (Saatchi et al. 2011b, Mitchard et al. 2011, Mermoz et al. 2015), and more than 200 to 300 Mg/ha at P-band wavelengths (~70) (Saatchi et al. 2011b, LeToan et al. 2011, Sandberg et al. 2011). By adding interferometric radar techniques as in PolInSAR and TomoSAR measurements, the sensitivity of radar sensors may increase over the entire biomass range in tropical forests (Hajnsek et al. 2009, Minh et al. 2015, Neumann et al. 2012). The high-resolution, two-dimensional radar measurements (backscatter power) have provided separation of tropical forest biomass based on their canopy gaps, structure, and spatial heterogeneity (Hoekman et al. 2000), and have been used as an important deforestation and degradation monitoring tool.

Lidar and radar remote sensing techniques are currently recognized as the best approaches for quantifying and monitoring forest AGB changes globally. Therefore, numerous space agencies are attempting to improve the presence of these techniques for spaceborne observation of forest bio-

LIDAR AND RADAR FOREST MEASUREMENTS

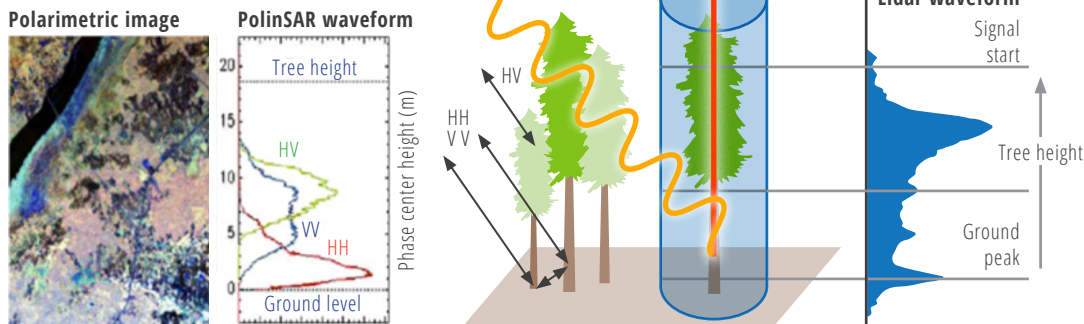


Figure 5.4 Lidar and radar forest inventory from air or space platforms capturing vertical and horizontal structure of forest ecosystems.

mass, with NASA and the European Space Agency (ESA) having already approved plans to develop and launch lidar and radar sensors in the near future (Fig. 5.4).

NASA's GEDI (launch 2018) and NISAR (launch 2021) missions, and ESA's Biomass (launch 2022), share similar objectives for developing regional or global estimates of forest structure and AGB. These missions will address one of NASA's key strategic goals for understanding changes in the Earth's climate by focusing on the most uncertain component of the global carbon cycle related to terrestrial carbon sources and sinks. All missions providing active remote sensing measurements of forest structure must be converted to AGB using algorithmic models and validated by ground-estimated AGB distributed globally in different forest types. These missions have significant overlaps in terms of science objectives and products, but each focuses on different observations, employs different algorithms, and retrieves different AGB ranges at different spatial and temporal scales. The success of these missions strongly depends on how their science products can advance scientific and societal benefits.

Biomass observations at P-band will be particularly useful for high biomass density forests in tropical regions where there is a large uncertainty in quantifying forest biomass due to the lack of national inventory data and low efficacy of existing radar and optical remote sensing techniques. ESA's Biomass mission's unique contribution to the global carbon cycle is to provide annual carbon stocks and changes

for old growth, secondary, and degraded tropical forests. It is expected that the Biomass mission's measurement sensitivity will allow for the estimation of high-biomass forests (>100 Mg/ha). However, for areas of low biomass density (<100 Mg/ha), NASA's NISAR mission at L-band frequency will perform better in terms of accuracy and spatial resolution (<100 m). GEDI lidar sampling measurements of forest height will be acquired approximately 12 to 18 months prior to Biomass and NISAR data acquisitions, allowing GEDI-derived forest structure to integrate with Biomass and NISAR algorithms for improving the radar estimations of forest structure and biomass.

5.2 Forest Biomass – Ground Inventory

In this section, forest inventory is discussed as the most reliable approach for quantifying AGB at the local scale, as well as using airborne small-footprint lidar measurements as the state-of-the-art remote sensing technique for most accurately estimating AGB at landscape scales. Currently, both techniques are used extensively in quantifying forest carbon stocks at the local, regional, and national scales and are considered the most reliable for integrating with radar observations to estimate AGB. Particularly, airborne lidar data will allow upscaling inventory measurements from small plots to a scale that can be useful in calibrating radar measurements and developing radar-based models and algorithms for AGB. This section will also be considered as the first step

toward understanding how AGB is quantified and to what extent knowledge gained from ground and lidar AGB estimates could improve the radar techniques for AGB estimation. This section provides general information about ground and lidar quantification of AGB and also provides an example discussed during the SAR tutorial for demonstration.

5.2.1. FOREST INVENTORY SAMPLING

Forest inventory measurements include both the direct measurement of biomass of individual trees from destructive harvesting, or indirect estimation through measurements of tree size and inference using allometric relationships (Gibbs et al. 2007, Brown 1997, Chave et al. 2005, Keller et al. 2001). However, before an allometric equation can be used, ground-based forest inventory data must be collected using standard techniques at local, regional, or national scales. Systematic or random sampling designs (either of the entire forest area or stratified segments) are two broad techniques used to collect data that allow mean biomass to be estimated with low uncertainty.

Stratification of sampling with broad forest types can greatly increase the efficiency of surveys by ensuring that major variations are captured. These approaches are well established within the forestry community in most developed countries and can be readily adopted in tropical regions if access, cost, and institutional infrastructure issues are resolved. However, despite the availability of numerous methodologies for quantifying forest biomass in tropical regions

from ground sampling, there are still fundamental problems associated with sampling, measurement, and allometric uncertainty that must be addressed by the research community (Chave et al. 2014, Saatchi et al. 2015, Ngomanda et al. 2014, Lima et al. 2012, Chen et al. 2015, Katerrings et al. 2001).

5.2.1.1 Statistical Sampling

The conventional methodology for estimating the forest AGB in any location relies on statistical sampling approaches and is recommended by various protocols and guidelines for GHG inventory in forestlands (IPCC Chapter 4 2006). These sampling techniques have been used in most NFI systems in developed countries and include systematic random sampling approaches, as in examples of U.S. forest inventory data (Fig. 2.1) (Heath et al. 2011), Swedish NFI (Reese et al. 2003), Finland NFI (Tomppo et al. 2011), Canada NFI (Stinson et al. 2011), and China NFI (Zeng et al. 2015). A concise summary of the sampling designs in European countries can be found in the literature (Tomppo et al. 2011, Lawrence et al. 2010). Most of these countries use either detached field sample plots or clusters of plots, and there are variations in sampling density and the associated uncertainty. The forest area represented by one plot varies from 50 ha in the Walloon region in Belgium to about 2,500 ha in the U.S. and 267,700 ha in Canada. There is also quite a high level of diversity in estimation methods and the use of tree allometry based on the measurements. The reports in Tomppo et al. (2010) present more detailed descriptions of these countries' inventory methods and changes in the designs (Zeng et al. 2015).

An approach similar to the NFI systems for boreal and temperate forests can be applied to tropical countries with the additional consideration of diversity of species, structure, and requirements for precision of estimates. The sample size and the shape and the configuration of the samples will be an important element in creating a probabilistic sampling design at the national or regional scale. Large plots and a higher number of samples provide more precise AGB estimates at the national or subnational scales. However, other factors such as the degree of difficulty in establishing large plots in complex terrains, costs,

and the time associated with field surveys significantly contribute to the choice of sampling size and configurations (McRoberts et al. 2013).

5.2.1.2 Inventory Measurements and Biomass Allometry

Inventory has a long history from tree-based size and density measurements for harvesting and timber extractions. In general, trees are constrained in their geometry and display striking regularities in their structures. These regularities allow tree diameter measurements to be transformed into other variables of interest. There are two prevalent explanations for these regularities: One involves the mechanical strength required to support standing wood structures, and the other involves the constraints of transporting water up through a tall structure composed of hollow tubes. Trees essentially respond to both of these constraints by developing a complex but regular architecture that can be characterized in either case by the use of statistically calibrated equations known as "allometric equations." Also, tree diameter can be related to other attributes such as total tree mass, the area of a tree's foliage, etc., by allometric equations (West & Brown 2005, Chave et al. 2005).

Most trees do not grow symmetrically over their lifespans. Small trees have a disproportionately larger amount of leaves and less woody tissue than large trees (Hallé & Oldemann 1975, Hallé et al. 1978). Structural models based on tree size and mechanical strength were derived for engineering problems for constructing ships where diameter, height, and type of wood were used to calculate the mass. In forestry, similar type measurements have been used to quantify the size of trees and the density of the wood for logging and commercial use of wood. An allometric relationship can be found between tree height and sapwood area that scales isometrically, on average, with the tree trunk cross section. This relationship varies as a consequence of morphological and ecophysiological species-specific responses to different habitats and hydraulic constraints. However, it will ultimately converge on an approximately two-thirds scaling rule as the size of the tree increases (McMahon 1973).



Figure 5.5 Trees with complex structure associated with tree buttress. Photo by Sassan Saatchi, Costa Rica, 2007.

The allometric models are developed for each forest type and are based on empirical relationships between mass and tree diameter and height. However, these empirical relationships are difficult to obtain logistically, particularly for remote locations and tropical forests. Most calibrations are sparse with respect to data on larger diameter trees. Since the equations are fitted to the data using a log-transformed model, the errors associated with the larger diameter trees are very large (Chave et al. 2005, Chambers et al. 2001). In mature natural forests, a large percentage of the total mass is associated with the largest trees, so this is potentially a significant source of error and bias (Shugart et al. 2010).

5.2.2 PRACTICAL GUIDE FOR PLOT DESIGN AND SAMPLING

Several guidelines exist for designing plots for forest or general vegetation inventory and for structure and biomass characterization. It is recommended that interested readers consult with documents such as the [RAINFOR protocols](#) for plot design and measurements and [Winrock International](#). The documents can be downloaded from the following links:

- <http://www.rainfor.org/upload/ManualsEn->

[glish/RAINFOR_field_manual_version_June_2009_ENG.pdf](#)

- https://www.winrock.org/wp-content/uploads/2016/03/Winrock_Terrestrial_Carbon_Field_SOP_Manual_2012_Version.pdf

The following guidelines are designed to help in establishing plots for remote sensing, specially SAR biomass estimation applications:

(1) Location. Select the general area of the plot locations for the study area. Depending on the remote sensing applications, the general location may be selected from an area with the following criteria:

- Reasonably homogenous soil parent material and soil type
- Adequate access
- Reasonably sloped or flat terrain to avoid complex plot establishment and difficult of relating it to radar or lidar data
- Sufficient long-term security from human disturbance
- Sufficient long-term institutional support in case of permanent and monitoring plots
- Avoid areas that have not had frequent disturbance, particularly if the plots are used for developing models for remote sensing mapping, or calibration and validation of remote sensing products

(2) Sample design also depends on the application. For most inventory applications, the landscape is divided based on some stratification of vegetation type, soil, or topography; and the samples are designed to represent the structure of each strata. Within strata, plots should be randomly located, to avoid 'majestic forest' bias and provide statistically unbiased estimate of the structure and biomass for each strata. If maps are available, plot location should be randomly assigned prior to going to the field. If not, in the field, the position of the plot starting point can be randomized by locating it in a random direction at a random distance of the original location.

(3) Plot Size, Shape, and Orientation. Sample plots can be designed in a variety of size, shape, and orientations depending on some trade-off between accuracy, time, and cost of measurements. In addition, the vegetation type and the terrain

may also influence the choice of plot characteristics. Different requirements for plots were discussed and presented earlier. The guidelines here will cover the plot size and shape for both the ground-estimation of biomass and for remote sensing data analysis.

- Plots can be circles, squares, or rectangles. Experience has shown that small circular plots are more efficient because the actual boundary around the plot does not need not to be marked. But these plots are often used for national inventory and may not be used to represent remote sensing pixels. Circular plots are easy to establish when they are small. Large circular plots are difficult to establish on the ground because of uncertainty in delineating the boundary. Rectangular plots are also easy to establish and depending on the size of the rectangle and its orientation, the plot can be easily matched with pixels. If the rectangular plots are elongated in shape when laid out on the ground, they may significantly longer edges than circular plots that may introduce errors in number of trees.

- The choice of plot size also depends on the application or remote sensing data, the accuracy of biomass estimation, and the type of forests. For SAR studies, large plot size >0.25 ha or >1-ha depending on the SAR pixel size and speckle noise is recommended. It is possible to calculate the appropriate plot size specifically for each project; however, this adds an additional complication and an additional effort to the process. The size of trees and the diameter threshold of trees may also influence the plot size. It is possible to calculate the size of the plot based on precision and effort and the application. Prior to initiation of plot measurement, it is recommended that limited sampling take place to determine the size of the largest trees. In a land cover stratum with few trees greater than 50 cm dbh, the minimum stem diameter measured within the largest nest may need to be adapted. For non-forest, savanna, and woodland strata, nest plot sizes, and stem diameter sizes will

need to be delineated.

- There are also nested plots that may help to have large plots and a cost efficient approach in collecting tree measurements. Nested plots are composed of several plots (typically 2 to 4, depending upon forest structure) plots and each plot in the nest should be viewed as being a separate plot. According to Winrock guidelines, in ecosystems with low structural variation, such as single species, even-aged plantations, or in areas where trees do not exist, a single plot can be effectively used.
 - For orientation, N/S and E/W directions for the principal axes of the plot are the most convenient and also most compatible with the remote sensing pixel comparison. Note that when establishing plots using GPS, record the true or magnetic north to be able to accurately delineate the boundaries of the plot in the remote sensing imagery.
- (4) Topography may impact the plot size and orientation in the field. It is important to record the planar distance if used to set up the plot and the angle of the slope. These values will allow calculating the area of the plots established on sloped terrains.
- (5) Measurements in the plots also depends on the size of trees and the type of vegetation. However, in general the measurements should include:
- The size of trees (diameter, height, crown size, etc.), identification of tree species for quantifying their wood density or specific gravity from existing data or measurements of wood density (see for example measurement protocols by Jerome Chave: [http://www.rainfor.org/upload/ManualsEnglish/wood_density_english\[1\].pdf](http://www.rainfor.org/upload/ManualsEnglish/wood_density_english[1].pdf)).
 - Plot dimensions and location by using GPS units. Latitude/longitude, among other measurements for the plot geometry and location will be elevation, bearings of plot boundaries, and local landmarks to assist plot relocation. It is recommended that GPS measurements include several plots along different axis of the plots (e.g., GPS for every 20 m within the plot for a 1-ha plot (100 m x 100 m) to increase the accuracy of plot location, size, and orientation.

5.3 Forest Biomass – Lidar Remote Sensing Inventory

AIRBORNE LIDAR CANOPY HEIGHT MODEL

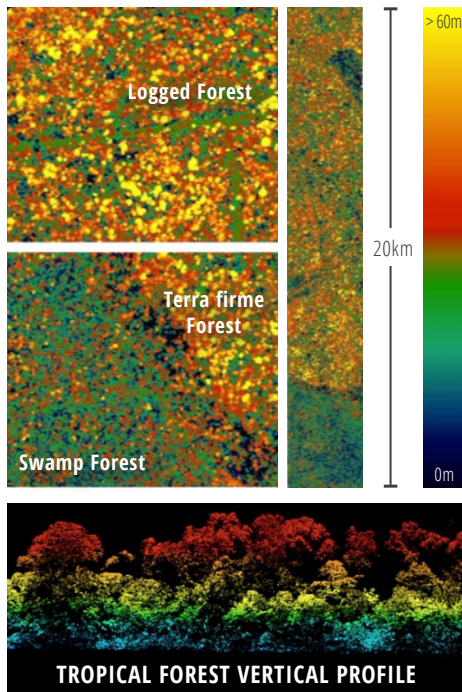


Figure 5.6 Example of forest canopy height measured by airborne lidar over old growth, degraded, and swamp forests of the Congo Basin in Democratic Republic of Congo (data from WWF/ UCLA Carbon Map and Model Project).

5.3.1 LIDAR FROM AIR AND SPACE

Airborne lidar measurements can be used for both mapping and sampling inventory of forest structure, as in most national inventory techniques (Figure 5.6). This is mainly due to the accuracy of high-resolution airborne lidar measurements for measuring tree height, vertical structure, and horizontal distribution of tree crowns and gaps (Ferraz et al. 2016). For airborne sensors, a significant area over the landscape (100–10,000 ha) can be readily mapped at about 1-m spatial resolution (Asner et al. 2010).

Capable of acquiring elevations with centimeter-level accuracy, small-footprint airborne lidar has had a revolutionary impact on 3D imaging of the Earth's surface and forest structure. More commonly, small-footprint airborne lidar sensors have been employed to detect vegetation and describe the canopy structure

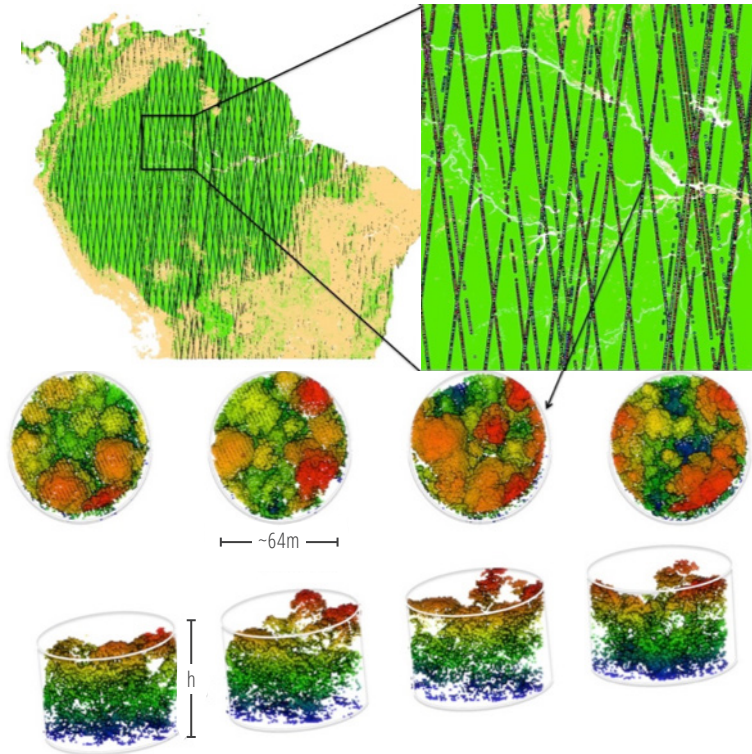


Figure 5.7 GLAS lidar measurements across tropical forests showing systematic sampling of forest vertical structure at large footprints suitable for estimating AGB for each sample location.

for applications such as habitat modeling, forest inventory, and biomass studies. Airborne small-footprint (<1 m) lidar measurements are mainly discrete-return or waveform sensors working in near-infrared (1,064 nm) wavelengths and flying at low altitudes, depending on the presence of cloud and lidar measurement requirements. Other new lidar technologies working in different optical wavelengths and photon counting capabilities are available for a combination of applications (Moussavi et al. 2014). Small-footprint lidar records multiple of points for each unit area (1 m²) with high precision of the altitude of each point within the canopy, allowing a detailed measurement of the forest vertical profile. The airborne sensors are widely available in tropical regions and can be used to acquire data over significant areas either for wall-to-wall coverage (Mascaro et al. 2011b, Meyer et al. 2013) or as inventory samples for regional and national carbon assessments (e.g., BioREDD in Colombia, the World Wildlife Fund (WWF) program in the Democratic Republic of the Congo (DRC), lidar inventory in Brazil, and the NASA Carbon Monitoring System (CMS) program

in Kalimantan). These airborne lidar inventory samples are all based on a Verified Carbon Standard (VCS) VT0005 methodology tool developed by Sassan Saatchi in Colombia and certified by Terra Global Capital (Tittmann & Saatchi 2015).

Existing spaceborne lidar technology works at only large-footprint (25- to 80-m radius) elliptical or circular plots over the landscapes along orbital tracks or sensor beams, providing a systematic sampling of forest structure (Lefsky 2010). In this case, the density of samples will increase as the satellite's orbit drifts along the Earth's surface. Large-footprint lidar measurements have the advantage of being treated as a plot including a large number of trees and being matched with ground measurements for relating the sensor forest height measurements to AGB.

Data acquired over global forests in 2003–2008 from the Geoscience Laser Altimeter System (GLAS) on board the Ice, Cloud, and land Elevation Satellite (ICESat) provided millions of footprints that can be treated as inventory samples (Fig. 5.7).

These footprints have an average size of approxi-

mately 0.25 ha (0.16–0.5 ha) spaced at about 172-m intervals along the orbits over the landscape (see Fig. 5.7). The GLAS lidar samples do not follow any *a priori* design, as they randomly capture different forest types and provide a reasonable set of data to be treated as forest inventory. A series of studies using GLAS data have successfully demonstrated GLAS data capabilities for estimating forest canopy heights (Lefsky et al. 2007, Rosette et al. 2008) and forest biomass (Lefsky et al. 2005, Nelson et al. 2009, Neigh et al. 2013). The studies consider the statistical nature of GLAS shots and the potential spatial correlations of samples for estimating regional mean and variance of forest structure or biomass (Neigh et al. 2013, Næsset et al. 2011, Saatchi et al. 2011a, Baccini et al. 2012).

5.3.2 LIDAR BIOMASS MODELS

Allometric models for converting lidar measurements of forest height or vertical structure into AGB have been developed for different forest types globally (Næsset et al. 2010, Nelson et al. 2010, Asner & Mascaro et al. 2014). These models are often in the form of power law and based on one or several lidar height metrics (Drake et al. 2002). The most common models use the mean top canopy height from small-footprint lidar or a height metric such as the height of the median energy (HOME) or percentile height from large-footprint lidar from air and spaceborne sensors (Asner & Mascaro 2014, Drake et al. 2002). Similar to ground estimation of AGB, the allometry models may vary from location to location, capturing differences in the tree growth and diameter height allometry of forests. Some examples of allometric model variations show significant variations in height to biomass models (Fig. 5.8). The use of multiple height metrics derived from the pseudo-waveforms from either small-footprint lidar or large-footprint lidar sensors can contribute to improving biomass estimation uncertainty over larger regions (Meyer et al. 2013, Saatchi et al. 2011, Neigh et al. 2013, Andersen et al. 2014). However, so far there is no universal model to convert the lidar height measurements into AGB on a continental scale, and by acquiring data in different forest types and calibrating the lidar data with ground forest inventory plots, new models are being developed.

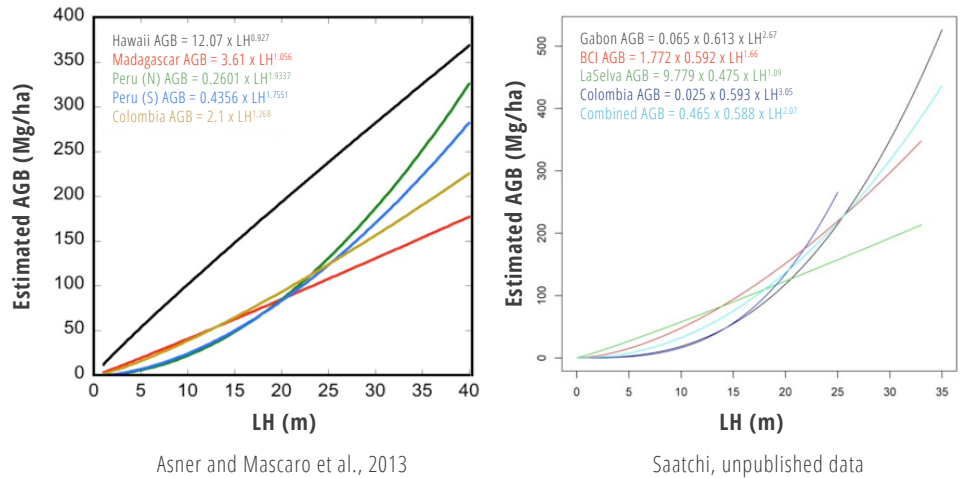


Figure 5.8 Examples of lidar biomass allometric models used in converting airborne lidar data to AGB. Variation across models suggests that the lidar models focused on one parameter only may vary significantly for different forest types, similar to ground allometric models

5.3.3 PRACTICAL GUIDE FOR PRODUCING LIDAR AGB MAPS

Lidar-biomass models are developed from ground plot level estimates of biomass and lidar height metrics. The following six steps must be considered in the model development:

- (1) Relation between ground estimation of biomass and lidar height metrics depends strongly on the plot size. For developing models, the plots sizes have to be large enough to include a large number of trees (50–100) such that the mean biomass density estimate of the plot from the allometric model has low uncertainty.
- (2) Depending on the forest types and size of trees, the plot size may vary. For boreal forests dominated by conifers, plots of >0.1 ha may contain enough trees and have accurate ground estimates of biomass. For tropical forests, plot sizes must be larger than 0.25 ha to guarantee the presence of enough trees for ground estimates of biomass with low uncertainty and lidar metrics that represent forest structure at a scale much larger than the crown of a large tree.
- (3) The shape of the plots may also influence the accuracy of the lidar-biomass models. Square plots are recommended as the best options for most forest types, because square plots

of any size are easy to establish and have smaller edge lengths compared to rectangular plots. Circular plots are difficult to establish unless they are small, particularly in tropical forests.

- (4) Models developed from small plots may introduce large bias in biomass estimation (see Fig. 5.9) due to edge effects and large variations of biomass at small scales that cannot be explained by forest height only. This is particularly the case in unmanaged forests in temperate and tropical regions (Chave et al. 2004, Meyer et al. 2013).
- (5) The height metrics used in developing a lidar-biomass model are important in large-scale applicability of the model. It is recommended that models are developed with height metrics that remain strongly related to AGB across the landscape when the forest structure varies due to variations of soil type and moisture, topography, and various levels of successional stages. For example, the mean top canopy height (MCH) is shown to be a robust metric for capturing the biomass variations across the landscape (Asner & Mascaro 2014, Meyer et al. 2013, Lefsky 2010). MCH from small-footprint lidar has not only information about the height of trees within the plot but also carries infor-

mation about gaps and spatial extent of tree cover. Theoretically, MCH includes the average of tree heights or crown areas within an area and therefore shows strong correlation to basal area, and hence AGB. The equivalent of MCH in ground measurements is not the mean height of trees but the basal area weighted height of the trees within the plot, the so-called “Lore’s Height of forest plot” (Lefsky 2010, Saatchi et al. 2011a).

(6) The form of the model may also become important in biomass estimation and error assessment. In most applications, the use of a power-law between the AGB and the height metrics provides the most reliable model for converting forest structure to biomass. A power-law or model also appears to be used extensively in allometric models developed from tree harvesting (Chave et al. 2005,

Brown et al. 2001). The use of a power law or logarithmic model between AGB and forest height metrics derived from airborne lidar data is recommended.

5.4 SAR Remote Sensing of Forest Biomass

SAR backscatter measurements are sensitive to vegetation AGB. Observations from a spaceborne SAR can thus be used for mapping AGB globally. However, radar sensitivity to AGB values changes depending on the wavelength and geometry of the radar measurements and is influenced by surface topography, structure of vegetation, and environmental conditions such as soil moisture and vegetation phenology or moisture. All algorithms or models used to estimate AGB from SAR measurements must account for all variables that impact SAR measurements. This

section provides a discussion of the overall sensitivity of radar backscatter to AGB to assist users in choosing the best combination of frequency, polarization, and incidence angles to develop AGB estimation models or algorithms. The impacts of forest structure spatial variation and errors associated with the geolocation of the plots used to relate the backscatter to biomass, the radar measurement geometry, and speckle noise all are important factors that influence radar sensitivity to forest structure and AGB.

5.4.1 RADAR SENSITIVITY TO FOREST STRUCTURE AND BIOMASS

Radar observations of vegetation have been studied for more than four decades, both theoretically and experimentally (Ulaby et al. 1982, Tsang et al. 1985, Ulaby & Dobson 1989, Cloude 2014). These studies have shown that the radar measurements depend strongly on the structure, dielectric proper-

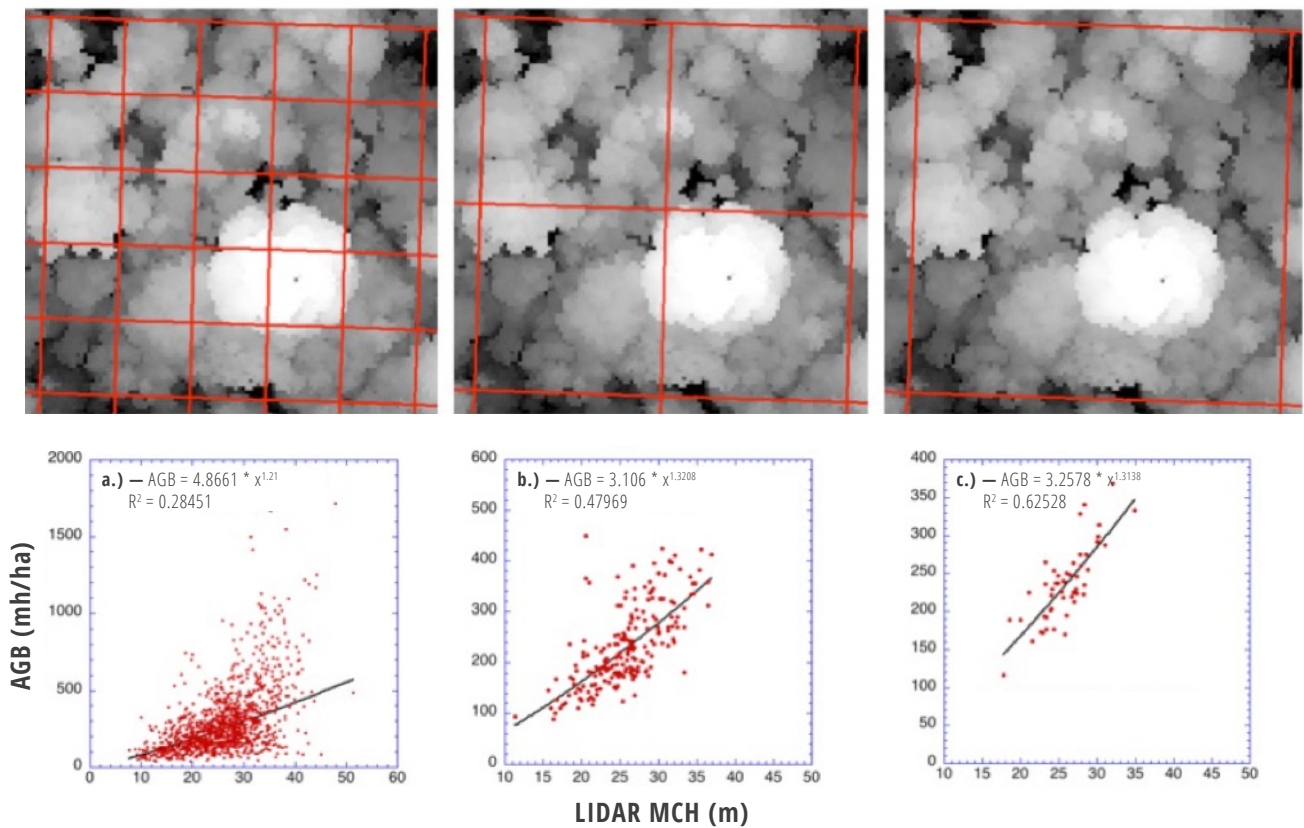


Figure 5.9 Ground plots of different size and lidar-derived models with MCH in tropical forests of Barro Colorado Island in Panama. The plots under the 1-m resolution lidar data suggest that at scale of 20 m x 20 m, (a) there is large bias in the model but gradually at areas of 50 m x 50 m, (b) 100 m x 100 m, and (c) the model improves, and the estimate of biomass can be done without significant bias.

ties of vegetation components, and underlying soil surface depending on the frequency of the operation (Saatchi et al. 1994, Saatchi & McDonald 1997, Ulaby et al. 1990). The soil is most commonly described as a homogeneous medium having a complex dielectric constant that is a function of the volumetric soil moisture, as well as the soil texture, temperature, and bulk density; several empirical models exist for this relationship (Dobson & Ulaby 1986, Hallikainen et al. 1985, Mironov et al. 2004, Peplinski et al. 1995). Studies of soil surface scattering and soil moisture remote sensing at L-band have shown that surface scattering can be expressed in terms of soil dielectric constant at the top 5 cm and the surface roughness characteristics in terms of Root Mean Square (RMS) roughness height and spatial correlation length (Fung et al. 1992). In most SAR-related models for the remote sensing of soil surfaces, it is assumed that the effect of the spatial correlation is reduced significantly during the SAR azimuthal processing and multi-looking, and that the radar signature sensitivity to soil surface RMS height variation remains as the dominant surface structure influencing the surface scattering (Oh et al. 1992, Shi et al. 1997, Dubois et al. 1995, Baghdadi et al. 2002, Bryant et al. 2007). Other landscape features such as directional row or tillage may impact radar cross sections at 100-m spatial resolution but are assumed irrelevant in natural vegetation such as forests and shrublands.

In general, the radar-transmitted energy, in the form of an electromagnetic pulse, penetrates into the forest canopy and reflects back from forest components such as leaves, branches, stems, and underlying soil. Knowing the magnitude of transmitted and received energy, a physical relationship based on electromagnetic theory has been developed to relate the ratio of these energies to properties of the forest. The radar measurements are performed in different frequencies or wavelengths, each providing a different penetration into the vegetation and soil and sensitivity to vegetation biomass.

The measurements are performed in a combination of transmit and receive polarizations (Horizontal (H) and Vertical (V)) at an off-nadir incidence angle and at a spatial resolution projected on the radar range direction. Therefore, radar backscatter sensi-

tivity to AGB at any frequency and polarization combination (e.g., HH, HV, VV) depends on two sets of parameters: (1) measurement geometry (such as incidence angle and location and size of the image pixels with respect to the size and the orientation of ground plots) and (2) forest structural parameters (such as the size (volume) and density of trees (number per resolution cell), orientation of forest components (leaves, branches, stems), underlying surface conditions (moisture, roughness, and slope)); and (3) the dielectric constant that in turn depends on the vegetation water content or specific gravity (i.e., the wood density) (Dobson et al. 1995, Saatchi & Moghaddam 2000). In the following subsections, the sensitivity of SAR measurements to these parameters are briefly examined, and examples and references for further reading are provided.

This section focuses on radar frequencies that are either operational or will be operational in future, and have strong sensitivity to vegetation AGB. Examples of SAR imagery are provided at C-band, L-band, and P-band frequencies. Among these frequencies, C-band (Sentinel, RadarSAT) and L-band (ALOS, PALSAR) are operational satellites and will be continued in the future for forest biomass monitoring in the L-band NISAR system (launch 2021). In 2022, ESA will launch a P-band SAR mission dedicated directly to monitoring forest structure and biomass globally.

5.4.2 RADAR WAVELENGTHS AND FOREST STRUCTURE

Usually SAR data are acquired at X-, C-, and L-band frequencies for remote sensing of the environment from airborne and spaceborne platforms. Other frequencies such as P-band and S-band have also been used for remote sensing applications but only on airborne platforms, with plans to be implemented for space observations in near future. A P-band sensor has been designed for ESA's future Earth Explorer Biomass mission, and an S-band sensor is ISRO's contribution to the NISAR mission. A summary for typical radar frequencies and wavelengths is shown in [Chapter 2, Table 2.3](#).

Excellent studies have been previously conducted on examining radar backscatter properties from forest areas (e.g., Freeman & Durden 1998, Dobson

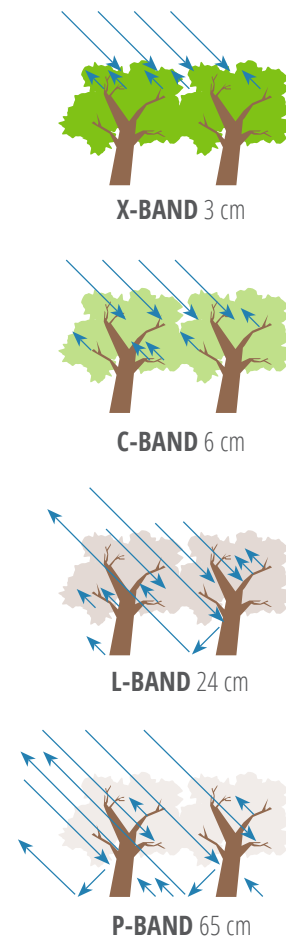


Figure 5.10 Sensitivity of SAR measurements to forest structure and penetration into the canopy at different wavelengths used for airborne or spaceborne remote sensing observations of the land surface.

et al. 1992, Ranson et al. 1997). Most scattering occurs when the particles are on the scale of the radar wavelength. Thus, in the case of forests, L-band backscatter arises more from the trunk and the branches of trees, whereas X-band backscatter arises more from their leaves and needles. Also, microwave penetration depth in forests varies depending on the frequency. While L- and P-band can penetrate deep into forests, X-band can get reflection from the canopy level. The backscatter sensitivity to forest components as seen by SAR systems operating at different frequencies is shown in [Figure 5.10](#). For biomass estimation, L-band and P-band sensors are therefore preferred over higher frequencies and smaller wavelengths for two reasons: (1) at these bands, the radar

waves or energy can penetrate the tree canopy and scatter from larger woody components of the forest, and (2) the scattering from larger tree components, unlike leaves, are more stable temporally and remain highly coherent over the acquisition period in the case of repeated measurements for change detection or interferometric applications (Le Toan et al. 1992).

At higher X- and C-band frequencies, SAR penetration will be limited to the upper forest canopy dominated by leaves and smaller branches unless used in very sparse forest covers such as woodlands and savannas. High-frequency radar systems such as Sentinel and RadarSAT operating at C-band and Terra-X SAR operating at X-band provide measurements that are more sensitive to the biomass in low-density forests (e.g., sparse savannas), shrublands, grasslands, or agricultural crops (Wigneron et al. 1999, Saatchi et al. 1994).

Recent studies have focused on the relationship between AGB and radar typically use spaceborne SAR data from ALOS PALSAR (L-band, $\lambda = 23.62$ cm), and airborne SAR data from both P-band and L-band frequencies (LeToan et al. 2011, Saatchi et al. 2011b).

The radar scattering forest stem and large branches at low frequencies or large wavelengths is considered the main reason radar sensors are used for estimating forest volume and biomass. to trunk and crown biomass and moisture content [16,25]. Past studies have found that the radar backscatter increases with increasing forest AGB from low to medium levels of AGB, but gradually loses its sensitivity to higher AGB levels and asymptotes to a saturation level, resulting in a logarithmic or sigmoidal relationship between AGB and backscatter (Dobson et al. 1992, LeToan et al. 1992, Saatchi et al. 2011). The asymptotic or the saturation level varies based on the radar wavelength and forest type and structure. Results from the airborne AIRSAR (Fig. 5.11) and E-SAR data suggest that saturation may vary between 80 and 150 Mg·ha⁻¹ for L-band radar (15–30 cm wavelength) and 200–350 Mg·ha⁻¹ for P-bands, with a wavelength of ~70 cm (Saatchi et al. 2011, LeToan et al. 2011, Mitchard et al. 2009, Bouvet et al. 2018, Villard et al. 2015).

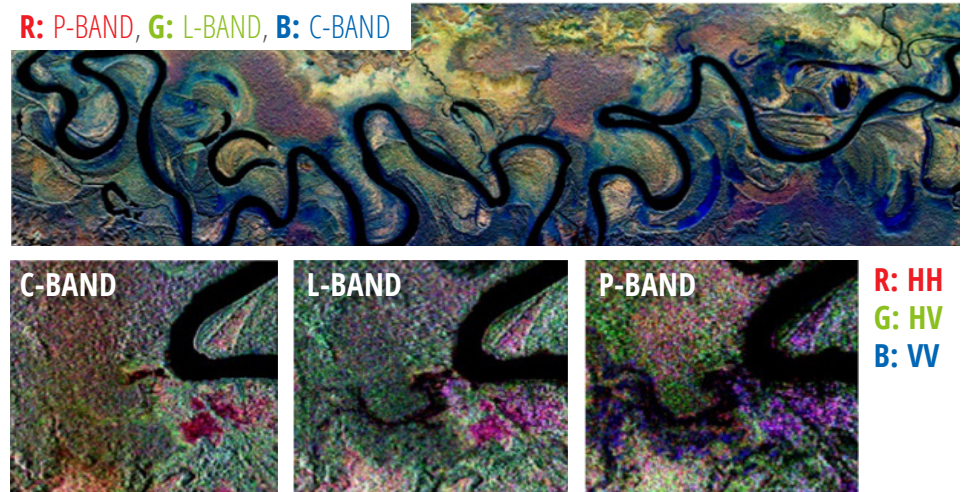


Figure 5.11 Examples of SAR imagery at C-, L-, and P-band frequencies from the AIRSAR system over tropical forests along the Ja River in Papua New Guinea showing differences of penetration and impacts of forest structure and underlying moisture on SAR false color composite (HH, HV, VV) imagery.

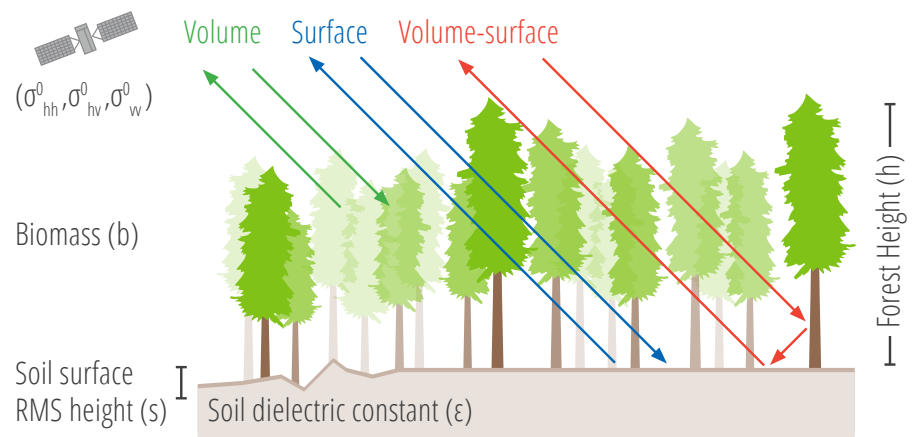


Figure 5.12 Dominant scattering mechanisms of L-band SAR measurements of forest ecosystems contributing to polarimetric backscatter observations.

5.4.3 RADAR SCATTERING AND FOREST STRUCTURE

The impact of vegetation structure and biomass on SAR data can be investigated by modeling the dominant scattering mechanisms controlling the SAR measurements. A variety of approaches exist for modeling vegetation media, including the characterization of forest vegetation structure, known as scatterers or scattering components such as stems, branches, and leaves in terms of canonical dielectric cylindrical or disk shapes with specified size and orientation distributions. The dielectric constants are assigned to each scattering component to reflect the live wood of trees and leaf material as well as their water content (Saatchi

et al. 1994, Saatchi & McDonald 1997, Saatchi & Moghaddam 2000, Yueh et al. 1992, Lang et al. 1983, Karam et al. 1992, Ulaby et al. 1990). The total SAR backscatter from vegetation arises from a combination of scattering and attenuation of individual scattering components that can be represented as a sparse scattering medium (Lang 1981, Saatchi et al. 1994, Chauhan et al. 1994). This approach requires knowledge of tree structure (size, orientation, and density; or equivalently species and biome), dielectric constant, and ground characteristics (RMS height, correlation length, and dielectric constant of soil surface). Figure 5.12 provides a general schematic of the three dominant SAR scattering mechanisms in the forest ecosystems.

The backscattering coefficient measurement by SAR systems can be expressed as the combination of three scattering components (Fig. 5.12): (1) volume (*vol*) scattering, (2) volume and surface interaction (*vol-surf*), and (3) surface scattering (*surf*):

$$\sigma_{pq}^0 = \sigma_{pq-vol}^0 + \sigma_{pq-vol-surf}^0 + \sigma_{pq-surf}^0 \quad (5.1)$$

where *p* and *q* denote polarization of transmitted and received radar signals, respectively, that can be assigned either vertical (V) or horizontal (H) for a linear polarization radar system. The three dominant scattering terms are derived from basic electromagnetic theory by solving Maxwell's equations in a discrete random media (Saatchi & Lang 1989, Lang 1981, Tsang & Kong 1988, Saatchi & McDonald 1997, Chauhan et al. 1991).

There are simpler approaches that only use the Vegetation Water Content (VWC) to provide analytical forms for attenuation and scattering effects. The most common model used in microwave frequencies is the Water Cloud Model, which includes two scattering components from vegetation volume and its underlying ground but ignores the volume-ground interaction (Attema & Ulaby 1978) that becomes dominant in forest ecosystems and for longer wavelength radar observations. Therefore, the Water Cloud Model is mainly applicable at shorter wavelengths (C-band and above) (Matzler 1994, Ulaby & El-rayes 1987) fails to represent the SAR vegetation interaction at longer wavelengths.

5.4.4 SAR POLARIZATIONS AND FOREST STRUCTURE

Transmitted and received radar signals propagate in a certain plane of polarization. Most radars are designed to transmit microwave radiation either horizontally polarized (H) or vertically polarized (V). Similarly, the radar antenna can receive either the horizontally or vertically polarized backscattered energy, and some radars can receive both. Different combination options for radar polarization (listed below) will provide different image characteristics:

- **Single-polarization**—the radar system

operates with the same polarization for transmitting and receiving the signal

- **Cross-polarization**—a different polarization is used to transmit and receive the signal
- **Dual-polarization**—the radar system operates with one polarization to transmit the signal and both polarizations simultaneously to receive the signal
- **Quad-polarization**—H and V polarizations are used for alternate pulses to transmit the signal and with both simultaneously to receive the signal (Fig. 5.13).

Among the quad-polarization configurations, there are also several variations as in the fully polarimetric measurements that include all components of amplitude and phase of the scattering matrix, and quasi-quad-polarization that includes only the amplitudes and not the phase due to switching the polarizations on different SAR transmit and receive pulses separating the HH/HV measurements from VV/VH (Raney 2007, Hensley et al. 2014).

Polarization is therefore the key characteristic of radar signals propagating into tree canopies or vegetation volume and scatter from individual vegetation components that collectively contribute to the backscatter energy measured by the radar receiver system. Polarization as the orientation of radar wave vectors (at H, V, or any other polarization) interact with vegetation components and backscatter according to the size and orientation of scatterers. For example, a standing live tree with near-vertical orientation depolarizes the incoming waves with different strengths than branches or leaves. Using radars that provide measurements in different polarizations allows separate vegetation with different structures to be reflected in the average size and orientation of different components. The best way to demonstrate this effect is by examining the radar imagery over agricultural landscapes with distinct crop types with uniform shapes and orientations (Fig. 5.14).

5.4.5. CONFOUNDING FACTORS IN RADAR SENSITIVITY TO BIOMASS

The confounding variables that impact SAR measurements and make interpreting those measure-

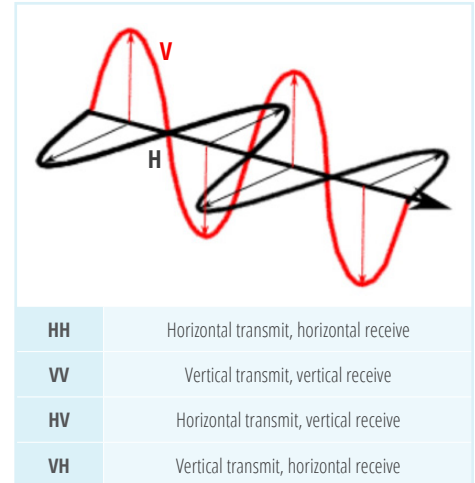


Figure 5.13 Electromagnetic waves radiated to the landscape in horizontal and vertical orientations providing different linearly polarized measurements.

ments ambiguous can be divided into two categories: (1) environmental and (2) geometrical.

5.4.5.1 Environmental Factors

- Two radar backscatter measurements of vegetated surfaces taken from the same instrument using exactly the same characteristics and observational geometry may be significantly different without any changes of the vegetation structure or biomass. The differences may be attributed to surface conditions or environmental changes (Fig. 5.15) between the two radar measurements and must be considered when analyzing the data (Table 5.1).

5.4.5.2 Geometrical Factors

Unlike optical passive and lidar sensors, SAR measurements are performed at an off-nadir look direction, and being an active sensor, both the geometry of the observations and the geometry of the targets (including both vegetated and non-vegetated surfaces) impact these measurements. The surface topography and the orientation of slopes and aspects of the observed surface are perhaps the most dominant effects on the radar measurements. However, other factors such as the orientation of trees, branches, leaves, and

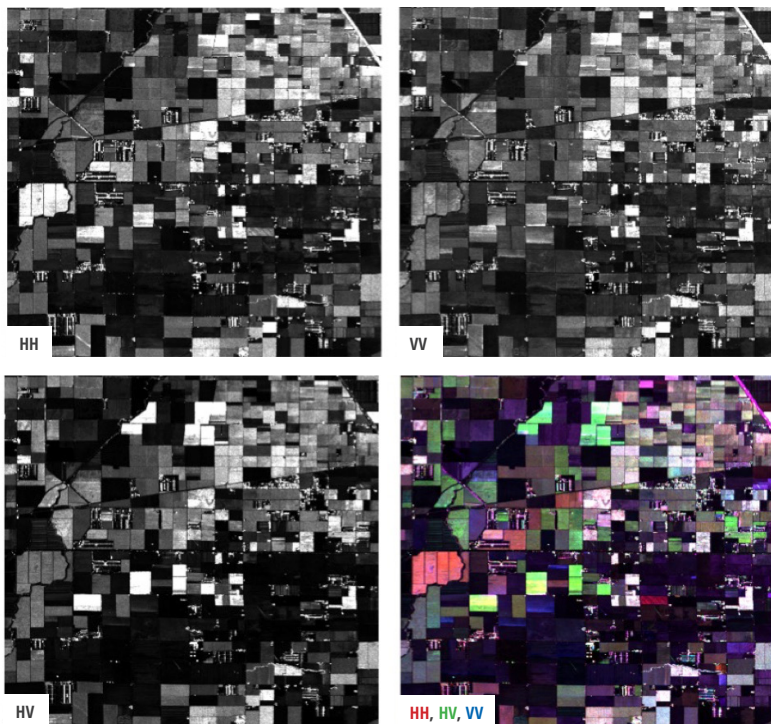


Figure 5.14 JPL UAVSAR image acquired by L-band radar showing three backscatter polarizations and the false-colored composites over an area in California's Central Valley covered by orchards and different crops. The strength of each polarized backscatter is shown, relatively suggesting how certain crops are relatively higher in one of the HH, HV, and VV polarizations.

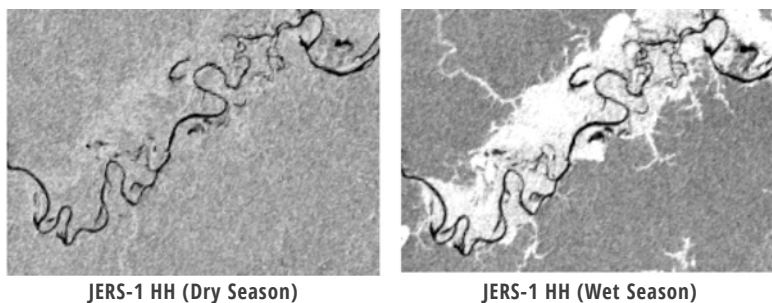


Figure 5.15 Changes of SAR backscatter in wetland forests acquired during the dry and wet seasons showing large backscatter difference due to inundation and an increase in the surface-volume scattering interaction in HH polarization.

VARIABLE	IMPACTS	BACKSCATTER CHANGES
Soil Moisture	SAR backscattered measurement of forests is sensitive to underlying moisture condition and any changes of soil moisture due to precipitation events or irrigation can influence backscatter values.	HH and VV backscatter, significantly and HV to a smaller degree, change with soil moisture depending on the density of vegetation cover. The volume-surface scattering mechanism and direct surface scattering are responsible for changes in backscatter. Similarly, SAR coherence between the data takes is impacted by changes of moisture.
Surface Inundation	Vegetated surfaces, particularly near rivers or in low elevation areas in wetlands, may be inundated seasonally or permanently due to the rise of the water level creating a smooth water body submerging the vegetation at different levels into the water.	Forest inundation increase the backscatter power by a large factor. The increase in power is significant in HH and VV due to volume-surface interactions. HV backscatter may also change due to inundation due to geometry and forest canopy density and the SAR wavelength.
Wind	Presence of wind may change the orientation of the leaves, twigs and small branches with respect to radar observational geometry.	The effects of wind often show up as random differences in the SAR backscatter between observations, introducing noise in backscatter, and reduction of coherence between two SAR observations.
Intercepted Water	After any rain events or early in the morning due to development of dews, there are water droplets on the leaves, causing both scattering and attenuation of the SAR signal.	Depending on the amount of intercepted water or the size of water droplets, and the wavelength, the radar backscatter may increase (at X-band and C-band) or reduce (at L-band and P-band) causing enhanced scattering or attenuation respectively.
Water Content	Changes of water content in trees and leaves from either stress, or diurnally and seasonally due to water loss and recharge of soil moisture impact radar backscatter.	Radar backscatter responds to dielectric constant of vegetation components and therefore the water content. Changes in water content can create significant changes (1-2 dB) in backscatter in all polarizations. Observations of the same time of the day and season can reduce this effect in SAR observations.

Table 5.1 Summary of environmental impacts on SAR measurements.

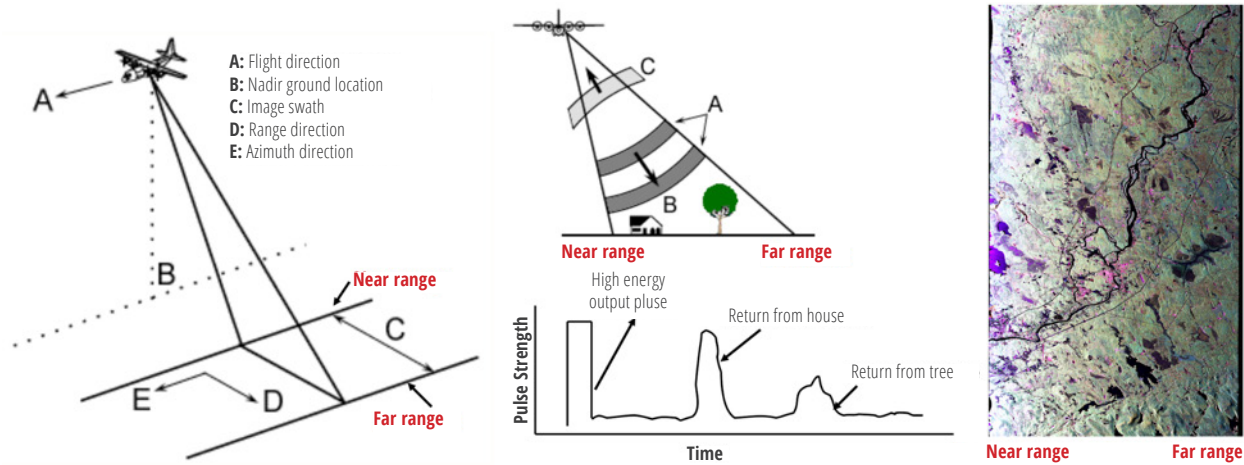


Figure 5.16 Fundamental arrangement and geometry of SAR measurements over the landscape showing (a) the radar look direction, imaging swath and near- and far-range locations, (b) radar pulses and returns across the slant range and the location of targets in the radar image, and (c) a UAVSAR image over mixed boreal forests of northern Maine at L-band polarizations showing the impact incidence angles on backscatter image.

other structures with the respect to the SAR observational geometry may also impact SAR measurements (Outlined in Fig. 5.16, Table 5.2).

5.5 SAR Processing Steps for Biomass Estimation

Before biomass estimation from SAR measurements, SAR data must be processed such that the pixel size and geometric attributes and environmental effects are all normalized and radiometrically calibrated. Although it may be possible to include all the SAR processing steps within the biomass estimation algorithm, preparing SAR imagery before algorithm implementation allows for separating the biomass estimation process from the data quality and calibration process.

5.5.1 SPECKLE AND IMAGE MULTI-LOOKING

One of the significant differences between active or coherent sensor imagery such as SAR (or laser) to passive sensors (such as that used in Landsat) is the effect of speckle in the spatial resolution of the sensor. Images obtained from coherent sensors are characterized by speckle. This is a spatially random, multiplicative noise due to coherent superposition of multiple backscatter sources within a SAR resolution element. In other words, speckle is a statistical fluctuation

VARIABLE	IMPACTS	BACKSCATTER CHANGES
Incidence angle	SAR measurements are acquired at off-nadir geometry. For each look direction, the radar beam scans the surface over a range of incidence angles. The range of incidence angles is larger for airborne systems (~ 20-70 degrees) but remains confined to only 6 to 10 degrees for spaceborne sensors.	The backscatter of vegetation surfaces vary by a factor of 2 or more from near range (e.g. 20 degrees) to far range (e.g. 70 degrees). If the terrain is topographically complex, the impacts of incidence angle variations will be larger. Often at near range angles the radar backscatter return is larger than at far range, due the larger path length of radar waves into the vegetation and stonger attenuation.
Surface Topography	SAR's side-looking geometry introduces displacements for tall objects and relief structures. The impacts of surface topography in radar imagery are of three kinds: shadows, foreshortening, and layover (Elachi et al. 1988). Radiometric Terrain Correction (RTC) techniques will help removing/reducing the effects of topography.	The changes of backscatter from surface topography can be significant depending on the slope and aspect of the surface and the incidence angle. Shadows appear dark in the image with very low backscatter. As the incidence angle of an image increases from near-range to far-range, shadowing becomes more prominent toward far-range. Foreshortening can cause compression of features in radar imagery. In the case of layover, the reflected signal from the upper portion of a surface feature is received before the return from the lower portion causing backscatter distortion.

Table 5.2 Summary of geometrical impacts on SAR measurements.

associated with the radar reflectivity (brightness) of each pixel in the image of a scene. The spatial resolution of a SAR sensor defines the minimum separation between measurements the sensor is able to discriminate and determines the amount of speckle introduced into the system. The higher the spatial resolution of the sensor, the more objects on the ground can be discriminated. The term "spatial resolution" is often confused with the pixel size, which is the spacing of the pixels in the azimuth and ground range direction after processing the data. A first step to reduce speckle—at the expense of spatial resolution—is usually performed during the multi-looking, where range

and/or azimuth resolution cells are averaged. The more looks used to process an image, the less speckle there is.

The SAR signal processor can use the full synthetic aperture and the complete signal data history in order to produce the highest possible resolution, albeit very speckled. The data often received from SAR data are in different formats: Single-Look Complex (SLC) or Multi-Look Complex (MLC). SLC image data are calibrated single-look complex files for each polarization (HH, HV, VH, and VV) that are often in floating point format, whereas MLC files are calibrated multi-looked cross products that may be in either amplitude or

power for each polarization and may be provided either as an integer (scaled amplitude) or floating point (backscatter power).

5.5.2 SAR PIXEL SIZE CHARACTERISTICS

For this application, the focus is on the multi-looked SAR imagery at pixel sizes that are square and can be readily projected on the ground using the local incidence angle. The user may improve the SAR image quality by further removing the speckle with spatial or temporal averaging at the expense of spatial and temporal resolution of the data. Speckle reduction is particularly important when using SAR data for estimating forest biomass or performing other operations such as classification and image segmentation.

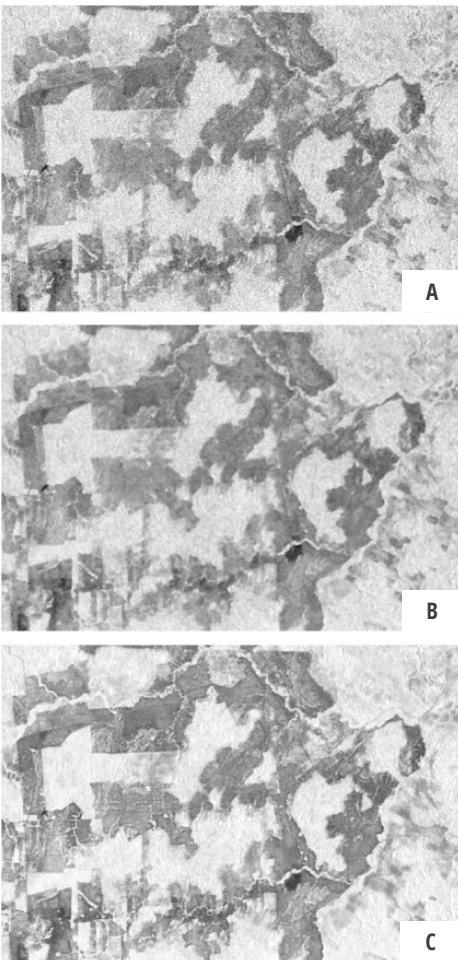


Figure 5.17 Speckle reduction of SAR imagery from (a) 25-m (5-look) resolution ALOS PALSAR image to (b) 45-look (effective 75-m) spatial filtering to (c) 25-look (5 ALOS images) temporal filtering.

When developing models with SAR backscatter and ground-estimated biomass from plots, the relation is significantly improved when speckle is reduced in SAR imagery. Examples of speckle reduction in imagery and SAR backscatter are shown in **Figure 5.17**.

The speckle reduction from spatial averaging impacts the radar backscatter measurements and improves the relationship between the SAR pixel and the ground or lidar measurements. The differences between side-looking SAR pixels and ground plot and lidar pixel are shown in **Figure 5.18**. SAR collects data along a slant range that samples only a slice of the forest medium under the pixel. For bare surfaces without a volume of vegetation, the projection of the pixel on the ground can readily relate the SAR measurements to the surface characteristics. However, in forest ecosystems, the sampling across the volumes always covers a sliced region into the canopy different from the footprint of lidar and the location of the ground plots.

5.5.3 SAR RADIOMETRIC CORRECTIONS

For a correct interpretation of backscatter signatures, correcting for the effects of local incidence angle due to topography and normalization for the true pixel area are necessary steps before biomass retrieval. Many studies have shown that uncompensated topographic effects induce a 2- to 7-dB dispersion of the L-band backscatter, which is about the same order of backscatter range used to distinguish forest and non-forest contrast in SAR imagery. The RTC, including the incidence angle normalization, will modify the backscatter values from σ^0 (sigma-nought) to γ^0 (gamma-nought). As the process of performing terrain correction is covered in other chapters, this section covers the basic information on how to convert σ^0 to γ^0 according to:

$$\gamma^0 = \sigma^0 \frac{A_{\text{flat}}}{A_{\text{slope}}} \left(\frac{\cos \theta_{\text{ref}}}{\cos \theta_{\text{loc}}} \right)^n, \quad (5.2)$$

where θ_{ref} and θ_{loc} respectively represent the reference angle for the normalization of the backscatter (e.g., the incidence angle at the mid swath of the SAR image) and local incidence angle derived from the geometry of radar with respect to the surface topog-

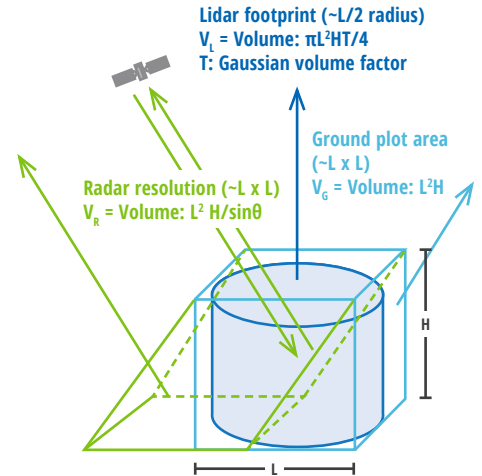


Figure 5.18 Schematic showing the SAR volume sampling of a forest ecosystem within a pixel in comparison with the ground plot and lidar samples. Differences between the volumes of each sensor are also shown. The difference in sampled area is much larger between SAR and ground or lidar when the pixel or plot size is small or over the topographically complex terrain due to edge effects and sampled areas. At larger pixels (~1 ha), the difference becomes small, and the relation between SAR measurements and ground- or lidar-estimated forest structure and biomass improves.

raphy (slope and aspect). A_{flat} and A_{slope} represent the local pixel area for a theoretically flat terrain and the true pixel area due to the sloped terrain, respectively. The power n represents the power of the fit of the angle correction due to radar backscatter variations across incidence angles. For a bare surface, the exponent is equal to 1, but for vegetated surfaces, it can be less than 1 due to variations in scattering mechanisms (volume over slope) originating from canopy gaps and different radar penetration into the canopy. The value of n may also vary with polarization. However, for simplicity, n may be considered to be 1 for all polarizations and for most practical cases.

All existing RTC algorithms are based on quantifying the local incidence angle and A_{slope} over terrain with significant topography. These approaches are based on estimating the local illuminated area A_{slope} through either (1) the estimation of the local incidence angle or the projection angle (Ulander 1996) or (2) the integration of the Digital Elevation Model (DEM) (Small 2011, Small et al. 1998). While methods based on

local incidence angle have the advantage of being simpler, methods that include DEM integration have been shown to be more accurate, particularly in steep terrain (e.g. [Fig. 5.19](#)). The DEM integration approach involves determining the number of DEM pixels belonging to each radar range and azimuth pixel through knowledge of the geocoding process. It is recommended that users of SAR imagery consult with existing tutorials on terrain correction available on [NASA](#) and [ESA](#) websites.

5.5.4 SAR Polarimetric Indices

The following section contains a brief discussion on how polarimetric signatures or indices can be used for monitoring forest cover or biomass in different landscapes. Use of signatures or indices are important because they are developed from a combination of radar measurements, which can improve the sensitivity for estimating or monitoring a surface characteristic and can reduce other impacts. For monitoring forest biomass, radar backscatter measurements can be impacted by variations in forest type and structural form (type and orientation), environmental conditions (e.g., moisture and phenology), or radar imaging geometry (e.g., incidence angle and topography). Choosing a combination of polarimetric or radar measurements that can reduce these effects and increase a radar image's sensitivity to forest cover or biomass can be regarded as a reliable monitoring index or parameter. Though there are more complex types that can be developed from either airborne polarimetric systems or from polarimetric interferometric measurements, two simple polarization indices—the Radar Vegetation Index (RVI) and the Radar Forest Degradation Index (RFDI)—are proposed below for monitoring forest types and which can be readily produced from existing satellite SAR systems:

$$RVI = \frac{8\gamma_{HV}^0}{\left(\gamma_{HH}^0 + \gamma_W^0 + 2\gamma_{HV}^0\right)}$$

where γ^0 represents the radiometrically and geometrically corrected SAR backscattering coefficient for each polarization combination in linear units (m^2/m^2). RVI is a ratio of cross-polarization to approximate the total power from all polarization channels;

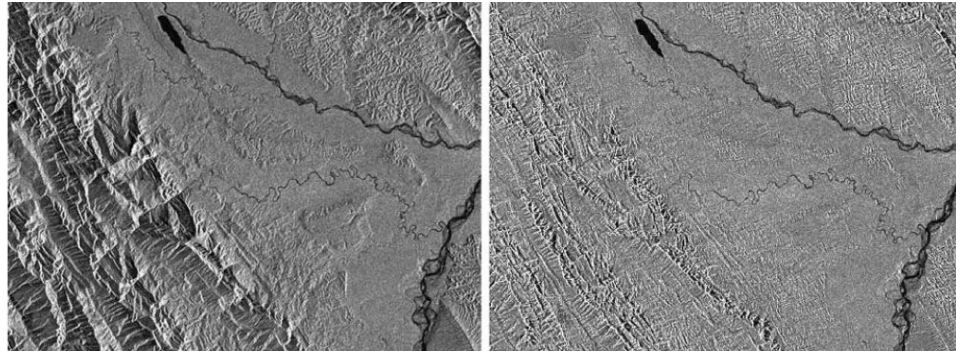


Figure 5.19 Examples of SAR imagery (a) before and (b) after RTC over a test site in mountains of Bolivia. A Sentinel SAR image before RTC (left) shows areas that are stretched and compressed due to the topography and geometry of image acquisition. These areas are shown corrected (right) as unstretched and adjusted for backscatter values after applying the RTC from the Gamma algorithm.

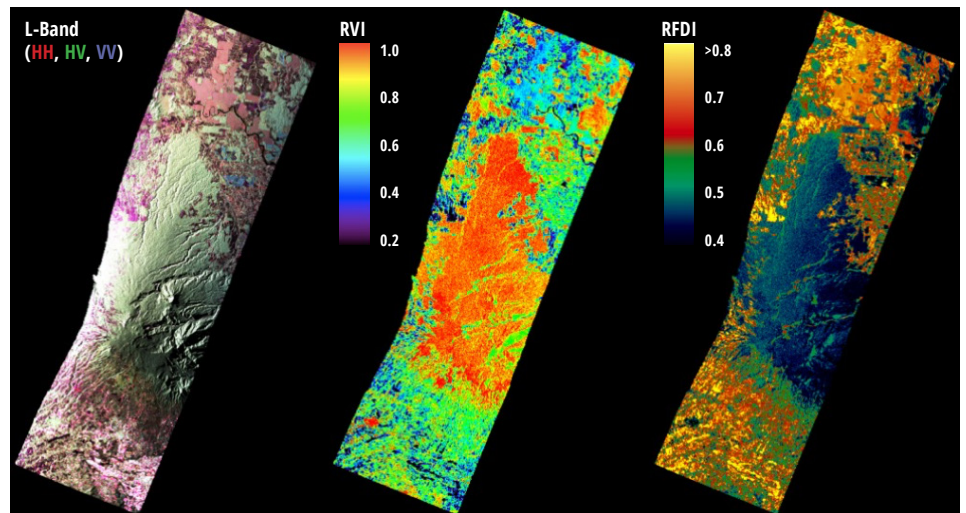


Figure 5.20 UAVSAR L-band polarimetric images and polarization indices over the La Selva Biological Station in tropical forests of Costa Rica showing: (a) three polarized channel color composite showing areas of relatively intact rainforest across a mountain range and low-biomass areas in the northern and southern parts of the image, (b) RVI image showing higher forest biomass areas in red and crops and agroforestry and secondary forests in green and blue, and (c) RFDI image showing more intact forests in dark blue and degraded, secondary, and low-biomass values in lighter blue, green, and red.

it generally ranges between 0 and 1 and is a measure of the randomness of scattering. The RVI is near 0 for a smooth bare surface, increases with vegetation growth, and has an enhanced sensitivity to vegetation cover and biomass. By being a ratio, the RVI has less sensitivity to radar measurement geometry and topography and remains insensitive to absolute calibration errors in radar data.

The RFDI is calculated as

$$RFDI = \frac{\gamma_{HH}^0 - \gamma_{HV}^0}{\gamma_{HH}^0 + \gamma_{HV}^0}$$

where the terms are all radiometrically corrected imagery. However, the ratio can also be used before any radiometric or geometric correction of the SAR imagery. The value of RFDI varies between 0 and 1 because in almost in all conditions, even in most topographically complex terrain, HH remains larger than HV. However, the values of RFDI remain mainly at >0.3 for dense forests, to values of about 0.4 or more for degraded forests, and >0.6 for deforested landscapes (e.g. [Fig. 5.20](#)). RFDI can be used with dual-polarization imagery such as the ALOS PALSAR Fine Beam Dual (FBD) datasets.

Using data from the same satellite orbits, the geometry and incidence angle do not vary over SAR pixels, allowing temporal analysis of RFDI without concerns for changes in geometry and incidence angle. In fact, RFDI from satellite imagery such as ALOS PALSAR or Sentinel can be computed without any correction for incidence angle and topography. The main application of RFDI is defined as an index to monitor changes in forest cover due to deforestation and degradation. The low values refer to forests where the effect of volume-surface interaction is either small (e.g., forests with shorter stems and dense canopies) or relatively equal in both channels (e.g., forests over slopes). The high values refer to forests with large differences between HH and HV, suggesting they are open or recently degraded forests, or inundated forests. Theoretically, RFDI can be used at any radar resolution; however, the best spatial resolution for developing RFDI depends strongly on the speckle noise in radar backscatter and the natural heterogeneity of forest structure and gap size variations over the landscape where the contribution of volume-surface interaction is larger in HH compared to HV backscatter. In general, RFDI can be used to detect both the loss of forest cover and its recovery from disturbances resulting from logging or other types of natural or anthropogenic events.

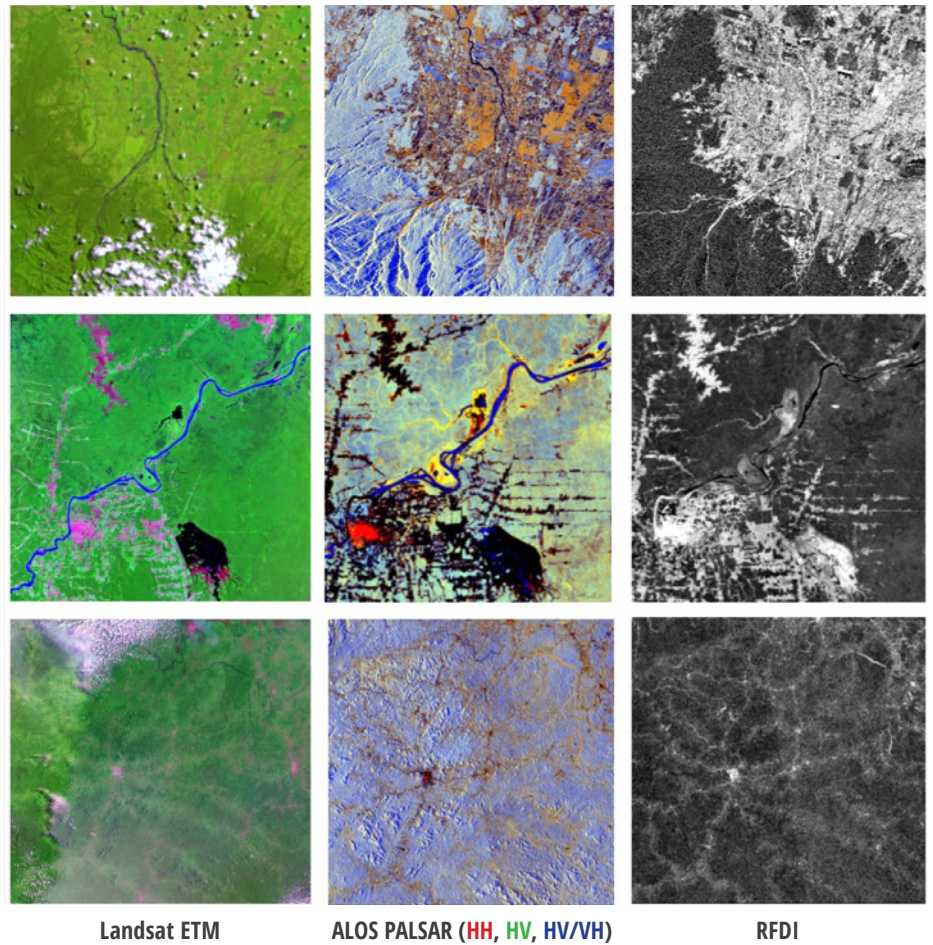


Figure 5.21 Satellite imagery over three tropical study areas, with Braulio Carrillo National Park in the top row; Rondônia, Brazil in the middle row; and Ebolowa in Cameroon in the bottom row. Images include false color Landsat ETM (RGB:543 bands) (left column), false color ALOS PALSAR images (RGB: HH, HV, HV/HH) (middle column), and RFDI (right column)

5.5.5 PRACTICAL SAR IMAGE PROCESSING FOR BIOMASS ESTIMATION

Five practical approaches for SAR processing before the data analysis for biomass estimation are summarized as follows:

- (1) Download the SAR intensity imagery in any format and create imagery in linear power (not in dB). Linear power data, which are often provided in floating point, are considered the calibrated radar imagery that can be used to relate to any surface parameter or integrated in the models. Note that working with backscatter values in dB may introduce large statistical errors in the analysis because all mathematical equations and algebraic relations must consider the logarithmic quantities.
- (2) SAR images can be multi-looked (simple averaging) to create images at coarser spatial resolution with reduced speckle. Speckle in SAR imagery can also be reduced by using various SAR filters (Lee

INDEX	APPLICATION	INTERPRETATION
Radar Vegetation Index (RVI)	Monitoring vegetation cover, water content, and aboveground biomass with quad-pol or quasi-quad-pol data.	Range (0-1): low values refer low vegetation cover and water content. The low threshold can be used to separate forest and nonforest.
Radar Forest Degradation Index (RFDI)	Detecting forest degradation and deforestation, biomass loss and gain with dual-pol or quad-pol data.	Range (0-1): Low values refer to high biomass and intact forests. Values change gradually to higher values for degraded and nonforest areas. The values remain independent of topography.

Table 5.3 SAR vegetation indices used with dual- and quad-polarized SAR measurements.

- et al. 1999).
- (3) All SAR images acquired from satellite or airborne datasets must be georeferenced such that each ground-projected pixel has geographic coordinate. Note that multi-looked SAR images with reduced speckle improve the relationship between ground measurements and SAR backscatter. De-

- pending on SAR data, the multi-looked imagery can have different resolutions. For example, for ALOS PALSAR data (originally at 20 m with 3 looks), a 100-m image can be regarded as an image of about 75 looks with significantly reduced speckle.
- (4) If the data downloaded do not include RTC, use any commercially or freely available software to

perform terrain correction. NASA's Alaska SAR Facility provides several software applications for SAR processing, including [MapReady](#) for terrain correction. RTC can be applied on multi-looked imagery given the geometry of the SAR observations and the terrain model (such as the Shuttle Radar Technology Mission (SRTM) data). This process includes finding the local incidence angle and the area normalization factors in map (in the final radar ground projection) coordinates for projection angle corrections.

- (5) Develop color composite images from SAR polarizations and SAR polarimetric indices to identify different features of landscape and vegetation covers in color without the impacts of topography and or SAR geometry.

5.6 SAR Biomass Estimation Algorithm

Performing all necessary SAR processing results in SAR imagery that has been corrected for terrain effects through RTC techniques and projected on the ground and multi-looked to a certain pixel spacing (e.g., 25 m–100 m) depending on the original image resolution. Basic techniques are presented here to develop a radar-biomass model or algorithm for estimating vegetation/forest AGB. This section is designed to show: (1) the general relationship between vegetation biomass and radar measurements, (2) development of site-specific statistical models from either airborne or satellite radar data, (3) development of a physically based model that includes different scattering matrix components, and (4) use of machine-learning algorithms for large-scale biomass mapping.

5.6.1 GENERAL RADAR-BIOMASS RELATIONSHIP

To demonstrate the relationship between radar measurements and AGB, this section concentrates on low-frequency (large-wavelength) radar systems at the L-band frequency due to its availability from space through ALOS PALSAR and due to its strong backscatter sensitivity to biomass at low- to mid-ranges. However, some results are shown and examples given from C- and P-band SAR imagery, as they are available from Sentinel series and, in the future, from ESA's Biomass mission.

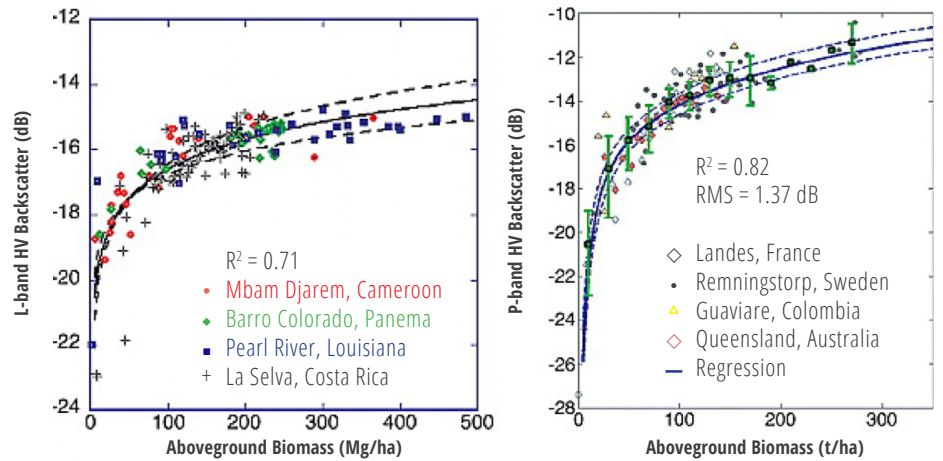


Figure 5.22 Sensitivity of radar backscatter measurement at L-band and P-band frequencies and HV polarization to forest AGB over sites distributed in boreal, temperate, and tropical ecosystems (Shugart et al. 2010).

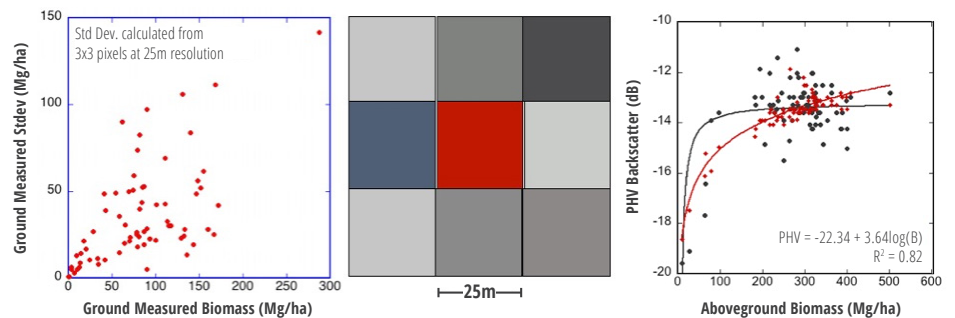


Figure 5.23 Impacts of geolocation error and small plot size on radar backscatter-biomass relationship shown by large variations of backscatter in small plots (25 m × 25 m) (left), the geolocation error causing the correct pixel (red) or plot location being misplaced by one of the surrounding pixels (center), and the impact of the geolocation error on radar backscatter relation and saturation (right). The use of correction location or larger plots will improve the relationship and the asymptote.

As discussed previously, the dominant scattering mechanisms as well as the size (volume) and dielectric constant (moisture or wood density) of forests determine the magnitude and behavior of the backscatter at each polarization to AGB. As a result, the backscatter radar energy at linear polarizations is related to the volume and biomass of forest components (**Fig. 5.22**).

The radar backscatter biomass relationships shown in **Figure 5.22** for both L-band data from ALOS PALSAR (Mitchard et al. 2009, Saatchi et al. 2011b) and airborne P-band data (Le Toan et al. 2011) from several study sites are based on a direct comparison of radar measurements and AGB from ground plots. The form of the relationship suggests that there is a rapid rise of backscatter with biomass for low-biomass plots, and then a slower increase to an asymptote at higher biomass values. For L-band, the asymptote may arrive

at values of about 100 Mg/ha or more depending on forest types (Yu & Saatchi 2016), and for P-band, the asymptote may reach 300 Mg/ha or higher. Note that both the form of the relationship and the asymptote or saturation values may change significantly depending on the data quality and analysis:

- (1) The plot data used for comparison of radar imagery are small; therefore, the backscatter power may be noisy due to the presence of speckle noise in radar measurements. The noisy data may introduce a false saturation at lower biomass values. Large plots >100 m in size will readily improve the relationship.
- (2) Geolocation errors in both SAR and ground plot locations will introduce noise in the data when comparing the ground plots and the radar backscatter (**Fig. 5.23**). Similar to the plot size,

the geolocation error can introduce false saturation. The use of larger plots and averaging SAR pixels (multi-looking) reduces geolocation errors.

- (3) Changes in SAR geometry across the plots may also introduce noise in the data, impacting the relationship and the saturation level of the radar-biomass relationship. If the image is not corrected radiometrically (RTC) and for incidence angle variations, plots with similar biomass may have significantly different backscatter (Fig. 5.24).
- (4) Environmental differences and changes in soil moisture on radar backscatter can introduce noise in the relationship. Using multitemporal SAR imagery will allow averaging out the moisture effects and will improve the backscatter values, allowing them to become more stable spatially and temporally for biomass estimation (Fig. 5.24).
- (5) Differences in the time of image acquisition and plot data can also introduce noise in the relationship. If the inventory plots are established a long time before or after the SAR acquisition, changes in biomass and forest structure from both disturbance and recovery during this period will influence the SAR backscatter. It is recommended that the dates between ground and radar acquisitions are minimized.

5.6.2 RADAR-BIOMASS STATISTICAL MODELS

Depending on the wavelength of the measurement, the radar backscatter from a forest can be related to scattering from live stems, branches, and foliage based upon their abundance and moisture content within a resolution cell as:

$$\gamma_{pq}^0 \propto f_{pq}(n_i, V_i, \epsilon_i), \quad (5.3)$$

where f_{pq} is a function averaged all possible orientation and size distributions, p and q represent the transmit and received polarizations (H, V), n_i represents the density of trees, V_i represents the volume of trees, and ϵ_i represents the moisture or dielectric constant of forest components (stems, branches, and leaves). This equation symbolically represents the radar backscatter relationship to forest structure and wood density that, along with orientation and tree size distributions, can be used to generate a model for estimating forest volume or biomass. In addition to forest structure and biomass, other parameters such as soil moisture and surface structure (slope and roughness) impact the function. The most important task in radar biomass estimation is the development of the model f_{pq} .

The analogy of this model in forestry applications is a parametric or regression-type relationship designed to directly estimate AGB with respect to forest structure. Here, some options of statistical models are pro-

vided that are developed by fitting a regression-type equation to backscatter relation to AGB. The following is the starting point in the analysis of data:

- (1) The radar backscatter is radiometrically corrected and normalized for incidence angle (γ_{pq}^0), and is converted into the linear unit and not in logarithmic scale (dB). To convert radar backscatter to a linear unit, $10^{(0.1 \text{ dB})}$ is used, where dB refers to the backscatter value in dB, which is often a negative number.
- (2) The plot size is large enough and has good geolocation and shape to match the radar pixels.
- (3) Radar backscatter data are from multi-looked imagery for large enough pixels with reduced speckle noise.
- (4) Plot-level radar backscatter at each polarization or for radar vegetation indices are derived from averaging pixel-based backscatter at the linear unit.

Here, a statistical model is introduced based on the nonlinear combination of radar backscatter for the estimation of biomass. Based on previous studies, the regression model is between an unknown power of AGB and a linear combination of backscatter measurements at three polarizations (Ranson & Sun 1994, Saatchi et al. 2007, Saatchi et al. 2011b):

$$\text{AGB}^\lambda = a_0 + a_1 \gamma_{HH}^0 + a_2 \gamma_{HV}^0 + a_3 \gamma_{VW}^0, \quad (5.4)$$

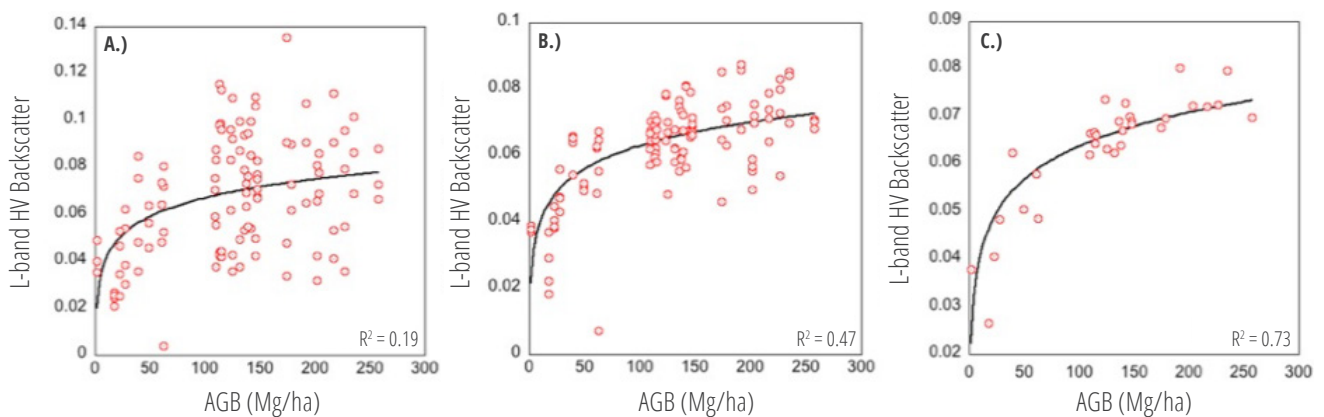


Figure 5.24 Radar backscatter and biomass relationship influenced by geometry and environmental conditions: (a) radar backscatter and AGB from ground plots acquired over different local incidence angles and different times, (b) correction of radar backscatter for the local incidence angle reducing the noise in the data, and (c) multitemporal averaging of backscatter (over five dates) reduce the noise due to environmental factors and moisture and improve the radar-biomass relationship (data from UAVSAR and ground plots in region of Howland, Maine, U.S.)

where the unknown coefficients (λ , a_0 , a_1 , a_2 , and a_3) will be determined statistically by using radar measurements and field data. The above model has the advantage of being flexible and can be used either for a single polarization, such as γ_{HV}^0 (Le Toan et al. 2011), or multiple polarization. It can also use other information such as the interferometric height estimation from radar or any other spectral information to improve the prediction of the model. The power λ for AGB is designed to adjust for the asymptote in the model (Saatchi et al. 2011b).

There are other options for AGB estimation from backscattering coefficients that have been used both in temperate and tropical forests (Saatchi et al. 2007):

$$\log(\log(AGB)) = a_0 + a_1 \gamma_{HH}^0 + a_2 (\gamma_{HH}^0)^2 + b_1 \gamma_{HV}^0 + b_2 (\gamma_{HV}^0)^2 + c_1 \gamma_{VV}^0 + c_2 (\gamma_{VV}^0)^2 \quad (5.5)$$

These equations have a larger number of coefficients to determine but may perform better in ensuring that the asymptote in the radar backscatter-biomass relationship is well-represented in the model. **Figure 5.25** shows the model fit of Eq. (5.4) for L- and P-band data over tropical forest of Costa Rica, and **Table 5.4** shows the coefficients derived from the model fit.

The power-law relationship defined in Eq. (5.4) is the optimum fit to the normalized backscatter data with respect to the aboveground dry biomass in all cases. At both frequencies, the scale of analysis did influence the form of the model between AGB and backscatter; however, as the scale of analysis increased from 0.25 to 1.0 ha, the r-squared correlation between backscatter and AGB improved, largely due to the spatial averaging of the radar data and the reduction of speckle noise. The improvement from 0.25 to 0.5 ha is due to both the reduction in speckle noise

and the errors due to geolocation and orientation of the plots, whereas the improvement from 0.5- to 1.0-ha plots is mostly due to averaging a larger number of pixels, hence the reduction of speckle noise. Although all polarizations show similar trends with respect to increasing AGB, there are clear distinctions among them in terms of backscatter level and sensitivity to biomass. In both frequencies, the HV sensitivity to biomass is much higher, and the relationship improves much higher than other channels as the scale of measurement increases. However, at L-band, the sensitivity to biomass decreases rapidly at 100 Mg ha⁻¹ at 0.25 ha and with slightly higher values of 100–150 Mg ha⁻¹ at the 1-ha scale.

The P-band results show a very strong relationship to AGB over the entire range with gradual loss of sensitivity at AGB > 200 Mg ha⁻¹. The r-squared correlation between P-band channels and AGB is almost above 0.7 in all cases and improves with the spatial scale.

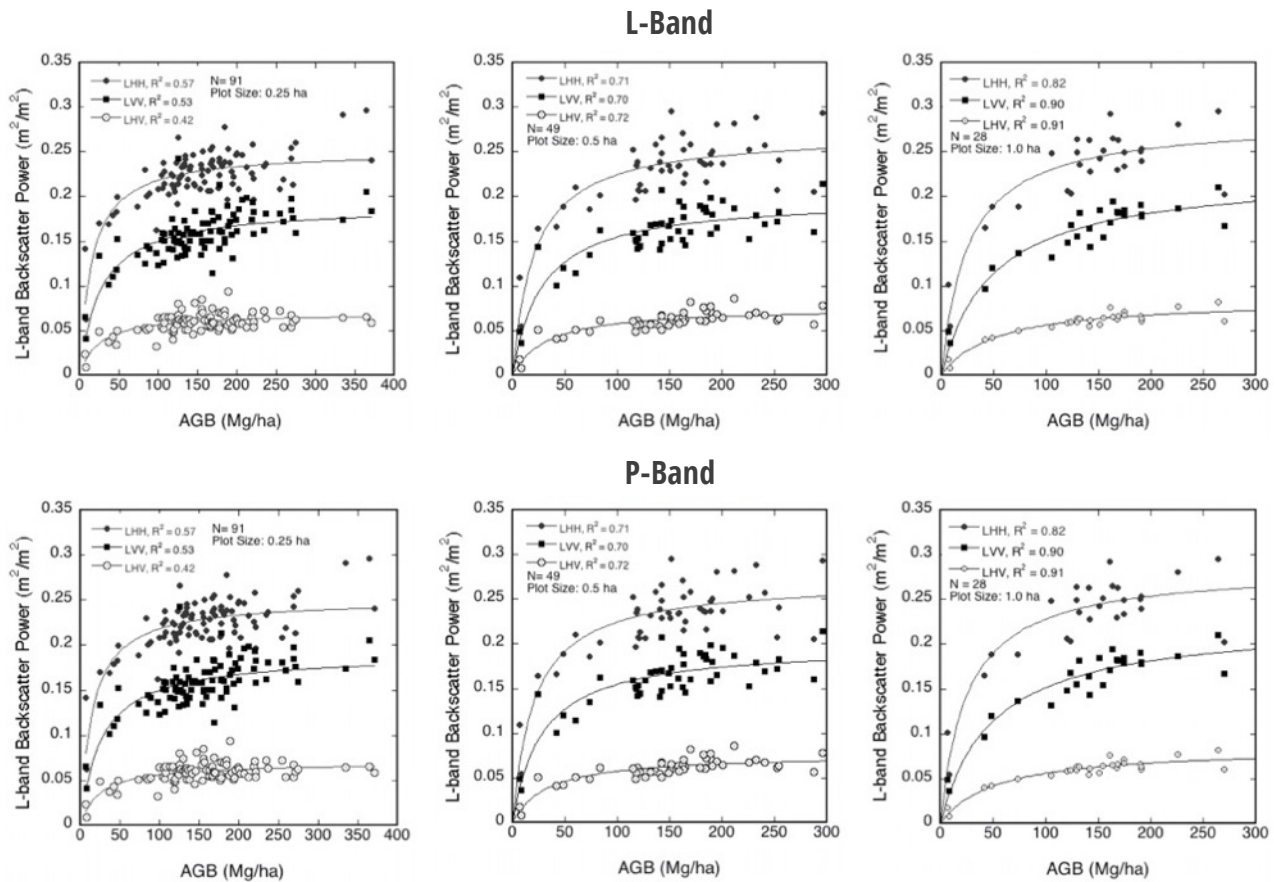


Figure 5.25 Model fits for the backscatter relationship with AGB for both L- and P-band at three polarizations of HH, HV, and VV at three different plot sizes of 0.25, 0.5, and 1.0 ha (Saatchi et al. 2011b).

RADAR CHANNELS	a0	a1	a2	a3
0.25 ha Scale				
LHH, LHV, LVV	-4.36	-41.68 ± 2.56	45.71 ± 6.05	2.08 ± 2.53
PHH, PHV, PVV	-1.23	64.11 ± 6.05	235.41 ± 22.80	119.41 ± 8.73
0.5 ha Scale				
LHH, LHV, LVV	-1.91	16.49 ± 3.32	63.76 ± 11.28	39.26 ± 3.93
PHH, PHV, PVV	-0.31	57.96 ± 6.36	313.29 ± 30.79	81.22 ± 11.07
1.0 ha Scale				
LHH, LHV, LVV	-0.67	-7.35 ± 4.87	106.63 ± 21.96	48.11 ± 6.72
PHH, PHV, PVV	0.73	42.13 ± 13.49	323.02 ± 64.41	71.51 ± 18.74

Table 5.4 Parameters of the model fit to Eq. (5.4) using airborne radar backscatter at L-band P-band with three polarization combination and three spatial scales.

Model Parameters	A	B	C	D	α	β
γ_{HV}^0	0.04 ± 0.01	0.06 ± 0.03	0.04 ± 0.1	0.00001	0.14 ± 0.05	0.019 ± 0.02

Table 5.5 Fitting coefficients and unknowns for a temperate/boreal mixed conifer forest site in Howland, Maine.

5.6.3 RADAR-BIOMASS PHYSICALLY BASED MODELS

Physically based models are often complex in formulation and include a large number of variables covering the remote sensing sensor characteristics, the geometry of measurements, and the forest characteristics. There are several types of physically based models that are used to simulate the radar measurements from forest canopies (Saatchi & McDonald 1997, Saatchi & Moghaddam 2000, Ulaby et al. 1990, Sun & Ranson 1995, Karam & Fung 1983, Karam et al. 1992, Oh et al. 1992). As discussed previously, the model is based on formulating the three dominant scattering mechanisms or radar backscattering power from vegetation layers. These include volume, volume-surface, and surface scattering:

$$\gamma^0 = \gamma_{vol}^0 + \Gamma_{surf} \gamma_{vol-surf}^0 + \Gamma_{vol} \gamma_{surf}^0, \quad (5.6)$$

where γ_{vol}^0 is the volume backscattering from vegetation, $\gamma_{vol-surf}^0$ is the volume forward scattering from vegetation, γ_{surf}^0 is scattering from the soil surface, $\Gamma_{vol} = \exp(-B \times AGB)$ is the volume attenuation (absorption), and Γ_{surf} is the soil surface reflectivity.

The above equation and terms can be repeated for each polarization separately. Here, the model fits for only one polarization is represented, and the

methodology for developing semi-empirical models that include the physical formulation is provided. The HV polarization typically has better sensitivity to forest AGB than the HH or VV polarizations and has less sensitivity to the soil surface scattering and moisture. Therefore, for demonstration, this chapter focuses on the HV polarization. Another focus is on the L-band data as it appears to be the widely used data from space from the ALOS PALSAR data. However, the methodology can work for both L-band and C-band over different ranges of biomass depending on the sensitivity of each sensor (Fig. 5.26).

In forests where the canopy is not as dense, such as the temperate conifers and boreal forests, the magnitude, sensitivity to biomass, and the contributions of each scattering component may be different. For example, in boreal forests, L-band backscatter can possibly have significant contributions from the surface-volume term with potentially enhanced sensitivity to forest biomass and soil moisture (Sandberg et al. 2011). This possibility is explored by fitting a functional form that includes both volume and the volume-surface scattering term:

$$\gamma^0 = AW^\alpha (1 - e^{-BW}) + (CW^\beta + D)Se^{-BW}, \quad (5.7)$$

where A, B, C, D, α , and β are fitting coefficients, and the unknowns are W (as the AGB) and S (as the soil surface condition). The term S includes the reflectivity of the surface which depends primarily on soil surface moisture. The temperate/boreal mixed conifer forest was selected as an example to demonstrate the effect of other scattering contributions, as observations from ALOS PALSAR HV and AGB from ground data are available from the site in Howland, Maine (Table 5.5).

After developing the model for the study site, the next step is to estimate AGB from the model. The biomass estimation process from the model relies on a least-squared approach such that the function can be inverted to estimate W and S . If the only data available are from ALOS PALSAR, which provides dual-polarization imagery in HH and HV over most of the world, the least-squared method can be readily written as:

$$Loss = \sum_{t=1}^n \left\{ \left[\eta_{HH} (f_{HH}(W, S_t) - \gamma_{HH,t}) \right]^2 + \left[\eta_{HV} (f_{HV}(W, S_t) - \gamma_{HV,t}) \right]^2 \right\}, \quad (5.8)$$

where $\eta = 1$ for HH, or 3.5 for HV. The Loss function will be minimized in a least-squared approach to es-

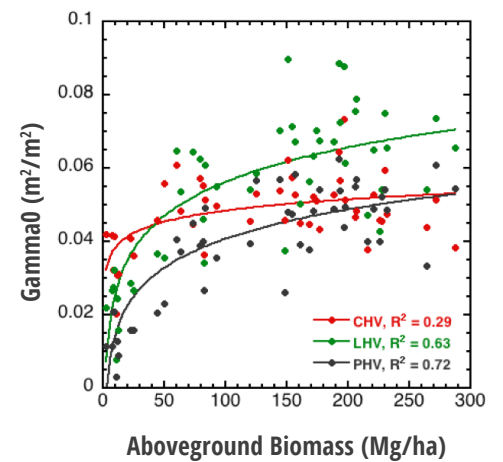


Figure 5.26 Relationship of backscatter in HV polarization at three frequencies of C, L, and P-band based on ground and backscatter data over Howland forest in Maine using biomass estimates from 0.1-ha plots AIRSAR data from one image. The backscatter values are different in magnitude and sensitivity, and the fit is based on a logarithmic model.

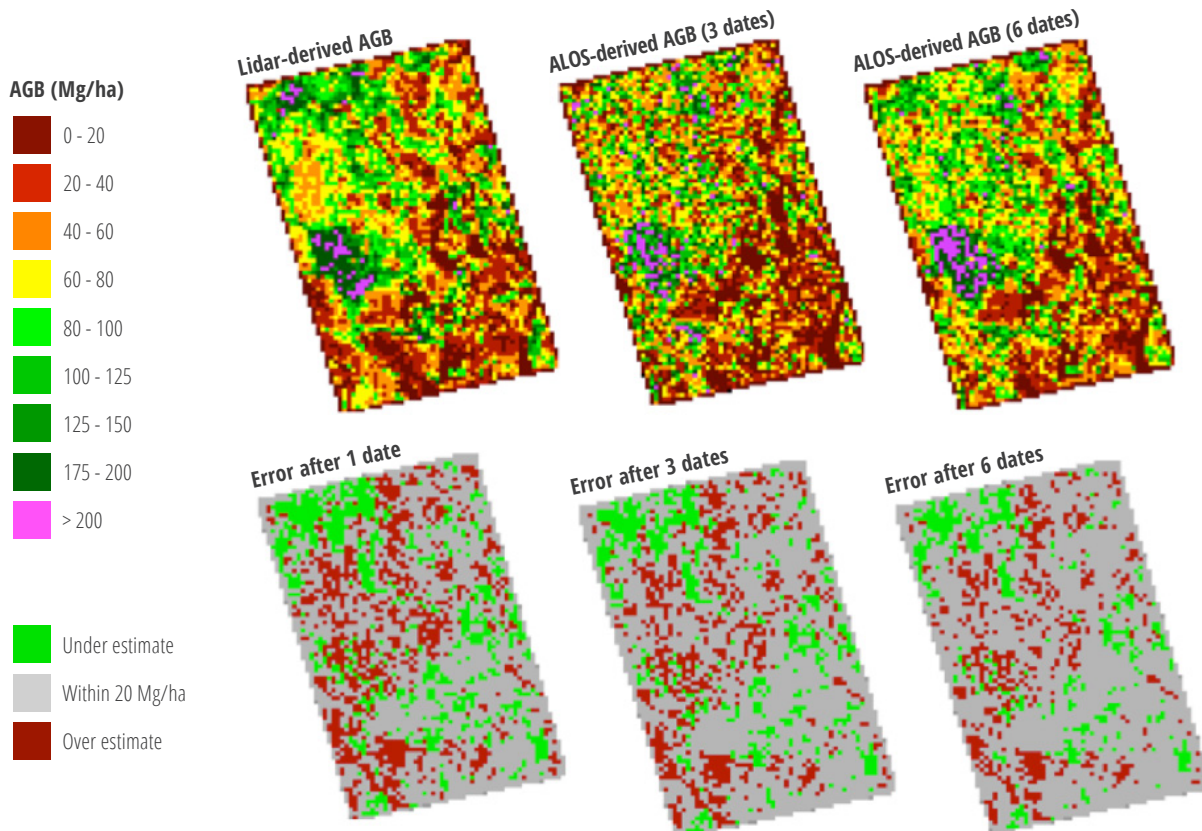


Figure 5.27 Application of the semi-empirical model on the ALOS PALSAR HH and HV images over Howland, Maine forests and comparison with the lidar-derived AGB as a reference map. The results shows using multi-temporal ALOS imagery, the SAR estimation of biomass approaches the Lidar estimation. With 6 ALOS images, over 75% of the image pixels are estimated within 20 Mg/ha of the reference values. The accuracy increases to 86% after using 9 images.

estimate W and S at each pixel. Note that with multiple SAR imagery acquired at different times t , the above equation is used by allowing the soil term S to change through time, but W (AGB) remains constant to improve the estimation approach. This assumes that for a period of a season or few months to stack multitemporal radar data, AGB remains constant or has some undetectable change unless a major disturbance occurs.

The above formulation was designed to demonstrate that a semi-empirical or physically based algorithm can be derived for an ecoregion or forest type and applied over large areas. This is mainly due to the fact that statistical models developed based on field data over a small region may have large errors when applied over areas far from the original test area due to potential variations in landscape topography, soil moisture and roughness, and vegetation structure. However, the

semi-empirical algorithm relies more on the physics of the problem and compensates for the landscape and regional variation. In a more rigorous implementation of the problem, the Loss function can also be optimized locally by updating the coefficients of the model (A , B , C , D) over a local window of pixels (3×3 or 5×5 or larger) to allow for the model to be better adjusted to local variations of the forest structure within an ecoregion.

A simpler version of the physically based algorithm has been applied in few cases. Yu and Saatchi (2016) use a model that weights more on the volume scattering and combines the surface effect in both volume-surface interaction and surface scattering as an unknown term:

$$\gamma^0 = AW^\alpha (1 - e^{-BW}) + C, \quad (5.9)$$

where W is AGB in Mg/ha; and A , B , C , and α are fitting coefficients. The above equation has been used

to model ALOS PALSAR variations over global vegetation biomass (Yu & Saatchi 2016). Bouvet et al. (2018) used a slightly simpler version of the model that can be inverted analytically, though with less flexibility for adjusting for the asymptote. In their version, the model is fit to the decibel values of the backscattering coefficient:

$$\gamma^0 = A(1 - e^{-BW}) + Ce^{-BW}. \quad (5.10)$$

This formulation ignores the volume-surface scattering and only considers the volume and surface scattering. The formulation corresponds to the modified Water Cloud Model (Santoro et al. 2002), an adaptation of the original Water Cloud Model (Attema & Ulabay 1978) that has been widely used for vegetation biomass estimation at higher frequencies such as C-band. The above model has already been used for L-band data by several authors (Cartus et al. 2012, Mermoz et al. 2014, Michelakis et al. 2014, Mitchard et al. 2011).

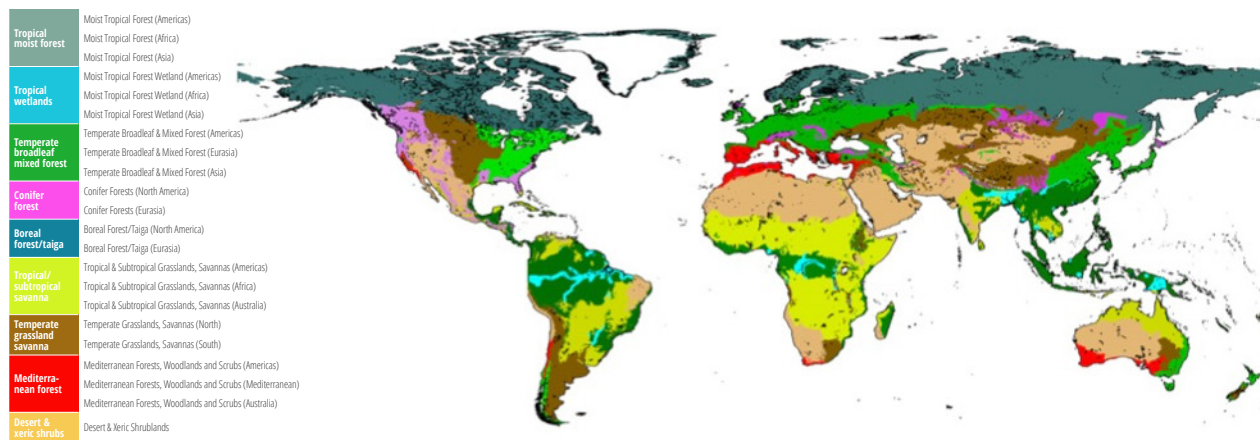


Figure 5.28 Global ecoregions derived from the WWF ecoregion map (Olson, et al. 2001) by separating the ecoregions in different continents.

5.6.4 RADAR-BIOMASS MODEL VARIATION ACROSS GLOBAL FORESTS

Radar-biomass algorithms will vary globally depending on the forest types. In order to provide a basic set of algorithms globally for rapid estimation of forest biomass in the absence of any reliable ground or lidar data, the development of preliminary algorithms for global vegetation ecoregions is summarized here. The primary objective of this section is to show how many different models can, on the average, represent the L-band radar sensitivity or relationship to biomass, starting with several datasets to develop the models:

- The radar backscatter data from ALOS/PALSAR, from the Japan Aerospace Exploration Agency (JAXA). JAXA has released the 2007–2010, 2015, 2016, and 2017 annual mosaics of ALOS/PALSAR data at fine-beam mode and dual polarization (HH, HV). The global mosaic is corrected for geometric distortion and topographic effects, with potentially significant residual distortions in areas of high slopes. HH and HV backscatter values from the 2007 mosaic have been used for this study. To achieve this, the backscatter digital numbers (DN) from the PALSAR product were converted to values of backscattering coefficient $[σ_{hh}^0]$ in units of linear power then aggregated to a 50-m resolution using simple averaging within a 2-x-2-pixel window. The ALOS PALSAR data and instructions for converting the DN values to backscatter power are given [here](#).

- The GLAS, onboard the ICESat (2003–2008), can be used to make global estimates of forest height and vertical structure. In turn, these data are used to derive estimates of forest biomass at the GLAS effective footprint size of approximately 50 m (0.25 ha). All GLAS waveform data were filtered depending on the signal-to-noise ratio and cloud flag in the GLAS GLA14 dataset to develop more than 7 million clean waveforms distributed over the global forests. GLAS data can be downloaded from the [NASA DAAC website](#).
- Starting with 22 global ecoregions from the WWF biome map (**Fig. 5.28**), these were reduced to 15 regions that are vegetated and have significant structural diversity to affect the radar signature (Olson et al. 2001). These data were used as the main source for separating the ecoregions globally. This WWF-derived map is based on a suite of datasets such as climate, topography, and seasonality, separating the key global vegetation life-forms that have distinct structure, landscape, and climate features. Additional separation of ecoregions across continents was allowed because of distinct biogeography and plant distributions, as well as other factors including history of climate and human impacts.

The ICESAT GLAS waveform data provide vegetation vertical structure and different height metrics that were converted to AGB for each waveform (Lefsky 2010, Yu & Saatchi 2016). The ALOS PALSAR pixel values for HH and HV from the global mosaics of 2007 will be, and the associated ecoregions from

the WWF-based map were extracted for all latitude/longitude center coordinates of the GLAS footprints. Each AGB value was then associated with two ALOS polarized backscatter and one ecoregion class from WWF map. To demonstrate the relations between radar measurements and AGB, the AGB values were placed into 5 Mg/ha bins and the corresponding backscatter values were averaged. For every bin within each forest category, the mean and standard deviation of the ALOS-HH and HV backscatter values within the bin were calculated. The mid-AGB value was used to represent each bin. The extreme end of this bin distribution was terminated once the number of points within the bin fell below 500. The biomass values were also limited to 200–300 Mg/ha, a factor of 2–3 beyond the sensitivity limits of the L-band data with respect to the biomass to allow for developing the backscatter-biomass models and detecting the saturation region for each ecoregion (**Fig. 5.29**).

Using the models developed for HV-polarized backscatter for all 22 global ecoregions, a statistical F-test to compare the models between two or three models depending on each ecoregion using a pairwise statistical test was developed based on the statistical significance of extra sum-of-the-squares F test and the AIC approach. This analysis allows for the definition of a p-value to be small enough to give criteria necessary to separate statistically and significantly different models from other possible models. The process was first performed on models with similar ecoregions such as boreal forests of the two continents and then between the boreal forest mod-

els and other ecoregions. The results of the statistical tests provided 15 distinct models across the global ecoregions (Fig. 5.30).

Both of the models in Eqs. (5.7) and (5.9) were used to fit the data and both performed well. Here, for simplicity and easier application of the model to the backscatter for biomass estimation, the coefficients for the global forests are provided for interested researchers or practitioners to apply on radar imagery to develop the biomass. The next sections provide specific instructions for practical implementation of the algorithms for different regions.

Note that because of the highly complex nonlinear nature of Eqs. (5.7) and (5.9), and the small number of fitting data points, the fitted coefficients may have large uncertainties for some ecoregions, as shown by the one-standard-deviation values of the fitted coefficients. While the more complex functional form of Eq. (5.7) may be closer to the physical representation of the full backscattering mechanism, caution must be taken in using these fitted coefficients to make physical interpretations because of the limited number of observational diversities. It is recommended that interested researchers develop more site-specific and regional models with improved ground or lidar data.

5.6.5 RADAR-BIOMASS NONPARAMETRIC MODELS

There are multiple ways of extrapolating samples of forest biomass data from ground or lidar measurement to a gridded map. These include parametric approaches such as the use of statistical regression models and semi-empirical models described previously that can be applied on individual radar pixels. However, maps of biomass have also been developed using a set of spatial environmental data from remote sensing and climate, and nonparametric approaches such as interpolation, co-kriging, classification, coloring by numbers, decision rule techniques, and machine-learning approaches as in the Random Forest (Xu et al. 2015), Maximum Entropy (MaxEnt) (Xu et al. 2015, Saatchi et al. 2011b), Super Vector Machine (Garcia et al. 2017), or Neural Networks (Del Frate & Solimini 2004). In some cases, the parametric models are not suitable for estimating biomass because the

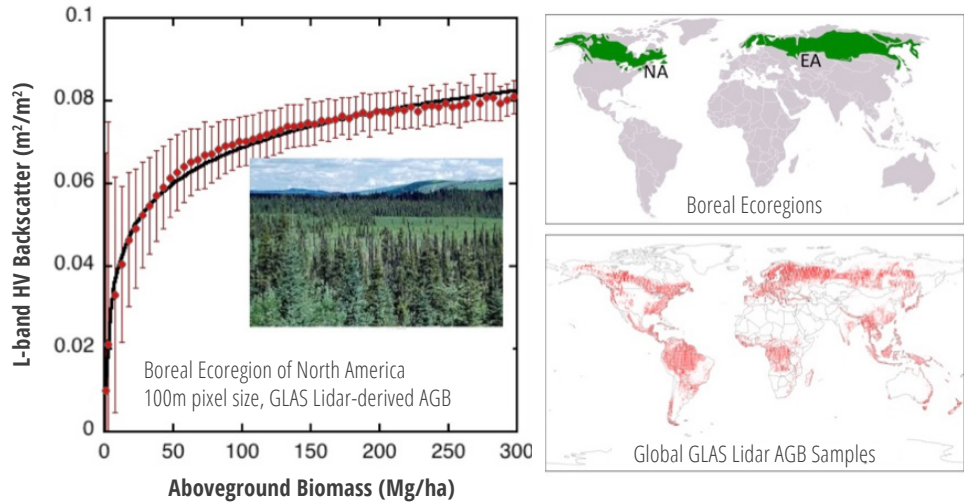


Figure 5.29 Sensitivity of L-band HV backscatter to AGB of boreal forests of North America dominated by conifers. The sensitivity is high up to 100 Mg/ha and starts declining for AGB >100 Mg/ha.

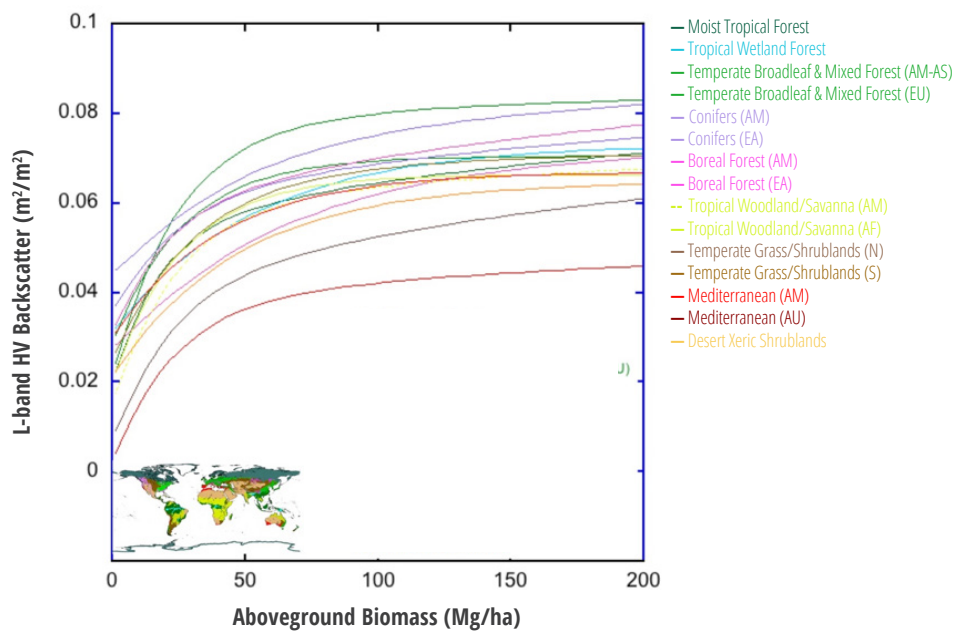


Figure 5.30 Distinct L-band HV models for 15 ecoregions globally. The models are derived from binned backscatter and AGB data derived from GLAS lidar data.

models are developed with limited data over small regions and are used for large-scale biomass estimation. Factors such as landscape variability, forest structure, and variations of moisture and other environmental variables impact the applicability of a simple statistical model developed with limited data in and over a relatively non-representative landscape. Nonparametric models are found to be more suitable

in large-scale geospatial and geostatistical analyses because they are not affected as much by noise in the model or issues associated with multivariate normality. Nonparametric models can also integrate variables with different statistical distributions and provide more stable and relevant information. Furthermore, forest structure and biomass often exhibit complex, nonlinear variations, autocorrelation, and variable in-

teraction across temporal and spatial scales. In these cases, nonparametric approaches often greatly outperform the parametric methods. Proposed here are nonparametric and machine-learning approaches for mapping forest biomass over large areas using SAR imagery or fusion with other datasets such as topographical data from SRTM or even Landsat imagery for regional and national-scale biomass mapping for the improvement of biomass estimation.

Among nonparametric models, two common approaches used extensively for large-scale mapping were selected (Saatchi et al. 2011, Baccini et al. 2012, Xu et al. 2015): the MaxEnt estimation algorithm and the Random Forest estimation model. To apply these methods, two sets of data are required:

(1) Training data—the model or machine-learning training data can be selected from AGB estimated from inventory plot data or lidar measurements. The training data must be widespread to cover the range of landscape and biomass variations over the region of interest, with the number of samples covering the biomass range and representative of areas similar or compatible with the pixel size of the remote sensing imagery.

(2) Spatial data layers—Here, the spatial layer is SAR imagery from any airborne or satellite data such as Sentinel and ALOS. However, spatial data can be selected from a range of imagery such as SRTM to represent the topography or Landsat imagery to allow data fusion and improvement of estimation. In the case of SAR, the images are preferred to be terrain corrected, multi-looked, or speckle filtered and projected at the spatial scale compatible with the ground plots or lidar estimated biomass.

5.6.5.1 MaxEnt Model

MaxEnt is a probability-based algorithm that seeks the probability distribution by maximizing the information contained in the existing measurements (Berger et al. 1996, Phillips et al. 2006). The method is used as a classification approach, and each class has some probability of occurrence $p(A_k)$, where A is a measurement event of the response variable, while the measurements are from training samples that belong to class k . The following constraint assumes that

GLOBAL VEGETATION TYPE	A	B	C	α
Africa Tropical Moist	0.056492	0.064689	0	0.038247
Asia Tropical Moist	0.045409	0.060518	0	0.060518
America Tropical Moist	0.040546	0.068784	0	0.098841
Temperate Conifer	0.0092565	0.057336	0.04	0.27162
Temperate Broadleaf/Mixed	0.041469	0.034296	0.026406	0.012282
Tropical Shrubland	0.016429	0.11013	0	0.2675
Tropical Dry Broadleaf	0.021563	0.042324	0.027519	0.1117
North America Boreal	0.018911	0.019744	0.029106	0.15723
Eurasia Boreal	0.0091605	0.038506	0.04	0.26141
Fresh Water Flooded	0.047845	0.045581	0.022164	0.0058592
Saline Water Flooded	0.013682	0.051846	0.02192	0.21116

Table 5.6 Proposed coefficients for simple ALOS PALSAR HV-based model as in Eq. (5.9) for several global ecoregions as examples for rapid estimation of forest biomass.

probabilities of all $p(A_k)$ must sum to 1.

$$\sum_k p(A_k) = 1. \quad (5.11)$$

From information theory, the most uncertain probability distribution is the one that maximizes the entropy term:

$$E = -\sum_k p(A_k) \ln p(A_k). \quad (5.12)$$

This process will ensure that the distribution is estimated by keeping the randomness of samples for the largest entropy. Equation for E naturally gives the maximum value for the entropy when all probabilities are equal (randomness) assuming no other constraints are applied to the system except for the equation where the sum of the probabilities are 1. If additional information is available (i.e., some known AGB observations and corresponding measurements in X as in ALOS PALSAR or any SAR data; these are referred to as the training set), the probability distributions are “conditioned” on the available observations:

$$p(A_k | X) = p_k(X) p^0(A_k) / p(X). \quad (5.13)$$

The right part of Eq. (5.13) follows the Bayes’ theorem, meaning that the posterior probability $p(A_k | X)$ depends on the distribution of X and equals to the product of prior probability $p^0(A_k)$ and the probability distribution $p_k(X)$ that finds X to be in the class k , and normalized by the probability distribution of

X for the entire domain of measurement variables (here, satellite images). The maximization of the entropy term in Eq. (5.14) is equivalent to finding the probability distribution $p_k(X)$ closest to $p(X)$, and the maximum entropy procedure gives the “raw” output: $p_k^{raw}(X) = p_k(X) / p(X)$ (Elith et al. 2011). The prior probability $p^0(A_k)$ is often unknown, as this quantity is the proportion of all observations over the entire scene that belongs to class k . Assuming that the training set is sampled randomly, $p^0(A_k)$ can be estimated as $p^0(A_k) = N_k / N_{total}$, where N_k is the number of samples in the training set labeled as class k , and N_{total} is the total number of samples in the training set.

For the interested variable AGB, the numeric values can be categorized into a set of classes: $k_1, k_2, k_3, \dots, k_n$, where $0 < k_1 \leq AGB_1 < k_2 \leq AGB_2 < \dots < k_n \leq AGB_{max}$. And each class has a nominal value of AGB—usually the mean value of each class AGB_k . To predict the AGB value for any pixel i with known measurements X_i , it is calculated as the expectation of all classes given the MaxEnt results retrieved from the training set:

$$\langle AGB_i \rangle = \frac{\sum_{k=1}^n [p(A_k | X_i)]^m p(A_k | X_i) AGB_k}{\sum_{k=1}^n [p(A_k | X_i)]^m}. \quad (5.14)$$

Empirical tests have found that the model performs better by assigning higher weights to more probable classes. Therefore, an extra exponential

parameter is added to the raw output in the above equation that is determined to be approximately 3 (Saatchi et al. 2011a)

5.6.5.2 Random Forest Model

The Random Forest model is an ensemble model of decision trees trained from randomly selected subset features and random sampling of the training set using the bagging method (Breiman 2001). Random Forest can be a regression method when using regression trees, and for the j th regression tree, the regression model can be built as

$$AGB = f_j(x) + \varepsilon, \quad (5.15)$$

where x , ε , and X are the bagged samples of the training set, and $f_j(\bullet)$ is the nonparametric function determined by the j th regression tree. The final prediction of Random Forest regression is the unweighted average of the collection of trees:

$$\widehat{AGB}(X) = \frac{1}{J} \sum_{j=1}^J f_j(x). \quad (5.16)$$

This averaging process inevitably creates results biased towards the sample mean, and large/small values of AGB are often underestimated/overestimated. Various bias correction methods have been proposed to post-Random Forest results. Introduced here is a simple regression method on the Random Forest RF prediction to correct the biases, so that every 5 percentiles of the training data are grouped to have its own bias correction:

$$AGB = \alpha + \beta \widehat{AGB}(X) + \sum_{m=1}^M \gamma_m (\widehat{AGB}(X) - b_m) D_m + \varepsilon. \quad (5.17)$$

Here, the results of Random Forest prediction $\widehat{AGB}(X)$ are further compared with the true AGB in the training set using segmented regression. Parameters α , β , and γ_m are all regression coefficients, b_m is the location of break points for the 5-percentile, 10-percentile, ..., and 95-percentile of AGB in the training set, and D is the dummy variable that equals to 1 when $\widehat{AGB}(X) > b_m$ and 0 otherwise. The bias-corrected Random Forest prediction is shown to have less underestimation of high AGB, which is important for biomass and carbon estimations.

To evaluate the performance of the machine-learning algorithms, recommend three statistical measures are recommended: (1) the coefficient of determination (R^2), (2) the Root-Mean-Square

Error (RMSE), and (3) the Mean Signed Deviation (MSD). Once all of these measures are applied to an independent test set where the original AGB is obtained from ground data or airborne lidar, while the predicted AGB is derived using the SAR and other remote sensing data layers and the model trained from the training set. In addition, it is recommended to use the Moran's I statistics to quantify the spatial autocorrelation in the data. The local Moran's I index confirms the need to select more spatial samples in heterogeneous areas like forests, as it can identify spatial clusters and outliers (see Xu et al. 2015, Xu et al. 2017).

5.6.6 PRACTICAL CONSIDERATION FOR SAR BIOMASS ESTIMATION

The following is recommended for practical use of SAR imagery for biomass estimation:

- (1) **Choice of SAR data**—Depending on the vegetation type and the scale of analysis and biomass range, the choice of radar data may be different. For all areas covered with low-vegetation biomass such as grasslands, shrublands, sparse woodlands, young secondary regeneration, and low-density wetlands, the C-band data from the Sentinel satellites are the most suitable datasets. If airborne SAR data are available for the study site, use of polarimetric C-band data at high spatial resolution is recommended. From low to moderately high biomass up to 100–150 Mg/ha, the use of L-band polarimetric or dual-pol data are recommended. ALOS-2 PALSAR imagery is the most suitable dataset because of its frequent observation (every 14 days), resolution (~20 m), and sensitivity to biomass. For all forests >150 Mg/ha of biomass, use of P-band data that are currently mainly from limited airborne sensors are recommended. P-band data can be used for estimating and monitoring tropical forest biomass.
- (2) **InSAR observations**—Although, the subject was not covered in this chapter, the use of Interferometric SAR (InSAR) for measuring the forest structure across some vertical depth may help with improving the biomass estimation particularly beyond the saturation level

in some forests. Unfortunately, reliable InSAR data are not readily available. The future Biomass mission (and to some extent the NISAR mission) may provide some InSAR data. However, the use of Sentinel, ALOS, and Terra-X SAR data have been used in InSAR models in different studies to explore the use of vertical structure derived from radar for biomass estimation.

- (3) **Multitemporal observations**—Due to the sensitivity of radar imagery to soil moisture, and to some extent variations of vegetation moisture seasonality, the use of time series images for reducing the effect of environmental factors for biomass estimation is recommended. The SAR biomass model often performs poorly if it is developed based on one SAR image and applied on an image acquired at a different season or date. One practical approach is to collect as many SAR images over the study areas as possible and average the data temporally to reduce the effect of the moisture before developing the model as shown in [Figure 5.25](#).
- (4) **Map unit and pixel size**—Choose map units of 100 m or more for improved results from the biomass estimation. It is recommended that SAR biomass models are developed with plots of at least 1 ha in size for a relatively unbiased estimate of the biomass within the range of biomass allowed for the SAR data. If reliable models are developed at smaller pixels or plot sizes (e.g., 0.25 ha) for some forest types (dry forests, woodlands, boreal), it is recommended to estimate the biomass at 0.25 ha and aggregate the result to 1 ha or more for applications. The error of biomass estimation will reduce with a factor of slightly less than \sqrt{n} , where n is the number of pixels for averaging (Weisbin et al. 2014).
- (5) **SAR measurement diversity**—Most models shown in this section were based on L-band HV backscatter measurements due to its improved sensitivity to biomass and moderate effects of moisture or other environmental factors. However, use of models that include

several polarizations or even measurements of two or three frequencies improve the model performance and the accuracy of the biomass estimation. In most practical studies, access to some ALOS PALSAR and Sentinel satellite imagery is possible. Combining the datasets in a statistical model as shown in this section can improve the accuracy of the biomass across different ranges.

5.7 Uncertainty Analysis

Uncertainty analysis has become an important ingredient of forest biomass estimation from both ground and remote sensing data due to Intergovernmental Panel on Climate Change (IPCC) guidelines (IPCC 2006). This section provides a summary of different types of uncertainty analysis from simple to more complex inferences of mean or total biomass (carbon stocks) of forests at regional or national scales. According to the IPCC ([Chapter 3](#)) and the [Carbon Fund Methodological Framework](#), all forest biomass and carbon assessments at the project, jurisdictional, and national levels must address the uncertainty related to the biomass estimation and all derived products such as emissions from deforestation and degradation by:

- (1) Identifying and assessing sources of uncertainty
- (2) Minimizing uncertainty where feasible and cost effective
- (3) Quantifying remaining uncertainty

The sources of uncertainty are identified in both the land-use or activity data and the biomass estimations for different land use and land cover classes and emission factors. Once the sources are identified, their relative contribution to the overall uncertainty of the biomass estimation at the regional for land cover types and hence emissions and removals can be quantified and reported. Here, the uncertainty analysis is summarized in three steps: (1) Cross Validation (CV) approach for developing uncertainty for SAR-biomass models and local area estimation of biomass when ground or reference data are available, (2) error propagation approach showing how uncertainty from different sources of errors can be combined to provide total uncertainty on the biomass estimation at the biomass map units or on the aver-

age for a region, and (3) inference of forest biomass at regional scales by calculating both the mean and the variance or uncertainty around the mean using uncertainty of sources of errors and spatial correlation of map units or derived biomass pixels.

5.7.1 CROSS VALIDATION

Cross validation is a modeling technique used to check the statistical learning consistency with independent data from the training set itself. Not only can it be used to check the performance of the SAR biomass model or spatial modeling by making predictions on new data that are never used in the training, but it is also often used as a technique of parameter tuning to avoid “overfitting.” For regression-based analysis, the mean-squared-error (MSE) is normally used as the scoring parameter in the CV process. There are several ways of cross validation commonly used to evaluate the performance, including k-fold approach, leave-one-out CV, repeated random subsampling (or Monte Carlo CV), and so on. Interested readers can consult several references for the use of validation approaches for quantitative remote sensing products (Browne 2000, Hawkins et al. 2003, Arlot & Celisse 2010).

5.7.2 ERROR PROPAGATION

The overall sources of uncertainty for estimating forest biomass from SAR or any remote sensing data can be summarized as follows:

- **Measurement Errors**—This error can be either random or systematic and results from errors in measuring, recording, and transmitting the information.
 - In ground data, there are several sources of the error that can impact the biomass estimation at the plot level (Chave et al. 2005). In addition, in measurements of trees, the size and location of the plot can introduce significant errors in biomass estimation as a reference data to be compared to the SAR measurement.
 - SAR measurements also may have errors associated with the absolute calibration of the system, the RTC method for removing topography and incidence angle effects, and geolocation of pixels when using the data to compare with

ground plots. Together these effects can cause bias and random errors in estimation of emissions. Discussion has already been presented as how to improve the errors associated with the SAR data processing and radiometric corrections.

- **Statistical and Sampling Errors**—To develop models of SAR backscatter with ground reference data or airborne lidar-derived biomass may also have errors associated with the sampling and the statistical representation of the plots and pixels. In general, plot data need to represent the landscape variations of biomass from low to high biomass and must follow the requirements of the size, orientation, and geolocation and number of samples.
- **Lack of representativeness of data**—This source of uncertainty is associated with a lack of complete correspondence between ground and SAR data. In addition, to develop the SAR biomass models, the pixels must be spatially representative in the SAR image and not all are from a certain incidence angle, at a certain elevation and slope in order to make sure that the relationship developed between the SAR data and ground are representative. Any errors in sample size and sampling characteristics can introduce both systematic and random errors.
- **Models**—Models developed from SAR data and biomass often have uncertainty due to both the choice of the model function and the fit of the model parameters. If data are noisy, the model fits may have large errors that include both the systematic (choice of wrong model equation) and random errors.
- **Statistical Random Error**—This source of error often appears in inventory data that are supposed to be a random sample of a finite size depending on the variance of the population. Here, the sample size is a key source of uncertainty.
- **Misclassification and missing data**—This uncertainty is due to incomplete, unclear, or faulty definition of data, and allometric models leading to bias in estimation of biomass. This will often occur when working with the ground plots.

For example, using biomass data from plots with different type of measurements, lack of availability of allometric models to estimate biomass (e.g., allometry for tropical wetland forests).

- **Missing data**—This uncertainty may result when measurements are below the detection limit causing a nondetected data that can, in turn, introduce both bias and random errors. By assuming that there are several sources of errors that introduce uncertainty in the pixel-level estimation of biomass, the total uncertainty associated with estimating AGB at the pixel level can be calculated by assuming all errors are independent and random, by using

$$\epsilon_{AGB} = \sqrt{\epsilon_{\text{measure}}^2 + \epsilon_{\text{model}}^2 + \epsilon_{\text{sampling}}^2 + \epsilon_{\text{prediction}}^2}, \quad (5.18)$$

where each of the terms are the relative errors at that pixel scale. Using the above equation, the errors at the pixel level will be propagated and a map of the uncertainty at the pixel level will be created. The main requirement for a pixel-level map of uncertainty is to be able to have a pixel-level prediction error from the model. The prediction error for SAR estimation of biomass at the pixel level is often developed through a boot-strapping approach where the model errors are simulated to generate different predictions for the pixel scale AGB and to produce the mean and use the variance as the prediction uncertainty or error.

5.7.3 REGIONAL INFERENCE OF BIOMASS

The goal of regional estimate of biomass and forest carbon stocks is to be able to develop emission factors for calculating emissions and removals from different types of human-induced disturbances in the forest such as deforestation, degradation, regeneration, or agroforestry. The problem then is to be able to use the estimates of biomass at the map units (pixel scale) from SAR data to estimate the mean and variance (uncertainty) of the biomass at large scales. The mean is estimated by the average of the biomass of all pixels for a region. However, for estimating the variance several components of errors must be included in the calculation, such as the errors associated with the spatial correlation of

biomass estimates at the pixel level.

5.7.3.1 Spatial Autocorrelation

To demonstrate the existence of spatial autocorrelations among the biomass estimates at the pixel level, the use of semivariogram analysis (Isaaks & Srivastava 1990) is recommended. The variogram-based approaches assume that the spatial autocorrelation of variables only depends on the distance h , while it has no other directional or locational dependence. The variogram $\gamma(h)$ is defined as

$$\gamma(h) = \frac{1}{2} E \left[\left(y_{x_i} - y_{x_j} \right)^2 \right] = [C(0) - C(h)], \quad (5.19)$$

where $||x_i - x_j|| = h$ and $C(h)$ is the covariogram depending on the distance h . In addition to above uncertainty at the pixel scale, to calculate the uncertainty at the regional level for forest biomass, the spatial correlation of the errors at the pixel level much be considered. The spatial correlation derived from semivariogram analysis will provide the variance to the estimate of the error using the following model

(see VT0005) (Weisbin et al. 2014).

$$\sigma_L^2 = P^{-1} \left[\frac{1}{m} \sum_{i=1}^m \sigma_{ui}^2 + 2 \sum_{i=1}^m \sum_{j<i}^m \rho(d) \sigma_{ui} \sigma_{uj} \right] \quad (5.20)$$

and

$$\rho(d) = \exp \left(-\frac{d}{\alpha} \right), \quad (5.21)$$

where

- $P = 1$ (representing the size of the pixel as 1 ha)
- i, j are the generic indices representing pixels in the biomass map
- n is the number of pixels within each LULC or stratum
- r is the range from semivariogram estimating the spatial correlation of errors associated with the AGB pixel level errors
- c is the parameter of fit for exponential spatial correlation function derived from semivariogram analysis. $c = 1/3$ is the default value (Chilès & Delfiner 2012) (unitless)
- d is the distance between pixels i and j within m (pixels)

ERROR PROPAGATION ESTIMATING AGB FROM SAR DATA

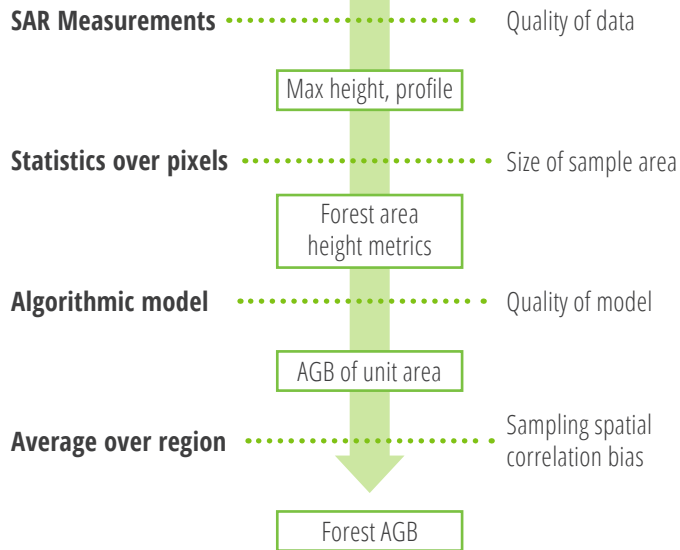


Figure 5.31 Schematic showing the main sources of uncertainty in SAR estimation of AGB and the process of error propagation for total uncertainty assessment.

- $\rho(d)$ is the spatial correlation function in terms of distance d based on exponential semivariogram model (unitless)
- σ_f^2 is the variance derived from a priori RS data, a pilot study, or default values of AGB density for the LULC class
- m is a dummy large number representing pixels in the map for each LULC. The number can be arbitrarily large or at least twice the default value of range r
- $\sigma_{wi,j}^2$ is the estimated variance associated with AGB values for each 1-ha pixel of the map

By assuming a pixel level uncertainty that is derived from the bootstrapping approach of SAR-biomass relationship or from the machine-learning algorithm of (σ_i) at each pixel, the uncertainty of the mean biomass at the regional scale can be evaluated using:

$$\begin{aligned} \sigma^2 = & \frac{1}{N^2} \left(\sum_{i=1}^N \sum_{j=1}^N \text{cov}(\sigma_{\varepsilon,i}, \sigma_{\varepsilon,j}) \right) \\ & + \frac{1}{N^2} \left(\sum_{i=1}^N \sum_{j=1}^N \text{cov}(\sigma_{f,i}, \sigma_{f,j}) \right) \\ & + \frac{1}{N^2} \left(\sum_{i=1}^N \sum_{j=1}^N \text{cov}(\sigma_{z,i}, \sigma_{z,j}) \right), \end{aligned} \quad (5.22)$$

where N is the total number of pixels, σ_ε , σ_f and σ_z are the pixel-level errors from (1) spatial mapping uncertainty, (2) allometric equation uncertainty, and (3) uncertainty of predictor variables from SAR backscatter, respectively. The three sources of errors are assumed independent, so that the overall uncertainty of regional estimates comes from the three covariance terms.

The first covariance using spatial autocorrelation is modelled

$$\begin{aligned} \sigma_\varepsilon^2 = & \frac{1}{N^2} \left(\sum_{i=1}^N \sigma_i^2 + \sum_{i=1}^N \sum_{j(j \neq i)}^N \rho_{ij} \sigma_i \sigma_j \right) \\ & \sum_{p=1}^m \sum_{q=1}^m \left(\underline{g}_p \text{cov}(\phi_p, \phi_q) \underline{g}_q \right), \end{aligned} \quad (5.23)$$

where ρ_{ij} is the correlation coefficient between pixels i and j , and it can be approximated from the variogram (Eq. (5.19)) normalized $C(h)$ under the assumption that spatial autocorrelation only changes with distance h .

The second covariance is related only to the allometric model coefficients and can be reformulated as

$$\begin{aligned} \sigma_f^2 = & \sum_{p=1}^m \sum_{q=1}^m \left(\frac{1}{N} \sum_{i=1}^N \frac{\partial f}{\partial \phi_p} \right) \text{cov}(\phi_p, \phi_q) \left(\frac{1}{N} \sum_{j=1}^N \frac{\partial f}{\partial \phi_q} \right) \\ = & \sum_{p=1}^m \sum_{q=1}^m \left(\underline{g}_p \text{cov}(\phi_p, \phi_q) \underline{g}_q \right), \end{aligned} \quad (5.24)$$

where $\underline{g}_p = \frac{1}{N} \sum_{i=1}^N \frac{\partial f}{\partial \phi_p}$ is the mean of first derivative with respect to the allometric model coefficient ϕ_p , and m is the total number of coefficients in the allometric model—or in lidar-AGB model, m equals to 2. In the case that the biomass values used to calibrate the SAR data are from ground plots and not the lidar-AGB model, one can assume a certain fixed value as the uncertainty of the biomass from the tree allometry (Chave et al. 2014, Chave et al. 2005), or assume the value is 0.

The third covariance is related to the measurement errors. In the case of the lidar-AGB model, σ_z is the error associated lidar mean canopy height. Without in-situ validation of height measurements, it is impossible to evaluate this type of error. Discussion in the main paper has shown that at least the model-based height interpolation is very accurate and the error in 1-ha resolution is negligible. In the case of SAR, this error may be related to backscatter error associated with the radiometric calibration. This uncertainty can be a fixed value (1 dB for all pixels) or a value that varies depending on the SAR range and azimuth or the local incidence angle as a result of the terrain topographical complexity. Calculating the measurement errors of terrain-corrected SAR backscatter may be difficult and beyond the scope of this chapter. Therefore, the use of a calibration error recommended by the SAR processing team or available in the literature is recommended. For further readings on the uncertainty of inference of biomass at the regional level see McRoberts et al. (2017), Ene et al. (2017), Naesset et al. (2016), and Xu et al. (2017).

5.7.4 PRACTICAL CONSIDERATION FOR UNCERTAINTY CALCULATION

For validation of SAR-derived biomass maps, methodologies that can help improve the uncertainty

estimates or reduce the uncertainty are identified as part of the IPCC good practice guidelines. The biomass map can be distributed to the community to be used for land use planning, REDD+ projects, and the Emission Reduction (ER) programs; and in all applications, formal uncertainty assessments are required. Regional evaluation of the map can be performed by using inventory plots or airborne lidar data and site-specific lidar biomass allometry that together allow the estimation of the potential bias and the evaluation of the spatial consistency of the map. The methodology to develop regional estimates of forest biomass must follow one of the many standard protocols established by forest inventory techniques or the IPCC guidelines. For lidar sampling, a certified methodology that can be used for regional forest biomass estimation has already been developed. The methodology was developed by Sassan Saatchi and recently developed as a VCS tool with the collaboration of Terra Global Capital as VT0005 (see the attached appendix). At the time of releasing the map, ground data was too limited to have a comprehensive evaluation of the map regionally or locally. Here, a set of protocols is recommended for those who are interested in evaluating the map further at the local or regional scale.

- The biomass map derived from SAR is considered to have both systematic and random errors. The uncertainty of the map depends strongly on the input biomass data used for training and evaluating the results. Any errors in ground-based allometry and the lidar derived biomass as reference can impact the estimation and the map's accuracy.
- The biomass estimates in the map can be readily updated and improved when more data becomes available. Increasing the number of ground-estimated forest biomass, use of forest specific models, use of multitemporal SAR images for biomass estimation are critical steps to improve the accuracy of the map.
- For evaluating the map at regional scales (>10,000 ha), samples of lidar and plot data can be used. Any plots that are designed statistically to estimate the mean biomass with a high confidence interval (90%) can be used to compare with the

map pixel values. At the scale of parks, concessions, and communities, the biomass map can be used along with any land cover map to develop mean biomass density and can be compared with independent inventory data available for the same region.

- The map can also be evaluated at the pixel scale (e.g., 1 ha). However, for the comparison, the following precautions must be considered:
 - The plots have to be a minimum of 1 ha or larger. Using smaller plots is not recommended, as the biomass of the forest is extremely heterogeneous, particularly at scales of less than 1 ha.
 - The 1-ha plots chosen for comparison with the map have to be aligned with the map pixel orientation. Any plots with different orientation may have large uncertainty when compared to the map because of the variations of the biomass at the 1-ha scale.
 - The map also includes an uncertainty number associated with the biomass of each pixel. Any comparison with the pixel value biomass should consider the error provided for the pixel.
 - The number of plots must be larger than a few. Comparison only makes sense when it is statistically designed. Using one or a few plots will not provide any realistic and fair comparison of the map. It is recommended that at least 20–30 plots be used in statistically evaluating the map and comparing the results with the uncertainty provided.

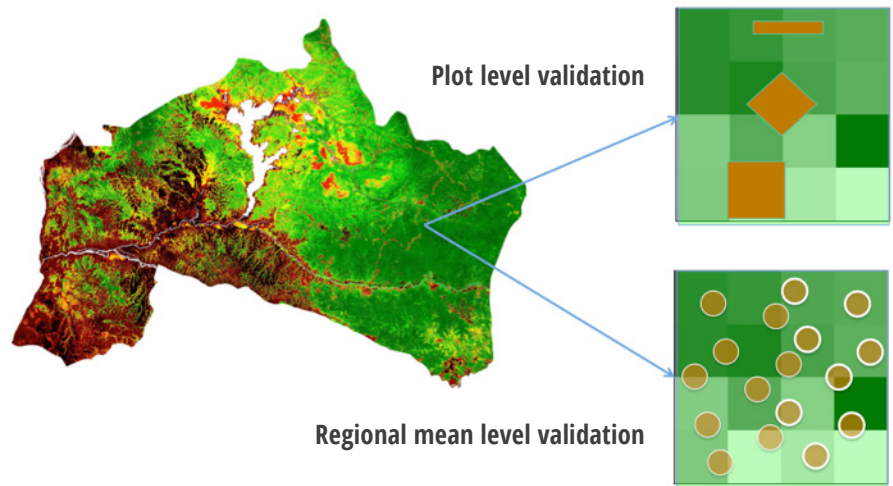


Figure 5.32 Methodology to evaluate the forest biomass map locally or at the pixel level using field inventory plots. For local evaluation, inventory plots must follow a statistical design to allow accurate mean AGB values. For pixel-level evaluation, plots must be equal to or larger than the pixel and must be oriented to maximize the overlay of the best spatial match between the pixel and the plot biomass.

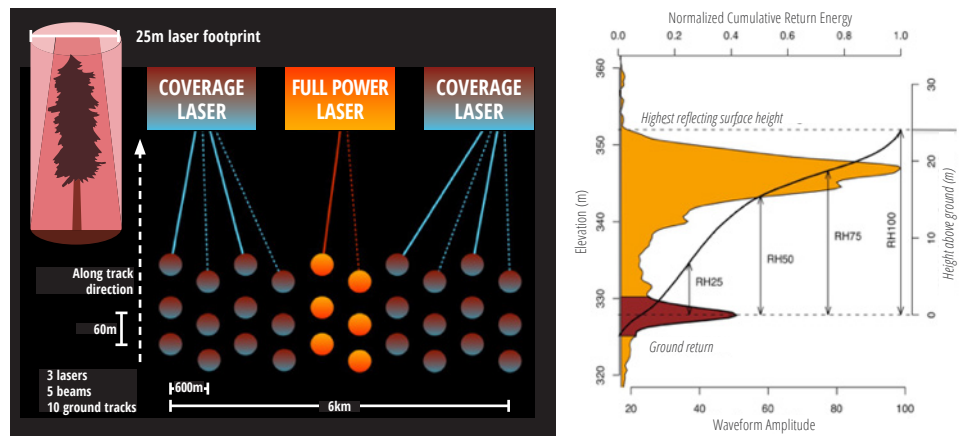


Figure 5.33 Distribution of GEDI footprints across the landscape from the three lasers and multiple beams (left panel) and the typical distribution of forest vertical structure captured by the GEDI footprint level waveforms.

5.8 Future Biomass Missions

5.8.1 GEDI (LAUNCH 2018–2019)

The scientific goal of GEDI is to characterize the effects of changing climate and land use on ecosystem structure and dynamics to enable improved quantification and understanding of the Earth's carbon cycle and biodiversity. Focused on tropical and temperate forests from its vantage point on the International Space Station (ISS), GEDI uses a lidar sensor (near infrared 1,064-nm wavelength) to provide the first global, high-resolution (25 m) sampling observations

of forest vertical structure. GEDI addresses three core science questions: (1) What is the aboveground carbon balance of the land surface? (2) What role will the land surface play in mitigating atmospheric CO₂ in the coming decades? (3) How does ecosystem structure affect habitat quality and biodiversity? Answering these questions is critical for understanding the future path of global climate change and the Earth's biodiversity.

GEDI informs these science questions by collecting ~12 billion cloud-free land-surface lidar waveform (vertical profile) observations over a two-year

mission lifetime. The instrument uses three laser transmitters split into five beams that are dithered to produce 10 parallel ground tracks of 25-m footprints (Fig. 5.33). GEDI will produce estimates of canopy height, elevation, and vertical canopy profile measurements. The 25-m (~0.0625 ha) footprint measurements are used to model AGB and then used to derive mean AGB and variance on a 1-km grid.

5.8.1.1 GEDI CAL/VAL Requirements

From its vantage point on the ISS, GEDI is focused on tropical and temperate forests between 51.5°S

and 51.5°N. The GEDI biomass calibration strategy is to develop globally representative pre-launch models for footprint AGB using near-coincident airborne laser scanning (ALS) data and plot inventory data. Mean and standard error of AGB for 1-km grid cells are then estimated from the modelled footprint AGB via statistical inference. The baseline requirement for GEDI is that the standard error of AGB estimates within 80% of Level 4B gridded product at 1-km cells will be <20 Mg ha⁻¹ or 20%, whichever is greater. The GEDI science products are developed using a series of airborne lidar and ground plots globally and models to estimate biomass from GEDI waveforms. These datasets are sampled globally to be representative of major forest types.

5.8.2 NISAR MISSION (LAUNCH 2021)

NISAR is a joint project between [NASA](#) and [ISRO](#) to co-develop and launch the first dual-frequency SAR satellite. NASA will provide the L-band (24-cm wavelength), and ISRO will provide the [S-band](#) (12-cm wavelength). The mission will acquire polarimetric and interferometric observations at an unprecedented coverage in space and time, which is optimized for studying changes of the global Earth surface.

NISAR will focus on the most dynamic ecosystems such as disturbed and recovering forests, inundated wetlands, and croplands. NISAR will measure aboveground woody vegetation biomass and its disturbance and recovery globally at the hectare scale; biomass accuracy shall be 20 Mg/ha or better for areas of woody biomass ≤100 Mg/ha over at least 80% of these areas. Therefore, the mission will focus on areas of low biomass, covering a significant portion of boreal, temperate, and savanna woodlands. It will provide seasonal to annual observations of biomass change in the most dynamic forests impacted by AGB disturbance and recovery. The NISAR mission will be able to provide L-band dual pol (HH, HV) observations every 12 days in ascending and descending orbits covering global forests every 6 days. These observations will be used to produce maps of the distribution of forest biomass at 1-ha grid cells. The NISAR radar is designed for global InSAR measurements, but the science products produced do not

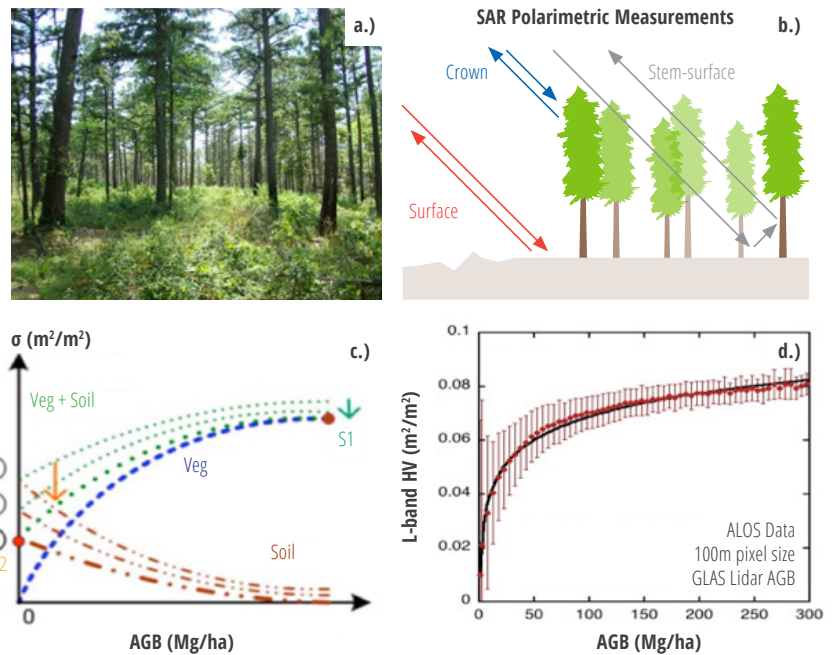


Figure 5.34 Schematic showing a typical northern conifer forest (a) simulated to an ensemble of trees with stems, branches, and leaves (b) exposed to L-band radar energy with dominant scattering from forest components, (c) suggesting the combined influence of structure and soil moisture on radar backscatter with reduced sensitivity to biomass at higher AGB values. The last panel (d) shows the sensitivity of radar backscatter at L-band HV polarization showing the sensitivity to biomass values < 100 Mg/ha with sample data from the entire northern coniferous forests (Yu & Saatchi 2016).

include direct information on the vertical structure of forests. Rather, AGB is estimated from backscatter measurements and exploits either empirical statistical approaches or inversion of physically-based scattering models that must be calibrated over study sites globally to capture the structural and composition differences of forests in different ecoregions.

The NISAR algorithm is based on an analytical semi-empirical model with coefficients that are calibrated with structure and biomass information from ground measurements. The forest inventory data available in a network of calibration plots distributed globally in different ecoregions (15 ecoregions as discussed in [Sec. 5.6](#)) and accompanied by airborne lidar observations to extend the ground observations and enable validation of the spatial variations of AGB. The size of plots used for calibration of the NISAR algorithm must be either >1 ha if used directly with the SAR data or smaller (~0.25 ha) if used in conjunction with the ALS observations. In addition, forest inventory data can be used to evaluate and report the

uncertainty of NISAR AGB at the national or regional scale and for carbon accounting and assessments.

5.8.3 BIOMASS (LAUNCH: 2022)

Biomass, the ESA's seventh Earth Explorer mission will be launched in the 2020–2021 timeframe and has the aim of providing crucial information about the state of the forests and how they are changing globally. The mission goal is to provide estimates of height and AGB in the world's forests. The science case on which Biomass was selected is based on its ability to provide estimates of AGB within dense tropical forests to monitor their storage and changes from disturbance at seasonal and annual frequency. The requirement for the Biomass mission is to estimate forest biomass with an accuracy of ≤20% for more than 67% of areas with biomass >50 Mg/ha on a 4-ha spatial grid cell (200-m x 200-m pixels) every six months for a period of five years of the mission duration. This requirement is achieved by using a P-band (70 cm wavelength) SAR sensor, because

of its unique capabilities to penetrate even dense tropical forest. The measurements will provide radar polarimetric backscatter (HH, HV, VH, VV) and interferometric observation with PolInSAR capability for forest height estimation and TomoSAR capability for backscatter vertical profile measurements.

In addition, the Biomass mission will provide global maps of forest height at the same 4-ha spatial scale for all forests >10-m height with 30% accuracy and include a 50-x-50-m deforestation map globally every six months. These measurements together, will significantly improve the ability to reduce the uncertainty in the global carbon cycle by providing spatially refined and temporally frequent observation of carbon fluxes in forest ecosystems.

The coverage of Biomass is global with a restriction, imposed by the U.S. Department of Defense Space Objects Tracking Radar (SOTR) stations, over Europe and the North and Central Americas. Under these restrictions, only 3% of AGB carbon stock coverage is lost in the tropical forest biome, which constituted 66% of global AGB carbon stocks in 2005. The loss is more significant in the temperate (72%), boreal (37%), and subtropical (29%) biomes. The calibration/validation (CAL/VAL) requirements of Biomass are primarily focused in tropical forest ecosystems, where the bulk of mission observations are located. The biomass and structure algorithms require large ground plots (>4 ha) or lidar-derived AGB estimates from airborne observations. These measurements must represent the variations of tropical forest structural types and allometric characteristics and must be repeated during the mission to allow validation of both biomass stocks and changes from disturbance and recovery.

5.8.4 CROSS-MISSION SYNERGISM

All three missions have significant overlaps in science objectives and products but focus on different observations, covering different regions, and retrieving different components of AGB at different spatial and temporal scales. The cross-mission synergism is based on the following observations and assessments from the breakout sessions:

- **Area coverage** and the science products from the space missions are immediately rec-

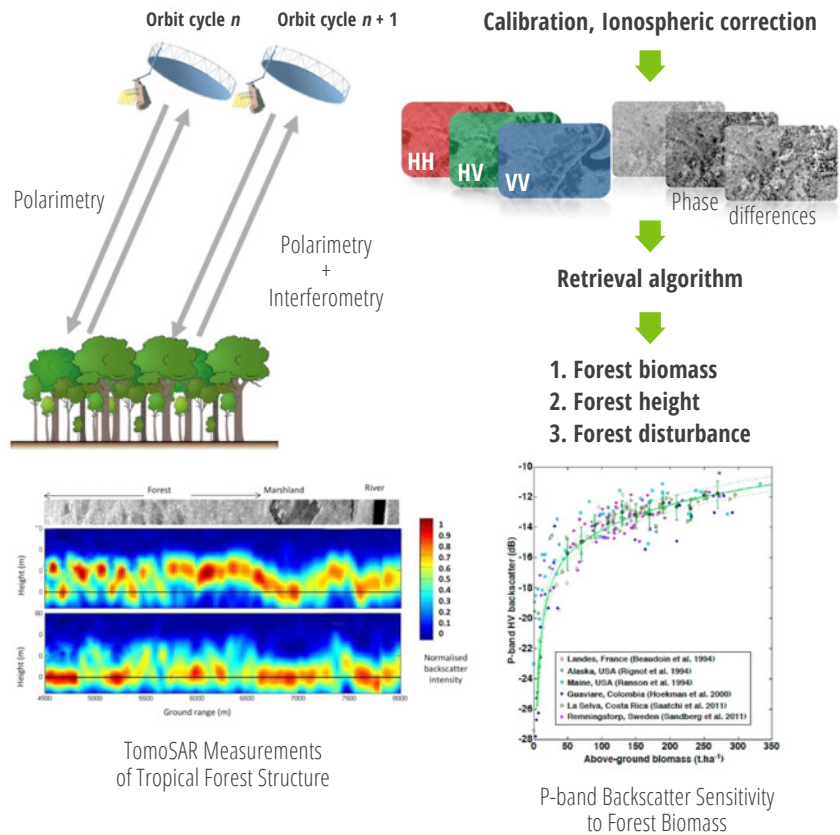


Figure 5.35 Biomass mission P-band SAR measurements showing the configuration of space measurements and the sensitivity of backscatter power and interferometry to forest structure.

ognized as complementary such that without the data from all the missions, wall-to-wall coverage, and estimation of the global forest biomass are impossible. Biomass focuses on tropical and subtropical woodlands at 4 ha, while NISAR is global but limited to areas of low forest biomass at 1 ha, and GEDI not limited by AGB, but with limited coverage collecting sample footprints within ± 50 degrees latitude.

- **Differences in biomass components** retrieved by each space mission suggest that a synergistic global AGB product cannot be mechanically produced by combining the maps, but rather requires a systematic data fusion approach. For reference, BIOMASS will estimate AGB when woody biomass is > 50 Mg/ha, NISAR will estimate AGB when woody and leafy biomass is < 100 Mg/ha, and GEDI will estimate AGB for the entire range from height measurements within each 25 m footprint.

- **Leverage the sensitivities of each measurement approach to cross-calibrate space mission products** can be achieved by using the measurements and products of one mission to CAL/VAL the algorithm or products of other missions. Although every space mission has a different method for estimating AGB, thus making it difficult to directly compare between products, an approach could be used that compares either similar lower level products or leverages different algorithm sensitivities (e.g., NISAR can provide more robust estimates for forests with 20 Mg/ha than for grasslands with ≤ 5 Mg/ha). For example, GEDI forest height may be used to develop and verify algorithms for the Biomass tomography-derived tree height. Similarly, height or backscatter products from NISAR and Biomass missions can provide information on the spatial variability of forest structure and biomass to improve the algorithm and resolu-

tion of GEDI height and biomass gridded products.

- **NISAR and Biomass measurements spatially overlap**, thus enabling data fusions such as (1) the combined measurements of L-band P-band for improving the estimates of low-biomass forests, (2) the use of higher temporal frequency NISAR observations to reduce the effects of soil moisture and vegetation

phenology on the BIOMASS estimation approach, (3) the deployment of a two-frequency algorithm to enable estimation of leaf, branch, and stem biomass, and (4) the use of combined measurements to increase sensitivity of the observations for detecting low-impact forest degradation and slow recovery.

- **Additional ecological science products** may be produced from synergistic integration

of data that enables exploration of the physical characteristics of each measurement. For example, other forest variables such as basal area, volume, branch, leaf, and stem biomass, and forest stand wood density may be derived using the combined sensitivity of radar observations to dielectric constants and tree stem and crown volumes, and ability of lidar waveforms to measure the vertical distributions and canopy gaps.

MISSION	Measurement	Product	Area Coverage	Grid Cell	Accuracy	Pre-launch Cal/Val Mission	Cal/Val needs	Post-launch Cal/Val	Sites
GEDI	Height	Height Metrics	50 deg. Latitude	25m footprint; 500m grid	~1m (canopy top footprint level)	ALS & LVIS flights RT modeling	LVIS samples globally	No validation requirement	International; crowd-sourced
	Waveform	Aboveground biomass (entire range)	50 deg. Latitude	25m footprint; 1 km grid	20 Mg or 20% at 1km, 80% px std. err.; mission	Footprint calibration equations; sampling simulations, ALS & LVIS flights	ALS-derived biomass from ground plot at 1 km grids	No validation requirement	NFI data supersites with ALS-derived biomass > 100 ha
BIOMASS	HH, HV, VH, VV Backscatter	Aboveground biomass (entire range)	Global (excluding North/Central America, Europe)	200 m (4 ha)	20% or 10 Mg/ha for biomass < 50 Mg/ha annual	Combined radar backscatter and TomoSAR & POLinSAR algorithm	Plots > 4 ha & ALS; across ecoregions	NFI & regional samples ALS & plots > 4 ha	NFI data CTFS; ForestGeo
	POLinSAR	Forest Height	Global (excluding North/Central America, Europe)	200 m (4 ha)	20% of total height	POLinSAR height algorithm	ALS & LVIS data distributed across ecoregions	Same approach as pre-launch	Distributed large plots
	TomoSAR Vertical Profile	TBD	Global (excluding North/Central America, Europe)	200 m (4 ha)	TBD	TomoSAR vertical structure	ALS & LVIS data distributed across ecoregions	Same approach as pre-launch	ALS and LVIS data
	Time Series	Forest Disturbance	Global (excluding North/Central America, Europe)	50 m (0.25 ha)	90% of pixels, annual	Optical imagery time series over selected sites	Landsat time series data, high-resolution imagery	Same approach as pre-launch	Distributed globally at deforestation hot spots
NISAR	HH & HV Backscatter	Aboveground biomass < 100 Mg/ha	Global low biomass areas	100 m (1 ha)	20 Mg/ha, 80% px < 100 Mg; annual	Radar biomass equations, algorithm	Plots > 1 ha & ALS data across ecoregions	NFI & regional samples ALS & plots > 1 ha	NFI data Distributed large plots & ALS data
	Time Series	Disturbance > 50% change in canopy cover	Global forests	100 m (1 ha)	80% of pixels, annual	High-res optical & ALOS/SAOCOM time series over selected sites	Landsat time series data, high-resolution imagery	Same approach as pre-launch	Distributed globally at deforestation hot spots

Table 5.7 Overall characteristics of the NASA and ESA missions to quantify the global forest structure and biomass that can be used to develop synergistic biomass products

5.9 References

- Andersen, H. E., S. E. Reutebuch, R. J. McGaughey, M. V. N. d'Oliveira, M. Keller. (2014). Monitoring selective logging in western Amazonia with repeat lidar flights. *Remote Sensing of Environment*, 151: 157 – 165.
- Arlot, S., and A. Celisse. (2010). A survey of cross-validation procedures for model selection. *Statistics Surveys*, 4, 40-79.
- Asner, G. P., J. Mascaro. (2014). Mapping tropical forest carbon: Calibrating plot estimates to a simple Lidar metric. *Remote Sensing of Environment*, 140, 614 – 624.
- Asner, G. P., G. V. N. Powell, J. Mascaro, D. E. Knapp, J. K. Clark, J. Jacobson, T. Kennedy-Bowdoin, A. Balaji, G. Paez-Acosta, E. Victoria, L. Secada, M. Valqui, and R. F. Hughes. (2010). High-resolution forest carbon stocks and emissions in the Amazon. *Proceedings of the National Academy of Sciences of the United States of America*, 107(38), 16738 – 16742.
- Attema, E. P. W., and F. T. Ulaby. (1978). Vegetation modeled as a water cloud. *Radio Science*, 13(2), 357 – 364.
- Baccini, A., S. J. Goetz, W. S. Walker, N. T. Laporte, M. Sun, D. Sulla-Menshe, J. Hackler, P. S. A. Beck, R. Dubayah, M. A. Friedl, S. Samanta, and R. A. Houghton. (2012). Estimated carbon dioxide emissions from tropical deforestation improved by carbon-density maps. *Nature Climate Change*, 2, 182-185.
- Baghdadi, N., C King, A. Bourguignon, and A. Remond. (2010). Potential of ERS and Radar-sat data for surface roughness monitoring over bare agricultural fields: Application to catchments in Northern France. *International Journal of Remote Sensing*, 23(17), 3427 – 3442.
- Berger, A. L., and V. J. D. Pietra. (1996). A maximum entropy approach to natural language processing. *Computational Linguistics*, 22(1), 39-71.
- Bonan, G. B. (2008). Forests and climate change. *Forcings, Feedbacks, and the Climate Benefits of Forests. Science*, 320(5882), 1444-1449.
- Boudreau, J., Nelson, R. F., Margolis, H. A., Beaudoin, A., Guindon, L., & Kimes, D. S. (2008). Regional aboveground forest biomass using airborne and spaceborne lidar in Québec. *Remote Sensing of Environment*, 112(10), 3876-3890.
- Bouvet, A., Mermoz, S., Le Toan, T., Villard, L., Mathieu, R., Naidoo, L., & Asner, G. P. (2018). An above-ground biomass map of African savannahs and woodlands at 25m resolution derived from ALOS PALSAR. *Remote Sensing of Environment*, 206, 156-173.
- Breiman, L. (2001) *Machine Learning* 45: 5.
- Brown, S. (1997). *Estimating biomass and biomass change of tropical forests: a primer* (Vol. 134). Food & Agriculture Org.
- Brown, S., 2002. *Measuring carbon in forests: current status and future challenges. Environmental pollution*, 116(3), pp.363-372.
- Bryant, R., M. S. Moran, D. P. Thoma, C. D. Holifield Collins, S. Skirvin, M. Rahman, K. Slocum, P. Starks, D. Bosch, M. P. Gonzalez Dugo. (2007). Measuring surface roughness height to parameterize radar backscatter models for retrieval of surface soil moisture. *IEEE Geoscience and Remote Sensing Letters*, 4(1), 137 – 141.
- Canadell, J. G., and M. R. Raupach. (2008). Managing forests for climate change mitigation. *Science*, 320(5882), 1456 – 1457.
- Cartus, O., M. Santoro, J. Kelldorfer. (2012). Mapping forest aboveground biomass in the northeastern United States with ALOS PALSAR dual-polarization L-band. *Remote Sensing of Environment*, 124, 466-478.
- Change, I. P. O. C. (2006). 2006 IPCC guidelines for national greenhouse gas inventories. 2013-04-28]. <http://www.ipcc-nggip.iges.or.jp/public/2006gl/index.html>.
- Chambers, J. Q., J. dos Santos, R. J. Ribeiro, N. Higuchi. (2001). Tree damage, allometric relationships, and above-ground net primary production in central Amazon forest. *Forest Ecology and Management*, 152(1-3), 73 – 84.
- Chauhan, N. S., D. M. Le Vine, R. H. Lang. (1994). Discrete scatter model for microwave radar and radiometer response to corn: Comparison of theory and data. *IEEE Geoscience and Remote Sensing Society*, 32(2), 416 – 426.
- Chauhan, N. S., R. H. Lang, K. J. Ranson. (1991). Radar modeling of a boreal forest. *IEEE Transactions on Geoscience and Remote Sensing*, 29(4), 627 – 638.
- Chave, J., Andalo, C., Brown, S., Cairns, M. A., Chambers, J. Q., Eamus, D., ... & Yamakura, T. (2005). Tree allometry and improved estimation of carbon stocks and balance in tropical forests. *Oecologia*, 145(1), 87-99.
- Chave, J., Condit, R., Aguilar, S., Hernandez, A., Lao, S., & Perez, R. (2004). Error propagation and scaling for tropical forest biomass estimates. *Philosophical Transactions of the Royal Society of London. Series B: Biological Sciences*, 359(1443), 409–420.
- Chave, J., Réjou-Méchain, M., Búrquez, A., Chidumayo, E., Colgan, M. S., Delitti, W. B., ... & Vieilledent, G. (2014). Improved allometric models to estimate the aboveground biomass of tropical trees. *Global change biology*, 20(10), 3177-3190.
- Chen, Q., Laurin, G. V., & Valentini, R. (2015). Uncertainty of remotely sensed aboveground biomass over an African tropical forest: Propagating errors from trees to plots to pixels. *Remote Sensing of Environment*, 160, 134–143.
- Chilès, J. P., and P. Delfiner. (2012). *Geostatistics: Modeling Spatial Uncertainty*. John Wiley & Sons, Inc: New York.

- Ciais, P., C. Sabine, G. Bala, L. Bopp, V. Brovkin, J. Canadell, A. Chhabra, R. DeFries, J. Galloy, M. Heimann, C. Jones, C. Le Quere, R. B. Myneni, S. Piao, and P. Thorton. (2013). Carbon and other biogeochemical cycles. In *Climate Change 2013. The Physical Science Basis. Contribution of Working Group I to the Fifth Assessment Report of the Intergovernmental Panel on Climate Change* [Stocker, T.F., D. Qin, G.K. Plattner, M. Tignor, S.K. Allen, J. Boschung, A. Nauels, Y. Xia, V. Bex, and P.M. Midgley (eds)]. Cambridge University Press, Cambridge, United Kingdom and New York, NY, USA.
- Cloude, S. (2010). *Polarisation: applications in remote sensing*. Oxford University Press.
- Clark, D. B., and J. R. Kellner (2012). Tropical forest biomass estimation and the fallacy of misplaced concreteness. *Journal of Vegetation Science*, 23, 1191 – 1196.
- Cugois, P. C., J. van Zyl, T. Engman. (1995). Measuring soil moisture with imaging radars. *IEEE Transactions on Geoscience and Remote Sensing*, 33(4), 915 – 926
- Del Frate, F., & Solimini, D. (2004). On neural network algorithms for retrieving forest biomass from SAR data. *IEEE Transactions on Geoscience and Remote Sensing*, 42(1), 24-34.
- Dobson, M. C., F. T. Ulaby, L. E. Pierce, T. L. Sharik, K. M. Bergen, J. Kellndorfer, J. R. Kendra, E. Li, Y. C. Lin, A. Nashashibi, K. Sarabandi, P. Siqueira. (1995). Estimation of forest biophysical characteristics in northern Michigan with SIR-C/X-SAR. *IEEE Transactions on Geoscience and Remote Sensing*, 33(4): 877 – 895.
- Dobson, M. C., F. T. Ulaby, T. LeToan, A. Beaudoin, E. S. Kasischke, N. Christensen. (1992). Dependence of radar backscatter on coniferous forest biomass. *IEEE Transactions on Geoscience and Remote Sensing*, 30(2), 412-415.
- Dobson, M. C., F. T. Ulaby. (1986). Preliminary Evaluation of the SIR-B Response to Soil Moisture, Surface Roughness, and Crop Canopy Cover. *IEEE Transactions on Geoscience and Remote Sensing*, GE-24(4): 517 – 526.
- Drake, J. B., Dubayah, R. O., Clark, D. B., Knox, R. G., Blair, J. B., Hofton, M. A., ... & Prince, S. (2002). Estimation of tropical forest structural characteristics using large-footprint lidar. *Remote Sensing of Environment*, 79(2), 305-319.
- Dubayah, R. O., & Drake, J. B. (2000). lidar remote sensing for forestry. *Journal of Forestry*, 98(6), 44-46.
- Dungan, J. L., Perry, J. N., Dale, M. R. T., Legendre, P., Citron-Pousty, S., Fortin, M. J., ... & Rosenberg, M. (2002). A balanced view of scale in spatial statistical analysis. *Ecography*, 25(5), 626-640.
- Elith, J., S. T. Phillips, T. Hastie, M. Dudik, Y. E. Chee, C. J. Yates. (2010). A statistical explanation of MaxEnt for ecologists. *Diversity and Distributions*, 17(1), 43 – 57.
- Ene, L. T., Næsset, E., Gobakken, T., Bollandsås, O. M., Mauya, E. W., & Zahabu, E. (2017). Large-scale estimation of change in aboveground biomass in miombo woodlands using airborne laser scanning and national forest inventory data. *Remote Sensing of Environment*, 188, 106-117.
- Englhart, S., Jubanski, J., & Siegert, F. (2013). Quantifying dynamics in tropical peat swamp forest biomass with multi-temporal lidar datasets. *Remote Sensing*, 5(5), 2368-2388.
- FAO. (2015). *Global Forest Resources Assessment 2015*, FAO, Rome, Italy.
- Ferraz, A., S. Saatchi, C. Mallet, V. Meyer. (2016). Lidar detection of individual tree size in tropical forests. *Remote Sensing of Environment*, 183, 318 – 333.
- Freeman, A. and S. L. Durden. (1998). A three-component scattering model for polarimetric SAR data. *IEEE Transactions on Geoscience and Remote Sensing*, 36(3), 963 – 973.
- Fung, A. K., and K. S. Chen. (1992). Dependence of the surface backscattering coefficients on roughness, frequency, and polarization states. *International Journal of Remote Sensing*, 13(9), 1663 – 1680.
- García, M., Saatchi, S., Casas, A., Koltunov, A., Ustin, S. L., Ramirez, C., & Baltzer, H. (2017). Extrapolating forest canopy fuel properties in the California Rim Fire by combining airborne lidar and Landsat OLI Data. *Remote Sensing*, 9(4), 394.
- Gibbs HK, Brown S (2000) Geographical distribution of woody biomass carbon stocks in tropical Africa: An updated database for 2000. Available at <http://cdiac.ornl.gov/epubs/ndp/ndp0555/ndp05b.html> from the Carbon Dioxide Information Center, Oak Ridge National Laboratory, Oak Ridge, TN. Accessed 2009.
- Gibbs, H. K., S. Brown, J. O. Niles, J. A. Foley. (2007). Monitoring and estimating tropical forest carbon stocks: Making REDD a reality. *Environmental Research Letters*, 2(4), 045023.
- Gibbs, H. K., S. Yui, R. Plevin. (2014). *New Estimates of Soil and Biomass Carbon Stocks for Global Economic Models*. Working Paper: Purdue University.
- Hajnsek, I., Kugler, F., Lee, S. K., & Papathanassiou, K. P. (2009). Tropical-forest-parameter estimation by means of Pol-InSAR: The INDREX-II campaign. *Geoscience and Remote Sensing, IEEE Transactions on*, 47(2), 481-493.
- Hallé, F., and R. A. A. Oldeman. (1975). *An essay on the architecture and dynamics of growth of tropical trees*.
- Hallé, F., R. A. A. Oldeman, and P. B. Tomlinson. (1978). Opportunistic tree architecture. In *Tropical Trees and Forests*, 269 – 331. Springer-Verlag, Berlin, Heidelberg.
- Hallikainen, M. T., F. T. Ulaby, M. C. Dobson, M. A. El-rayes, L. Wu. (1985). Microwave dielectric behavior of wet soil – part 1: empirical models and experimental observations. *IEEE Transactions on Geoscience and Remote Sensing*, GE-23(1), 25 – 34.
- Hansen, M. C., Potapov, P. V., Moore, R., Hancher, M., Turubanova, S. A., Tyukavina, A., ... & Townshend, J. R. G. (2013). High-resolution global maps of 21st-century forest cover change. *science*, 342(6160), 850-853.
- Harding, D. J., & Carabajal, C. C. (2005). ICESat waveform measurements of within-footprint topographic relief and vegetation vertical structure. *Geophysical research letters*, 32(21).

- Harris, N. L., Brown, S., Hagen, S. C., Saatchi, S. S., Petrova, S., Salas, W., ... & Lotsch, A. (2012). Baseline map of carbon emissions from deforestation in tropical regions. *Science*, 336(6088), 1573-1576.
- Hawkins, D. M., Basak, S. C., & Mills, D. (2003). Assessing model fit by cross-validation. *Journal of chemical information and computer sciences*, 43(2), 579-586.
- Hayashi, M., Saigusa, N., Yamagata, Y., & Hirano, T. (2015). Regional forest biomass estimation using ICESat/GLAS spaceborne lidar over Borneo. *Carbon Management*, 1-15.
- Heath, L. S., Smith, J. E., Skog, K. E., Nowak, D. J., & Woodall, C. W. (2011). Managed Forest Carbon Estimates for the US Greenhouse Gas Inventory, 1990-2008. *Journal of Forestry*, 109(3), 167-173.
- Hensley, S., Oveisgharan, S., Saatchi, S., Simard, M., Ahmed, R., & Haddad, Z. (2014). An error model for biomass estimates derived from polarimetric radar backscatter. *IEEE Transactions on Geoscience and Remote Sensing*, 52(7), 4065-4082.
- Hoekman, D. H., & Quiriones, M. J. (2000). Land cover type and biomass classification using AirSAR data for evaluation of monitoring scenarios in the Colombian Amazon. *Geoscience and Remote Sensing, IEEE Transactions on*, 38(2), 685-696.
- Houghton, R. A., A. Baccini, W. S. Walker. (2018). Where is the residual terrestrial carbon sink? *Global Change Biology*, 24(8), 3277 - 3279.
- Hyde, P., Dubayah, R., Walker, W., Blair, J. B., Hofton, M., & Hunsaker, C. (2006). Mapping forest structure for wildlife habitat analysis using multi-sensor (lidar, SAR/InSAR, ETM+, Quickbird) synergy. *Remote Sensing of Environment*, 102(1), 63-73.
- Isaaks, E., and R. Srivastava. (1990). *An Introduction to Applied Geostatistics*. Oxford University Press, Oxford, UK.
- Karam, M. A., A. K. Fung, R. H. Lang, N. S. Chauhan. (1992). A microwave scattering model for layered vegetation. *IEEE Transactions on Geoscience and Remote Sensing*, 30(4), 767-784.
- Karam, M. A., A. K. Fung, R. H. Lang, N. S. Chauhan. (1992). A microwave scattering model for layered vegetation. *IEEE Transactions on Geoscience and Remote Sensing*, 30(4), 767-784.
- Karam, M. A., and A. K. Fung. (1983). Scattering from randomly oriented circular discs with application to vegetation. *Radio Science*, 18(4), 557 - 565.
- Keller, M., M. Palace, G. Hurtt. (2001). Biomass estimation in the Tapajos National Forest, Brazil: Examination of sampling and allometric uncertainties. *Forest Ecology and Management* 154(3), 371-382.
- Ketterings, QM, Coe, R, Noordwijk, M, Ambagau, Y, Palm, CA (2001) Reducing uncertainty in the use of allometric biomass equations for predicting above-ground tree biomass in mixed secondary forests. *Forest Ecology and Management*, 146, 199 - 209.
- Lang, R. (1981). Electromagnetic backscattering from a sparse distribution of lossy dielectric scatterers. *Radio Science*, 16(1), 15 - 30.
- Lang, R. H., and J. S. Sighu. (1983). Electromagnetic backscattering from a layer of vegetation: A discrete approach. *IEEE Transactions on Geoscience and Remote Sensing*, GE-21(1), 62 - 71.
- Lawrence, M, RE McRoberts, E Tomppo, T Gschwantner, K Gabler. 2010. Comparisons of National Forest Inventories. In: Tomppo E., Gschwantner T., Lawrence M, R McRoberts (eds) *National Forest Inventories*. Springer, Dordrecht.
- Lee, J. S., M. R. Grunes, G. de Grandi. (1999). Polarimetric SAR speckle filtering and its implication for classification. *IEEE Geoscience and Remote Sensing*, 37(5), 2363 - 2373.
- Le Quere, C., R. M. Andrew, P. Friedlingstein, S. Sitch, J. Hauck, J. Pongratz, P. Pickers, J. I. Korsbakken, G. P. Peters, J. G. Canadell, A. Ameth, V. K. Arora, L. Barbero, A. Bastos, L. Bopp, F. Chevallier, L. P. Chini, P. Clais, S. C. Doney, T. Gkritzalis, D. S. Goll, I. Harris, V. Haverd, F. M. Hoffman, M. Hoppema, R. A. Houghton, T. Ilyina, A. K. Jain, T. Johannesen, C. D. Jones, E. Kato, R. F. Keeling, K. K. Goldewijk, P. Landschutzer, N. Lefevre, S. Lienert, D. Lombardozzi, N. Metz, D. R. Munro, J. E. M. S. Nabel, S. Nakaoka, C. Meill, A. Olsen, T. Ono, P. Patra, A. Peregon, W. Peters, P. Peylin, B. Pfeil, D. Pierrot, B. Poulter, G. Rehder, L. Resplandy, E. Robertson, M. Rocher, C. Rodenbeck, U. Schuster, J. Schwinger, R. Seferian, I. Skjelvan, T. Steinhoff, A. Sutton, P. P. Tans, H. Tian, B. Tilbrook, F. N. Tubiello, I. T. van der Laan-Luijckx, G. R. van der Werf, N. Viovy, A. P. Walker, A. J. Wiltshire, R. Wright, S. Zaehle. (2018). Global carbon budget 2018. *Earth System Science Data*, 10, 2141-2194.
- Le Toan, T., A. Beaudoin, J. Riom, D. Guyon. (1992). Relating forest biomass to SAR data. *IEEE Transactions on Geoscience and Remote Sensing*, 30(2), 403-411.
- Le Toan, T., A. Beaudoin, J. Riom, D. Guyon. (1992). Relating forest biomass to SAR data. *IEEE Transactions on Geoscience and Remote Sensing*, 30(2), 403-411.
- Le Toan, T., S. Quegan, M. W. J. Davidson, H. Balzter, P. Paillou, K. Papathanassiou, S. Plummer, F. Rocca, S. Saatchi, H. Shugart, L. Ulander. (2011). The BIOMASS mission: Mapping global forest biomass to better understand the terrestrial carbon cycle. *Remote Sensing of Environment*, 115(11), 2850 - 2860.
- Lefsky, M. A. (2010). A global forest canopy height map from the Moderate Resolution Imaging Spectroradiometer and the Geoscience Laser Altimeter System. *Geophysical Research Letters*, 37(15).
- Lefsky, M. A., Cohen, W. B., Parker, G. G., & Harding, D. J. (2002). Lidar Remote Sensing for Ecosystem Studies: Lidar, an emerging remote sensing technology that directly measures the three-dimensional distribution of plant canopies, can accurately estimate vegetation structural attributes and should be of particular interest to forest, landscape, and global ecologists. *BioScience*, 52(1), 19-30.
- Lefsky, M. A., Keller, M., Pang, Y., De Camargo, P. B., & Hunter, M. O. (2007). Revised method for

- forest canopy height estimation from Geoscience Laser Altimeter System waveforms. *Journal of Applied Remote Sensing*, 1(1), 013537-013537.
- Mascaro, J., Asner, G. P., Muller-Landau, H. C., van Breugel, M., Hall, J., & Dahlin, K. (2011b). Controls over aboveground forest carbon density on Barro Colorado Island, Panama. *Biogeosciences*, 8(6), 1615-1629.
- Matzler, C. (1994). Microwave (1-100 GHz) dielectric model of leaves. *IEEE Transactions on Geoscience and Remote Sensing* 32(4): 947 – 949.
- McMahon, T. (1973). Size and shape in biology. *Science* 179(4079), 1201 – 1204.
- McRoberts, R. E., Chen, Q., & Walters, B. F. (2017). Multivariate inference for forest inventories using auxiliary airborne laser scanning data. *Forest Ecology and Management*, 401, 295-303.
- McRoberts, R. E., Næsset, E., & Gobakken, T. (2013). Inference for lidar-assisted estimation of forest growing stock volume. *Remote Sensing of Environment*, 128, 268-275.
- Mermoz, S., Réjou-Méchain, M., Villard, L., Le Toan, T., Rossi, V., & Gourlet-Fleury, S. (2015). Decrease of L-band SAR backscatter with biomass of dense forests. *Remote Sensing of Environment*, 159, 307-317.
- Mermoz, S., T. L. Toan, L. Villard, M. Rejou-Mechain, J. Seifert-Granzin. (2014). Biomass assessment in the Cameroon savanna using ALOS PALSAR data. *Remote Sensing of Environment*, 155, 109-119.
- Meyer, V., Saatchi, S. S., Chave, J., Dalling, J. W., Bohlman, S., Fricker, G. A., ... & Hubbell, S. (2013). Detecting tropical forest biomass dynamics from repeated airborne lidar measurements. *Biogeosciences*, 10(8), 5421-5438.
- Michelakis, D., N. Stuart, G. Lopez, V. Linares, and I. H. Woodhouse. (2014). Local-scale mapping of biomass in tropical lowland pine savannas using ALOS PALSAR. *Forests*, 5(9), 2377-2399.
- Minh, D. H. T., Tebaldini, S., Rocca, F., Le Toan, T., Villard, L., & Dubois-Fernandez, P. C. (2015). Capabilities of BIOMASS tomography for investigating tropical forests. *Geoscience and Remote Sensing, IEEE Transactions on*, 53(2), 965-975.
- Mironov, V. L., M. C. Dobson, V. H. Kaupp, S. A. Komarov, V. N. Kleshchenko. (2004). Generalized refractive mixing dielectric model for moist soils. *IEEE Transactions on Geoscience and Remote Sensing*, 42(4), 773 – 785.
- Mitchard, E. T. A., Saatchi, S. S., Lewis, S. L., Feldpausch, T. R., Woodhouse, I. H., Sonké, B., ... & Meir, P. (2011). Measuring biomass changes due to woody encroachment and deforestation/degradation in a forest-savanna boundary region of central Africa using multi-temporal L-band radar backscatter. *Remote Sensing of Environment*, 115(11), 2861-2873.
- Mitchard, E. T. A., S. S. Saatchi, I. H. Woodhouse, G. Nangendo, N. S. Ribeiro, M. Williams, C. M. Ryan, S. L. Lewis, T. R. Feldpausch, and P. Meir. Using satellite radar backscatter to predict above-ground woody biomass: A consistent relationship across four different African landscapes. *Geophysical Research Letters*, 36, L23401.
- Mitchard, E. T., Feldpausch, T. R., Brienen, R. J., Lopez-Gonzalez, G., Monteagudo, A., Baker, T. R., ... & Pardo Molina, G. (2014). Markedly divergent estimates of Amazon forest carbon density from ground plots and satellites. *Global ecology and biogeography*, 23(8), 935-946.
- Mitchard, E. T., Saatchi, S. S., Baccini, A., Asner, G. P., Goetz, S. J., Harris, N. L., & Brown, S. (2013). Uncertainty in the spatial distribution of tropical forest biomass: a comparison of pan-tropical maps. *Carbon balance and management*, 8(10), 1-13.
- Mokany, K., Raison, R., & Prokushkin, A. S. (2006). Critical analysis of root: Shoot ratios in terrestrial biomes. *Global Change Biology*, 12(1), 84–96.
- Morel, A. C., Saatchi, S. S., Malhi, Y., Berry, N. J., Banin, L., Burslem, D., Nilus, R., & Ong, R. C. (2011). Estimating aboveground biomass in forest and oil palm plantation in Sabah, Malaysian Borneo using ALOS PALSAR data. *Forest Ecology and Management*, 262, 1786–1798.
- Moussavi, M. S., W. Abdalati, T. Scambos, A. Neuenschwander. (2014). Applicability of an automatic surface detection approach to micro-pulse photon-counting lidar altimetry data: implications for canopy height retrieval from future ICESat-2 data. *International Journal of Remote Sensing*, 35(13), 5263 – 5279.
- Næsset, E., Gobakken, T., Solberg, S., Gregoire, T. G., Nelson, R., Ståhl, G., & Weydahl, D. (2011). Model-assisted regional forest biomass estimation using lidar and InSAR as auxiliary data: A case study from a boreal forest area. *Remote Sensing of Environment*, 115(12), 3599-3614.
- Næsset, E., Ørka, H. O., Solberg, S., Bollandsås, O. M., Hansen, E. H., Mauya, E., ... & Gobakken, T. (2016). Mapping and estimating forest area and aboveground biomass in miombo woodlands in Tanzania using data from airborne laser scanning, TanDEM-X, RapidEye, and global forest maps: A comparison of estimated precision. *Remote sensing of Environment*, 175, 282-300.
- Neigh, C. S., Nelson, R. F., Ranson, K. J., Margolis, H. A., Montesano, P. M., Sun, G., ... & Andersen, H. E. (2013). Taking stock of circumboreal forest carbon with ground measurements, airborne and spaceborne lidar. *Remote Sensing of Environment*, 137, 274-287.
- Nelson, R., Ranson, K. J., Sun, G., Kimes, D. S., Kharuk, V., & Montesano, P. (2009). Estimating Siberian timber volume using MODIS and ICESat/GLAS. *Remote Sensing of Environment*, 113(3), 691-701.
- Neumann, M., S. Saatchi, L. M. H. Ulander, J. E. S. Fransson. (2012). Assessing performance of L- and P-band polarimetric interferometric SAR data in estimating boreal forest above-ground biomass. *IEEE Transactions on Geoscience and Remote Sensing* 50(3), 714 – 726.

- Ngomanda, A., N. L. E. Obiang, J. Lebamba, Q. M. Mavouroulou, H. Gomat, G. S. Mankou, J. Loumeto, D. M. Iponga, F. K. Ditsouga, R. Z. Koumba, K. H. B. Bobe, C. M. Okouyi, R. Nyangadouma, N. Lepengue, B. Mbatchesi, N. Picard. Site-specific versus pantropical allometric equations: Which option to estimate the biomass of a moist central African forest? *Forest Ecology and Management* 312, 1-9.
- Nogueira, E. M., Nelson, B. W., Fearnside, P. M., França, M. B., & de Oliveira, A. C. A. (2008). Tree height in Brazil's 'arc of deforestation': Shorter trees in south and southwest Amazonia imply lower biomass. *Forest Ecology and Management*, 255(7), 2963–2972.
- Oh, Y., K. Sarabandi, F. T. Ulaby. (1992). An empirical model and an inversion technique for radar scattering from bare soil surfaces. *IEEE Transactions on Geoscience and Remote Sensing*, 30(2), 370 – 381.
- Olofsson, P., Foody, G. M., Stehman, S. V. and Woodcock, C. E. (2013). Making better use of accuracy data in land change studies: estimating accuracy and area and quantifying uncertainty using stratified estimation. *Remote Sensing of Environment*, 129:122-131
- Olson, D. M., Dinerstein, E., Wikramanayake, E. D., Burgess, N. D., Powell, G. V. N., Underwood, E. C., D'Amico, J. A., Itoua, I., Strand, H. E., Morrison, J. C., Loucks, C. J., Allnutt, T. F., Ricketts, T. H., Kura, Y., Lamoreux, J. F., Wettengel, W. W., Hedao, P., Kassem, K. R. (2001). Terrestrial ecoregions of the world: a new map of life on Earth. *Bioscience*, 51(11), 933-938.
- Peplinski, N. R., F. T. Ulaby, M. C. Dobson. (1995). Dielectric properties of soils in the 0.3 – 1.3-GHz range. *IEEE Transactions on Geoscience and Remote Sensing*, 33(3), 803 – 807.
- Phillips, S. J., R. P. Anderson, R. E. Schapire. (2006). Maximum entropy modeling of species geographic distributions. *Ecological Modelling*, 190(3-4), 231-259.
- Raney, R. K. (2007). Hybrid-polarity SAR architecture. *IEEE Transactions on Geoscience and Remote Sensing*, 45(11), 3397-3404.
- Ranson, K. J., G. Sun, J. F. Weishampel, R. G. Knox. (1997). Forest biomass from combined ecosystem and radar backscatter modeling. *Remote Sensing of Environment*, 59(1), 118 – 133.
- Ranson, K. J., G. Sun. 1994. Mapping biomass of a northern forest using multifrequency SAR data. *IEEE Transactions on Geoscience and Remote Sensing*, 32(2), 388 – 396.
- Reese, H., M. Nilsson, T. G. Pahlen, O. Hagner, S. Joyce, U. Tingelof, M. Egberth, and H. Olsson. Countrywide estimates of forest variables using satellite data and field data from the national forest inventory. *AMBIO: A Journal of the Human Environment*, 32(8).
- Rosette, J., P. North, J. Suarez. (2008). Stemwood Volume Estimates for a Mixed Temperate Forest using Satellite Lidar. *Japan Society of Forest Planning*, 13, 205 – 214. Rosette, J., J. Suarez, R. Nelson, S. Los, B. Cook, and P. North. (2012). Lidar remote sensing for biomass assessment. In *Remote Sensing of Biomass –Principles and Applications* [L. Fatoyinbo (ed)], Intech.
- Saatchi, S. S., Harris, N. L., Brown, S., Lefsky, M., Mitchard, E. T., Salas, W., ... & Morel, A. (2011). Benchmark map of forest carbon stocks in tropical regions across three continents. *Proceedings of the National Academy of Sciences*, 108(24), 9899-9904.
- Saatchi, S. S., Houghton, R. A., Dos Santos Alvala, R. C., Soares, J. V., & Yu, Y. (2007). Distribution of aboveground live biomass in the Amazon basin. *Global Change Biology*, 13(4), 816-837.
- Saatchi, S. S., R. H. Land. (1989). Self consistent approach to average waves in a one dimensional discrete random medium. *PIERS: Progress in Electromagnetics Research Symposium. Proceedings of the symposium held July 25-26, 1989 in Boston, Massachusetts, USA*. P. 277.
- Saatchi, S. S., D. M. Le Vine, R. H. Lang. (1994). Microwave backscattering and emission model for grass canopies. *IEEE Transactions on Geoscience and Remote Sensing*, 32(1), 177 – 186.
- Saatchi, S., Marlier, M., Chazdon, R. L., Clark, D. B., & Russell, A. E. (2011b). Impact of spatial variability of tropical forest structure on radar estimation of aboveground biomass. *Remote Sensing of Environment*, 115(11), 2836-2849.
- Saatchi, S., Mascaro, J., Xu, L., Keller, M., Yang, Y., Duffy, P., ... & Schimel, D. (2015). Seeing the forest beyond the trees. *Global Ecology and Biogeography*, 24(5), 606-610.
- Saatchi, S. S., and K. C. McDonald. (1997). Coherent effects in microwave backscattering models for forest canopies. *IEEE Transactions on Geoscience and Remote Sensing*, 35(4), 1032- 1044.
- Saatchi, S.S. and M. Moghaddam. (2000). Estimation of crown and stem water content and biomass of boreal forest using polarimetric SAR imagery. *IEEE Transactions on Geoscience and Remote Sensing*, 38(2), 697 – 709.
- Sabine, C. L., M. Heimann, P. Artaxo, D. C. E. Bakker, CA Chen, C. B. Field, N. Gruber, C. Le Quere, R. G. Prinn, J. E. Richey, P. R. Lankau, J. A. Sathaye, R. Valentini. (2004). Current status and past trends of the global carbon cycle. In *The Global Carbon Cycle: Integrating Humans, Climate, and the Natural World* [C. B. Field and M. R. Raupach (eds)], Island Press, Washington, D.C.
- Sandberg, G., L. M. H. Ulander, J.E. S. Fransson, J. Holmgren, T. Le Toan. (2011). L- and P-band backscatter intensity for biomass retrieval in hemiboreal forest. *Remote Sensing of Environment* 115(11), 2874 – 2886.
- Santoro, M., Askne, J., G. Smith, J. E. S. Fransson. (2002). Stem volume retrieval in boreal forests from ERS-1/2 interferometry. *Remote Sensing of Environment*, 81(1), 19-35.
- Schimel, D., B. B. Stephens, J. B. Fisher. (2015). Effect of increasing CO2 on the terrestrial carbon cycle. *Proceedings of the National Academy of Sciences of the United States of America*, 112(2), 436 – 441.

- Schimel, D., R. Pavlick, J. B. Fisher, G. P. Asner, S. Saatchi, P. Townsend, C. Miller, C. Frankenberg, K. Hibbard, P. Cox. (2014). Observing terrestrial ecosystems and the carbon cycle from space. *Global Change Biology*, 21(5), 1762 – 1776.
- Sellers, P. J., D. S. Schimel, B. Moore III, J. Liu, A. Eldering. (2018). Observing carbon cycle-climate feedbacks from space. *Proceedings of the National Academy of Sciences of the United States of America*, 115(31), 7860 – 7868.
- Shi, J., J. Wang, A. Y. Hsu, P. E. O'Neill, E. T. Engman. (1997). Estimation of bare surface soil moisture and surface roughness parameter using L-band SAR image data. *IEEE Transactions on Geoscience and Remote Sensing*, 35(5), 1254 – 1266.
- Shugart, H. H., Saatchi, S., & Hall, F. G. (2010). Importance of structure and its measurement in quantifying function of forest ecosystems. *Journal of Geophysical Research: Biogeosciences (2005–2012)*, 115(G2).
- Small, D. (2011). Flattening gamma: Radiometric terrain correction for SAR imagery. *IEEE Transactions on Geoscience and Remote Sensing*, 49(8), 3081 – 3093.
- Small, D., F. Holecz, E. Meier, D. Nuesch. (1998). Absolute radiometric correction in rugged terrain: A plea for integrated radar brightness. *IGARSS '98. Sensing and Managing the Environment. 1998 IEEE International Geoscience and Remote Sensing Symposium Proceedings*.
- Stinson, G., Kurz, W. A., Smyth, C. E., Neilson, E. T., Dymond, C. C., Metsaranta, J. M., . . . & Blain, D. (2011). An inventory-based analysis of Canada's managed forest carbon dynamics, 1990 to 2008. *Global change biology*, 17(6), 2227–2244.
- Sun, G., and K. J. Ranson. (1995). Three-dimensional radar backscatter model of forest canopies. *IEEE Transactions on Geoscience and Remote Sensing*, 33(2), 372 – 382.
- Tittmann, P., & Saatchi, S. S. (2015). Tool for measuring ALBF using remote sensing v1.0, (March), 1–32. Accessed Dec 2018: <https://verra.org/wp-content/uploads/2018/03/VT0005-Tool-for-measuring-ALBF-using-remote-sensing-v1.0.pdf>
- Tomppo, E., M. Gschwantner, M. Lawrence, and R. E. McRoberts. (2010). *National Forest Inventories: Pathways for Common Reporting*. Springer, Dordrecht.
- Tomppo, E., J. Heikkinen, H. M. Henttonen, A. Ihalainen, M. Katila, H. Makela, T. Tuomainen, N. Vainikainen. (2011). *Designing and Conducting a Forest Inventory of Finland*. Springer, Dordrecht.
- Tsang, L., & Kong, J. A. (2004). *Scattering of electromagnetic waves: advanced topics (Vol. 26)*. John Wiley & Sons.
- Tsang, L., J. A. Kong, and R. T. Shin. 1985. *Theory of Microwave Remote Sensing*. John Wiley, New York.
- Ulaby, F. T., A. Aslam, M. C. Dobson. (1982). Effects of vegetation cover on the radar sensitivity to soil moisture. *IEEE Transactions on Geoscience and Remote Sensing*, GE-20(4), 476 – 481.
- Ulaby, F. T., and M. A. El-rayes. (1987). Microwave dielectric spectrum of vegetation – Part II: Dual-dispersion model. *IEEE Transactions on Geoscience and Remote Sensing*, GE-25(5), 550 – 557.
- Ulaby, F. T., M. C. Dobson. (1989). *Handbook of Radar Scattering Statistics for Terrain*. Artech House, Norwood MA.
- Ulaby, F. T., T. H. Bengal, M. C. Dobson, J. R. East, J. B. Garvin, D. I. Evans. (1990). Microwave dielectric properties of dry rocks. *IEEE Transactions on Geoscience and Remote Sensing*, 28(3), 325 – 336.
- Ulander, L. M. H. (1996). Radiometric slope correction of synthetic-aperture radar images. *IEEE Transactions on Geoscience and Remote Sensing*, 34(5), 115 – 1122.
- Villard, L., & Le Toan, T. (2015). Relating P-Band SAR Intensity to Biomass for Tropical Dense Forests in Hilly Terrain: γ_0 or t_0 . *IEEE Journal of Selected Topics in Applied Earth Observations and Remote Sensing*, 8(1), 214-223.
- Weisbin, C. R., Lincoln, W., & Saatchi, S. (2014). A systems engineering approach to estimating uncertainty in above-ground biomass (AGB) derived from remote-sensing data. *Systems Engineering*, 17(3), 361–373.
- West, G. B., and J. H. Brown. (2005). The origin of allometric scaling laws in biology from genomes to ecosystems: towards a quantitative unifying theory of biological structure and organization. *Journal of Experimental Biology* 208: 1575-1592.
- Wigneron, J. P., P. Ferrazzoli, A. Olioso, P. Bertuzzi, A. Chanzy. (1999). A simple approach to monitor crop biomass from C-band radar data. *Remote Sensing of Environment*, 69(2), 179-188.
- Wulder, M. A., and S. E. Franklin. (2012). *Remote Sensing of Forest Environments: Concepts and Case Studies*, Springer, New York.
- Xu, L., Saatchi, S. S., A. Shapiro, V. Meyer, A. Ferraz, Y. Yang, J. Bastin, N. Banks, P. Boeckx, H. Verbeeck, S. L. Lewis, E. T. Muanza, E. Bongwele, F. Kayembe, D. Mbenza, L. Kalau, F. Mukendi, F. Ilunga, D. Ebuta. (2017). Spatial distribution of carbon stored in forests of the Democratic Republic of Congo. *Scientific Reports*, 7, 15030.
- Xu, L., Saatchi, S. S., Yang, Y., Myneni, R. B., Frankenberg, C., Chowdhury, D., Bi, J. (2015). Satellite observation of tropical forest seasonality: Spatial patterns of carbon exchange in Amazonia. *Environmental Research Letters*, 10, 084005.
- Xu, L., Saatchi, S. S., Yang, Y., Yu, Y., & White, L. (2016). Performance of non-parametric algorithms for spatial mapping of tropical forest structure. *Carbon balance and management*, 11(1), 18.

- Yu, Y. and S. Saatchi. (2016). Sensitivity of L-band SAR Backscatter to aboveground biomass of global forests. *Remote Sensing*, 8(6), 522.
- Yu, Y., Saatchi, S. Fore, A. et al. (In Review) Carbon Stocks in World's Forests and Shrublands.
- Yueh, S. H., J. A. Kong, J. K. Jao, R. T. Shin, T. L. Toan. (1992). Branching model for vegetation. *IEEE Transactions on Geoscience and Remote Sensing*, 30(2), 390 – 402.
- Yun, S.-H., Hudnut, K., Owen, S., Webb, F., Simons, M., Sacco, P., Gurrola, E., Manipon, G., Liang, C., and Fielding, E., 2015b, Rapid Damage Mapping for the 2015 Mw 7.8 Gorkha Earthquake Using Synthetic Aperture Radar Data from COSMO-SkyMed and ALOS-2 Satellites: *Seismological Research Letters*, v. 86, no. 6, p. 1549-1556.
- Zeng, W., E. Tomppo, S. P. Healey, and K. V. Gadov. (2015). The national forest inventory in China: history-results-international context. *Forest Ecosystems* 2:23.
- Zolkos, S. G., S. J. Goetz, R. Dubayah. (2013). A meta-analysis of terrestrial aboveground biomass estimation using lidar remote sensing. *Remote Sensing of Environment*, 128, 289 – 298.
- Zhang X., Ni-meister W. (2014) Remote Sensing of Forest Biomass. In: Hanes J. (eds) *Biophysical Applications of Satellite Remote Sensing*. Springer Remote Sensing/Photogrammetry. Springer, Berlin, Heidelberg

DR. SASSAN SAATCHI is a senior scientist with the carbon cycle and ecosystems section at the Jet Propulsion Laboratory (JPL), California Institute of Technology and an adjunct professor at the UCLA Institute of the Environment and Sustainability and the Center for Tropical Research. He received his PhD in Electrophysics and Applied Mathematics from Georgetown University in 1988, and held a postdoctoral fellowship at the NASA/GSFC hydrospheric branch before joining JPL in 1991. During the past 20 years, Dr. Saatchi has participated in several NASA-supported interdisciplinary and international projects as principal investigator and has developed remote sensing techniques and algorithms for regional-scale ecological and hydrological variables for NASA airborne and spaceborne missions.

Dr. Saatchi's present research interests include the global carbon cycle, in particular forest biomass/carbon dynamics, land use and land cover change, forest structure and regeneration, and the impact of climate change and variability such as droughts on global forest function and resilience. He is currently directing several interdisciplinary research projects studying the carbon cycling of tropical forests, particularly in the Amazon and Congo Basin using satellite remote sensing data. As an adjunct professor at UCLA, he has also been collaborating with biologists to integrate satellite observations for mapping species functional diversity and habitat characteristics, and with social scientists to model and understand how human activities have impacted vegetation ecosystems. Dr. Saatchi has been developing new active remote sensing techniques from airborne and spaceborne platforms to quantify vegetation structure and water status and creating a data assimilation and modeling framework to improve understanding of processes that impact forest carbon and water cycling. He is actively involved in planned NASA's NISAR and ESA's BIOMASS satellite missions by developing algorithms for retrieving changes of vegetation above ground biomass across different landscapes and ecoregions.

I would like to thank the SERVIR program for providing the opportunity, support, and guidance for the material presented in this chapter. I particularly like to thank Daniel Irwin for inviting me to participate in this effort and for his leadership role in making SERVIR a successful program and extending the data and technical resources and capacity available at NASA to a larger international community. The content of this chapter was improved significantly after the reviews and recommendations provided by the SERVIR program. I also wish to acknowledge the contributions of those cited below in providing data, figures, and examples that helped with the tutorial material and the content of this chapter: Alan Xu, Yan Yang, Antonio Ferraz, Yifan Yu, Victoria Meyer. The methods and products presented in this chapter were developed from my past and present research in the field of ground and remote sensing of forest structure and carbon stocks and dynamics. I also wish to thank the Africa Flores for her guidance and persistence in developing the material for the chapter and Dr. Rajesh Bahadur Thapa, as the SERVIR capacity building lead for organizing the SAR biomass tutorial in Kathmandu, Nepal and his hospitality and technical discussions during my visit.